Biochemistry

pubs.acs.org/biochemistry Article

Targeting Parallel Topology of G-Quadruplex Structures by Indole-Fused Quindoline Scaffolds

Satendra Kumar,[†] Sushree Prangya Priyadarshinee Pany,[†] Sruthi Sudhakar, Sushma B. Singh, Chaitra S. Todankar, and P. I. Pradeepkumar*

Cite This: *Biochemistry* 2022, 61, 2546−2559 Read Online

ACCESS | Metrics & More | Article Recommendations | Supporting Information

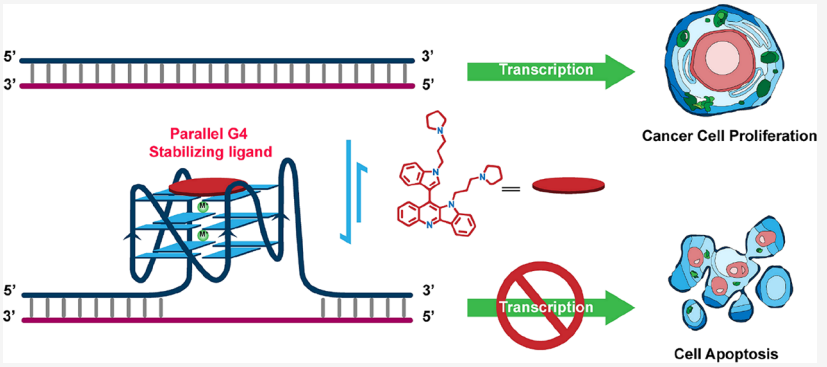

ABSTRACT: Preferential stabilization of G-quadruplex (G4) structures using small-molecule ligands has emerged as an effective approach to develop anticancer drugs. Herein, we report the synthesis of three indole-fused quindoline derivatives with varying lengths of side chains (**InqEt1**, **InqEt2**, **and InqPr2**) as selective ligands for promoter G4 structures. The ligands stabilize the parallel topology of *c-MYC* and *c-KIT1* promoter G4 DNAs over telomeric and duplex DNAs, as evident from the circular dichroism melting and polymerase stop-assay experiments. The lead ligand, **InqPr2**, downregulates the gene expression of *c-MYC* and c-*KIT* in HeLa and HepG2 cells, respectively, leading to apoptotic cell death. Molecular modeling and dynamics studies support the 2:1 binding stoichiometry revealed from the Job plot analysis and show the ligand's structural features that enable the preferential binding to the parallel G4 structures over other topologies. Our studies show that indole-fused quindoline derivatives can be harnessed as new molecular scaffolds for selective targeting of parallel G4 topologies.

INTRODUCTION

In addition to forming duplexes by Watson-Crick base pairing, guanines can form square planar structures termed G-tetrads *via* Hoogsteen hydrogen bonding.[1,2] More than two G-tetrads give rise to stable G4 structures with suitable metal salts.[1] G4 structures have gained immense attention because of their implications in various biological processes. Potential G4-developing sequences are found at the promoter regions of multiple proto-oncogenes and the end part of chromosomes.[2] Several significant biological functions, such as maintaining telomere length and modulation of oncogenic expression, are influenced by the formation of stable G4 structures.[23] In most cancer cells, overexpression of *c-MYC* is observed and is therefore considered as a significant therapeutic target.[4] Transcription of *c-MYC* gene is known to be controlled by nuclease hypersensitivity element (NHE III_1), which harbors G-rich sequences.[5] Expression of the *c-MYC* oncogene can be halted by stabilizing the G4 structure using small-molecule ligands.[6] A myriad of small molecules such as porphyrin, quindoline, carbazole, and so forth have been reported to inhibit *c-MYC* expression.[6] Identification of small molecules that regulate gene expression by targeting specific G4 topology is highly desirable.[2] Although targeting a particular G4 topology is quite challenging, varying dimensions of different G-quartets and the unique sizes of their loops can render specificity toward a specific topology. Though several ligands that stabilize G4 structures have been reported over the years,[2] only a few show preferential binding to promoter G4 structures.[3,6−8] Therefore, designing new molecular scaffolds, selectively binding to the promoter G4s with parallel topology, provides promising avenues for anticancer drug discovery.

Herein, we have synthesized G4-binding small molecule ligands based on a quindoline scaffold substituted with indole

Received: June 22, 2022
Revised: October 13, 2022
Published: October 31, 2022

https://doi.org/10.1021/acs.biochem.2c00373
Biochemistry 2022, 61, 2546−2559

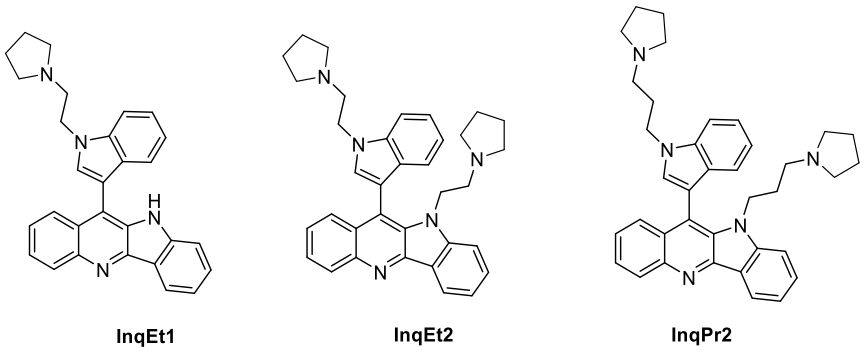

Figure 1. Structure of indole-fused quindoline derivatives used as G4-stabilizing ligands.

moieties (Figure 1). Various biophysical techniques were used to evaluate their binding affinities toward the G4 structures, and their cellular activities were also explored. The results obtained from these studies revealed that these ligands could preferentially bind to the parallel G4 DNAs of *c-MYC* and *c-KIT1* promoters and inhibit gene expression at the cellular level.

EXPERIMENTAL SECTION

Synthetic Procedure. Details of the synthetic methods and compound characterization data are described in the Supporting Information.

Single Crystal X-ray Diffraction Methodology. The crystal data of compound **4** and the alkylated product **InqPr1** were obtained on a Rigaku Saturn 724+ CCD diffractometer at 293 K (Radiation source: Mo K_α; λ = 0.7107 Å). The data were reduced with the help of CrysalisPro Red 171.41_64.93a software, and the structure was solved using Olex2[9] with the ShelXT[10] structure solution program and further refined with the SHELXL[11] refinement package using the least-squares minimization. The full-matrix least-squares technique with anisotropic thermal data for nonhydrogen atoms on F^2 was utilized for the final refinement of the structure. Refinement of the nonhydrogen atoms was carried out anisotropically, and the hydrogen atoms were refined at calculated positions as riding atoms with isotropic displacement parameters. Deposition numbers (CCDC: 2009565 [compound **4**] and 2113444 [**InqPr1**]) contains the supplementary crystallographic data for this paper. These data are provided free of charge by the joint Cambridge Crystallographic Data Centre and Fachinformationszentrum Karlsruhe Access Structures service.

Ligand Stock Solution. The 5 mM stock solution of the ligand was prepared using the appropriate amount of DMSO and diluted to 2.5 mM by using 1 mM HCl in H_2O.

Oligonucleotides. The oligonucleotides listed in Table S5 were used for all the biophysical experiments. All the oligonucleotides are synthesized in house using a MerMade 4 synthesizer. The oligonucleotides were purified with 20% PAGE with 7 M urea and 10x TBE, utilizing the standard protocols. The desalting of these purified oligonucleotides was performed using the SePak column, and the concentration was estimated with the UV−Vis spectrophotometer at 260 nm wavelength using appropriate molar extinction coefficients (ε).

CD Titration Studies. The circular dichroism (CD) titration studies were recorded in a Jasco J-1500 CD spectrometer between 200 and 600 nm wavelength ranges using a quartz cuvette of 1 mm path length. The scanning speed was at 100 nm/s with a response time of 8 s at 25 °C. The concentration of oligonucleotide used for the study was 10 μM in 10 mM lithium cacodylate, pH 7.2 in the presence of salt (10 mM KCl and 90 mM LiCl for Telomeric and *c-KIT1* DNAs, 1 mM KCl and 99 mM LiCl for *c-MYC* DNA, and 50 mM KCl and 50 mM LiCl for *h-RAS*1 G4 DNA). On the sequential addition of the ligand to the DNA solution, the solution was equilibrated for 3 min each time. Each spectrum was taken as an average of three measurements. All spectra are baseline-corrected and further analyzed using Origin 8.0 software.

CD Melting Studies. Melting experiments were performed using 10−15 μM DNA in 10 mM lithium cacodylate buffer, pH 7.2, along with the specific amount of LiCl and KCl, and 5 molar equivalents of ligands were used. *c-KIT1*, telomeric DNA, and duplex DNA solutions were prepared in 10 mM KCl and 90 mM LiCl, *c-MYC* DNA in 1 mM KCl and 99 mM LiCl, and *h-RAS1* in 50 mM KCl and 50 mM LiCl. After annealing these DNA solutions by heating at 95 °C for 5 min and cooling at room temperature over 3−4 h, 5 molar equivalent of ligand was added and kept at 4 °C overnight. Thermal melting was monitored at 263 nm for c-*MYC* and c-*KIT1*, at 295 nm for telomeric, 290 nm for *h-RAS1*, and 242 nm for duplex DNA using a 1 mm path length quartz cuvette at a heating rate of 1 °C min^{-1}. The results are the mean values of three replicates. To obtain the $T_{1/2}$, the sigmoidal curve was fitted with the Boltzmann function in Origin 8.0 software.

Fluorimetric Titration. The fluorimetric titration experiment was carried out by a HORIBA fluorimeter (Fluoromax 4) using a 100 μL micro quartz cuvette with a 1 cm path length. The ligand (100 μM) was excited at 412 nm, and the emission spectra were recorded at the 420−700 nm range, having a slit width of 3 nm. The fluorescence of ligand was recorded, and to it annealed DNA samples (0−9 μM DNA, 100 mM KCl, and 10 mM lithium cacodylate buffer, pH 7.2) were added, and the emission spectra were recorded after equilibration of 3 min for each addition. The normalized fluorescence intensity was plotted against the logarithm of the concentration of the DNA. The binding constant values were calculated by fitting the curve using Hill 1 eq 1

$$F_N = F_0 + (F_S - F_0)\left(\frac{[\mathrm{DNA}]^n}{[K_d]^n + [\mathrm{DNA}]^n}\right) \quad (1)$$

Normalized fluorescence intensity (F_N) was derived using the equation

https://doi.org/10.1021/acs.biochem.2c00373
Biochemistry 2022, 61, 2546−2559

$$F_N = \frac{(F_i - F_S)}{(F_O - F_S)}$$

where F_i = fluorescence intensity of the bound ligand at each titration point, F_0 = fluorescence intensity in the absence of a ligand, F_S = fluorescence intensity at the saturation concentration of a ligand, n = Hill coefficient, and K_d (dissociation constant) = $(1/K_a)$. All the spectra were analyzed by using Origin 8.0 software.

Job Plot Analysis. With an excitation wavelength of 412 nm and emission spectra in the 420−700 nm range, Job plot analyses for **InqPr2** with *c-MYC* and *c-KIT1* were carried out. The total ligand with DNA concentration of each sample was kept constant at 15 μM. The mole fractions of **InqPr2** in the samples varied from 0−1. Emission spectra of the samples were recorded in a Horiba fluorimeter (Fluoromax-4) by using a 100 μL micro quartz cuvette with a 1 cm path length and a 3 nm slit width. The stoichiometry for ligand−DNA complexes was calculated by plotting mole fractions of **InqPr2** against fluorescence intensities. Origin 8.0 was used to analyze all of the curves.

***Taq* DNA Polymerase Stop Assay.** The polymerase assay was executed using a formerly reported protocol with slight modifications. A suitable concentration of FAM-labeled primer (0.2 μM) and template DNA (0.1 μM) in annealing buffer (5 mM Tris (pH 8.0), 10 mM NaCl, and 0.1 mM EDTA) was annealed by heating at 95 °C for 5 min followed by slow cooling to room temperature. The annealed primer-template solution and 1× polymerase buffer (50 mM Tris−HCl (pH 8.0), 0.5 mM DTT, 0.1 mM EDTA, 5 mM $MgCl_2$, and 5 mM KCl for *c-MYC* and 10 mM KCl for telomeric DNA template; 1 μg μL^{-1} BSA in 5% glycerol; and 0.2 mM dNTPs) were mixed together further. An appropriate concentration of the ligand (0−100 μM) was added to the reaction mixture (10 μL) and incubated for over 30 min at room temperature. To achieve a primer extension reaction, 1 U of the *Taq* DNA polymerase enzyme was added to the reaction mixtures and heated at 40 °C for the telomeric and 55 °C for *c-MYC* for 30 min. Finally, 10 μL of the fast dye (80% formamide, 1× TBE, 50 mM EDTA (pH 8.0), and 0.025% bromophenol blue) was added to the reactions to stop the primer extension reaction. The extension products were then determined by 15% denaturing PAGE containing 7 M urea in 1× TBE (89 mM of Tris−HCl and boric acid each and 2 mM EDTA, pH 8.2) running buffer. The gel was scanned on an Amersham Typhon 600 (GE Healthcare) and quantified with the help of the Image Quant 5.2 software. IC_{50} values were determined with the help of Origin 8.0 software by plotting the percentage of the stop product against ligand concentrations.

Cell Culture. HeLa (human cervical cancer) cells and liver hepatocellular cancer cell lines (HepG2) were maintained in Eagle's minimum essential media (MEM), and Lenti- X were grown in Dulbecco's modified Eagle medium and supplemented with 10% fetal bovine serum with 1% of the antibiotic antimycotic solution. Cells were cultured in a humidified atmosphere (Memmert, ICO) containing 5% of CO_2 at 37 °C.

Cytotoxicity Studies. HeLa and HepG2 cells were seeded at a density of 6×10^3 cells per well in 96-well plates. After 24 h of seeding, the cells reached a confluency of about 60−70%. For Lenti-X cells, 10^4 cells per well in 96-well plates were seeded. After 24 h, the confluency was allowed to reach 70%. Then the media was removed, and the cells were washed with 100 μL of 1x PBS (137 mM NaCl, 2.7 mM KCl, 10 mM Na_2HPO_4, and 1.8 mM KH_2PO_4, pH 7.4) and treated with various concentrations of **InqPr2** (0.5, 1 2, 3, 4, 5, and 10 μM). For Lenti-X, various concentration of **InqPr2** ranging from 2−20 μM was used. After 24 h of incubation with the ligand, the plate containing treated/untreated cells was kept under a laminar flow hood for 30 min at room temperature for equilibration. To this, 100 μL of CellTiter Glo (Promega) reagent was added, and the plate was placed for 2 min in an orbital shaker. Subsequently, the cells were incubated 10 min for equilibration, and then, the luminescence values were acquired on a luminometer (Promega E5311, glowmax 20/20). The luminescence of a cell is directly related to the amount of ATP and thereby the number of viable cells present in the culture. The percentage cell viability was plotted against the logarithmic concentration of ligand, and the IC_{50} value was calculated by fitting the curve using the dose response equation in Graph pad Prism 8.3.0 using a previously reported procedure.[8]

RNA Isolation and Purification. HeLa cells were seeded at a density of 2×10^5 cells per well in 6-well plates and allowed to adhere for 24 h at 5% CO_2 and a 37 °C atmosphere. The dead cells from the wells were discarded along with the media, and the adhered cells were washed with 1x PBS, pH 7.4 (1 mL). The cells were exposed to the ligand **InqPr2** (2 μM) and incubated for 24 h under 5% CO_2. The next day, the media was discarded, and the cells were washed with PBS buffer (1 ml) followed by trypsinization. 100 μL of trypsin was added to the adhered cell and kept inside the 5% CO_2 incubator for 2−3 min. The trypsin activity was quenched by 1 mL of the media, and the media containing suspended cells was transferred to a 1.5 mL centrifuge tube and centrifuged at 2500 rpm for 5 min. The supernatant was discarded, and the cell pellets were taken for the RNA isolation. RNA was isolated using the GeneJET RNA purification kit (Thermo Scientific) according to the manufacturer's protocol. The cell pellets were collected and resuspended in the lysis buffer containing 2 M DTT solution (600 μL). The lysis buffer containing cells was vortexed and homogenized using a 20-gauge needle. The ethanol (600 μL) was added to it, and the solution was transferred to a RNA GeneJET column and centrifuged at 12 000 rpm for 1 min. The wash buffer I (700 μL) was added to the column and centrifuged at 12000 rpm for 1 min, followed by the addition of wash buffer II (600 μL). Finally, the RNA was eluted from the column using 100 μL of nucleus-free water. The isolated RNA was quantified by a nanophotometer (IMPLEN) and used as a template in c-DNA synthesis.

cDNA Synthesis. The cDNA synthesis was performed in a 20 μL reaction using the verso cDNA synthesis kit (Thermo Scientific, catalogue number AB1453A) employing the manufacturer's protocol. 500 ng RNA template, 1X cDNA synthesis buffer (4 μL), 500 μM dNTP mix (2 μL), 500 ng RNA primer (1 μL), RT enhancer (1 μL), verso enzyme mix (1 μL), and nucleus−free water (10 μL) were added, and the mixture was heated at 42 °C for 30 min for cDNA synthesis. Then, the mixture was heated at 92 °C for 2 min for the inactivation of the enzyme.

qRT-PCR Studies. The real-time quantitative polymerase chain reaction (qRT-PCR) was performed on an AriaMx Real-Time PCR system (Agilent Technologies) by using the Brilliant III Ultra-Fast SYBR green QPCR master mix

https://doi.org/10.1021/acs.biochem.2c00373
Biochemistry 2022, 61, 2546−2559

(Agilent Technologies, Catalogue Number 600882) and the cDNA library as the template. The forward and reverse primers used in the experiment are mentioned in Table S6. The amount of cDNA was optimized by dilution to get a significant threshold value for the housekeeping and the target gene within the range (40 cycles). The polymerase chain reaction (PCR) sample (10 μL) contains the 2X SYBR green master mix (5 μL), cDNA, (1 μL), 0.4 μM of each primer (20 μL), and nuclease-free water (3.2 μL). The PCR was executed in 96-well plates and amplified by using the quantitative PCR method. The thermal cycle was programed as follows: denaturation at 95 °C for 3 min, followed by 40 cycles with denaturation at 95 °C for 30 s, annealing at 57 °C for 30 s, and elongation at 72 °C for 30 s.[12] The relative expression of the gene of interest and the housekeeping gene, β actin, was determined by the arithmetic calibrator $2^{(-\Delta\Delta Ct)}$ method.[13] First, the threshold values for both housekeeping and target genes were obtained from the experiment. Each experiment was run in triplicate. Error bars represent the standard deviations derived from three independent experiments.

Statistical analysis was used to determine the expression of the gene of interest in treated and untreated cells. The *p*-value was calculated by the *t*-test using GraphPad Prism 6. For the analysis, *p*-values of less than 0.05 were considered significant.

Apoptosis Assay by Flow Cytometry Using Propidium Iodide/Annexin V-FITC. An apoptosis assay was performed using propidium iodide (PI)/Annexin V-FITC dyes by flowcytometry. HeLa cells of 2.0×10^5 density were seeded into the cell culture plate in C-MEM and allowed to adhere and grow at 37 °C in 5% CO_2 incubator for 24 h. After 70−80% confluency, the cells were treated with ligand **InqPr2** (2.0 and 4.0 μM) and again incubated in a 5% CO_2 incubator for 24 h. After incubation for 24 h, the cells were trypsinized, centrifuged at 2500 rpm for 10 min, and resuspended at 10^6 cells/mL in the 1× Annexin V binding buffer (100 μL). Cell suspensions (100 μL) were added with Annexin V-FITC (1 μL) and incubated for 15 min at room temperature in the dark. The cell suspension was further diluted with 400 μL of the Annexin V binding buffer, followed by the addition of 100 μg/mL of propidium iodide (1 μL) prior to flowcytometry (Becton Dickinson, Aria SORP). Statistical analysis to quantify the percentage of cells was performed by GraphPad Prism 6, and the *p*-value was calculated using the two-way Anova method. For the analysis, *p*-values of less than 0.05 were considered significant.

Molecular Dynamics Studies. The structure of the ligand **InqPr2** was prepared in GaussView 6.0 and optimized in the Gaussian 16 B.01 software at the HF/6-31+G** level of theory. The optimized structure of the ligand was used for further docking studies with *c-MYC* (PDB ID: 1XAV), *c-KIT1* (PDB ID: 2O3M), antiparallel telomeric (PDB ID: 143D), and telomeric Hybrid 2 G4 DNA (PDB ID: 2JPZ). The docking studies were done in the Autodock 4.2.6 software. To facilitate docking, the 5′-end dA was removed from *c-KIT1*. A grid size to enclose the whole macromolecule was used. A genetic algorithm was used to generate 500 independent conformations of the ligand with each of the G4 DNA. The docked conformers were then explored according to their binding energy and binding modes, and the best conformers were used for MD simulations using AMBER 18. The simulation procedure was adapted from a previously reported protocol by Neidle and Haider.[14] The electrostatic potential (ESP) charges for the selected docked conformers were calculated at the HF/6-31G* level of theory in Gaussian 16 B.01, and restrained electrostatic potential (RESP) fitting of these were completed using the antechamber[15] module of AMBER 18. The Generalized AMBER force field (GAFF)[16] and the OL15[17] force field were used for the ligand and G4, respectively. The systems were neutralized by adding K^+ as counter ions, and the TIP3P water model was used for solvation up to a 10 Å rectangular box. All the systems were prepared in tleap of AMBER 18. The systems were then subjected to 10 000 steps of minimization by the steepest descent method with a restraint of 2.0 kcal/mol.Å^2 on the ligand and G4. This was followed by 100 ps of heating and 100 ps of density equilibration with restraints of 50 and 2.0 kcal/mol·Å^2, respectively on the **InqPr2**-G4 complex. The system was further equilibrated for 800 ps in the *NPT* ensemble. Then, an unrestrained MD simulation was performed on the system using the *NPT* ensemble for 500 ns in GPU accelerated version of PMEMD in AMBER 18. SHAKE algorithm was applied to subject the hydrogen atoms to bond length constraints. The temperature was maintained at 300 K using the Langevin[18] thermostat with a collision frequency of 2 ps^{-1}. The pressure was maintained at 1 bar using Berendsen[19] barostat with a relaxation time of 2 ps. All the nonbonded interactions were calculated using the Particle Mesh Ewald (PME) method with a cut-off of 10 Å. The root mean square deviation (RMSD), root mean square fluctuation (RMSF), distances, clustering and other calculations were done using the CPPTRAJ[20] module of AMBER 18. The cut off used to calculate electrostatic distances was 5.0 Å. Binding energy was calculated using the molecular mechanics Poisson−Boltzmann surface area (MM-PBSA) module of AMBER 18 for the last 20 ns of the simulations. Images were rendered using PyMOL (www.pymol.org), and UCSF chimera[21] was used to visualize the trajectories.

RESULTS AND DISCUSSION

Ligand Design and Synthesis. Quindoline, an alkaloid having an indolo[3,2-*b*]quinoline tetracyclic ring system, is isolated from *Cryptolepis Sanguinolenta*.[22] This core exhibits a wide range of antiangiogenic, antiviral, and antitumor activity.[23,24] A derivative of quindoline has already been reported to downregulate the *c-MYC* oncogene expression.[25,26] So far, most of the quindoline derivatives reported are shown to interact with a variety of G4 topologies.[27−30] Considering all these factors, we designed the ligands with the tetracyclic quindoline core substituted with another indole moiety with side chains of varying lengths (Figure 1). We hypothesize that the ligands can potentially stack over the planar G-quartet surface, utilizing the aromatic core, and additionally, the indole moiety attached to the fused ring can impart selectivity toward folded G4 structures over duplex DNA. The presence of indole and the ethyl and propyl side chains can offer preference for the parallel G4 topology due to steric and conformational restraints. Moreover, the positively charged terminal pyrrolidine group can mediate electrostatic interactions involving the negatively charged phosphate groups of the loop and groove regions, and steric hindrance due to the pyrrolidine group can potentially fine-tune noncovalent interactions.[31]

https://doi.org/10.1021/acs.biochem.2c00373
Biochemistry 2022, 61, 2546−2559

Scheme 1[a]

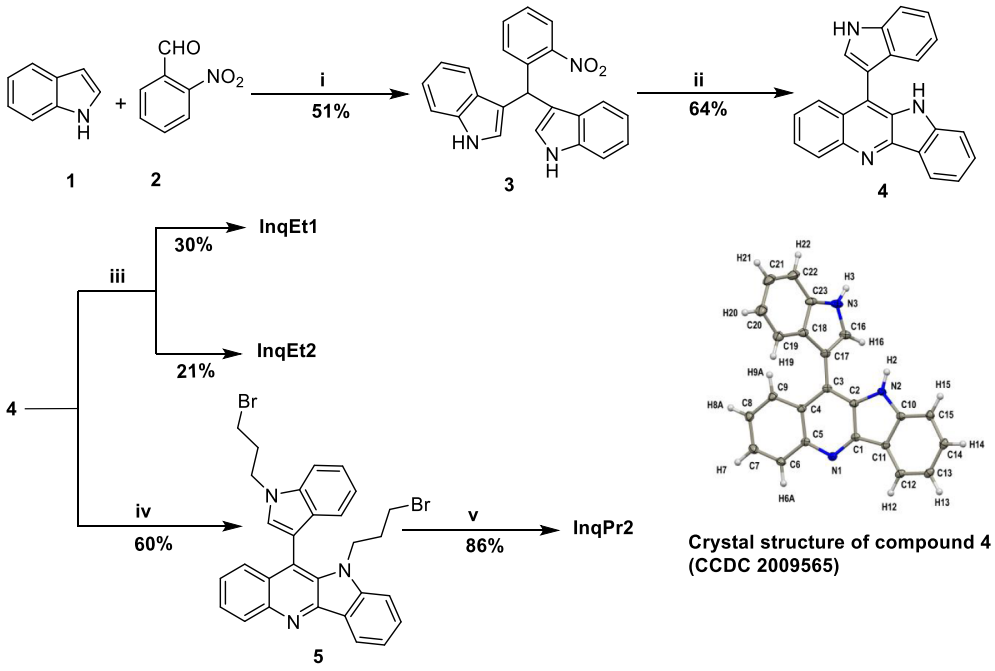

[a](i) I_2 and acetonitrile (ACN), rt, 20 min; (ii) $SnCl_2{\cdot}2H_2O$ and MeOH, 64 °C, 5 h; (iii) 1-(2-chloroethyl)pyrrolidine Hydrogen Chloride, Cs_2CO_3, and ACN, 80 °C, 48 h; (iv) 1,3-Dibromopropane, Cs_2CO_3, and ACN, 80 °C, 24 h; and (v) Pyrrolidine and ACN, 80 °C, 12 h.

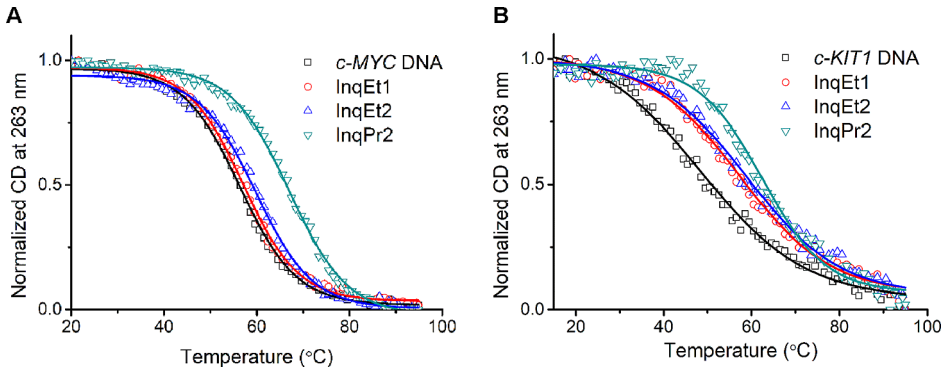

Figure 2. Normalized CD melting curves of *c-MYC* and *c-KIT1* G4 DNAs (10 μM in 10 mM lithium cacodylate buffer, pH 7.2) in the absence and presence of 5 molar equivalents of ligands. (A) *c-MYC* DNA (1 mM KCl and 99 mM LiCl); (B) *c-KIT1* DNA (10 mM KCl and 90 mM LiCl).

The synthetic procedure used to access G4 ligands in this work is shown in Scheme 1. The synthesis of all the derivatives was achieved from the starting materials indole **1** and 2-nitrobenzaldehyde **2**. Bisindole derivative **3** was prepared in 51% yield by reacting **1** with **2** in the presence of iodine.[32] The fused indolo[3,2-*b*]quinoline core **4** was prepared using a previously established procedure.[32] The indole-fused quindoline compound **4** was obtained in 64% yield by treating compound **3** with $SnCl_2{\cdot}2H_2O$. The detailed mechanism for the formation of **4** is shown in Scheme S1 of Supporting Information.

Compound **4** was alkylated with 1-(2-chloroethyl)-pyrrolidine hydrogen chloride under a basic medium using Cs_2CO_3 to furnish mono- and di-alkylated ligands **InqEt1** and **InqEt2** in 30% and 21% yield, respectively. Additionally, compound **4** was treated with 1,3-dibromopropane to synthesize the dialkylated product **5** exclusively in 60% yield. Bromide in compound **5** was further replaced by pyrrolidine to produce **InqPr1** in 86% yield. All the ligands were protonated by using 2% of 0.5 mM HCl/H_2O and utilized for further biophysical experiments.

Single crystal X-ray crystallographic technique was employed to acquire the crystal structure of compound **4**, and the ORTEP diagram is shown in Scheme 1. Crystallographic data, bond lengths, and angles of compound **4** are given in Tables S1 and S2, Supporting Information. The crystal structure revealed that both N1 and N2 nitrogen atoms (marked in **4** in Scheme 1) are positioned opposite, contrary to the structure reported in the literature in which the two fused ring nitrogen atoms face the same side.[32] In order to confirm the alkylation site in compound **4**, the crystal structure of the alkylated product was also obtained (**InqPr1**, Scheme S2, Supporting Information). The crystal structure clearly shows that the alkylation happens at the atoms N2 and N3 of compound **4** (Scheme S2, Tables S3 and S4, Supporting Information).

https://doi.org/10.1021/acs.biochem.2c00373
Biochemistry 2022, 61, 2546−2559

Table 1. Thermal Stabilization of Various Quadruplex and Duplex DNAs Determined from CD Melting Experiments

	[a]Δ $T_{1/2}$				
ligands	telomeric (K^+)	*c-MYC*	*c-KIT1*	*h-RAS1*	duplex (ds-17)
InqEt1	−1.1 ± 0.2	0.7 ± 0	9 ± 0.1	0.5 ± 0.2	0 ± 0.1
InqEt2	−0.2 ± 0.1	3.6 ± 0.1	10.7 ± 0.2	3.4 ± 0.2	0.2 ± 0
InqPr2	1 ± 0.2	9.8 ± 0.1	14.2 ± 0.1	−1.7 ± 0.1	−0.6 ± 0.1

[a]Δ $T_{1/2}$ represents the difference in the thermal melting temperature [$\Delta T_{1/2} = T_{1/2}$ (DNA + 5 molar equivalent ligand)—$T_{1/2}$ (DNA)]. The reported values are the average of three independent experiments with estimated standard deviations. All the experiments were performed using 10 μM quadruplex DNA or 15 μM duplex DNA in 10 mM lithium cacodylate buffer, pH 7.2. The $T_{1/2}$ values in the absence of ligands are 53.2 ± 0.2 for the telomeric DNA in the K^+ ion (10 mM KCl and 90 mM LiCl), 57.8 ± 0.4 for *c-MYC* DNA (1 mM KCl and 99 mM LiCl), 46.6 ± 0.6 for *c-KIT1* DNA (10 mM KCl and 90 mM LiCl), 53.8 ± 0.4 for *h-RAS1* DNA (50 mM KCl and 50 mM LiCl), and 64.0 ± 0.2 for duplex DNA (10 mM KCl and 90 mM LiCl).

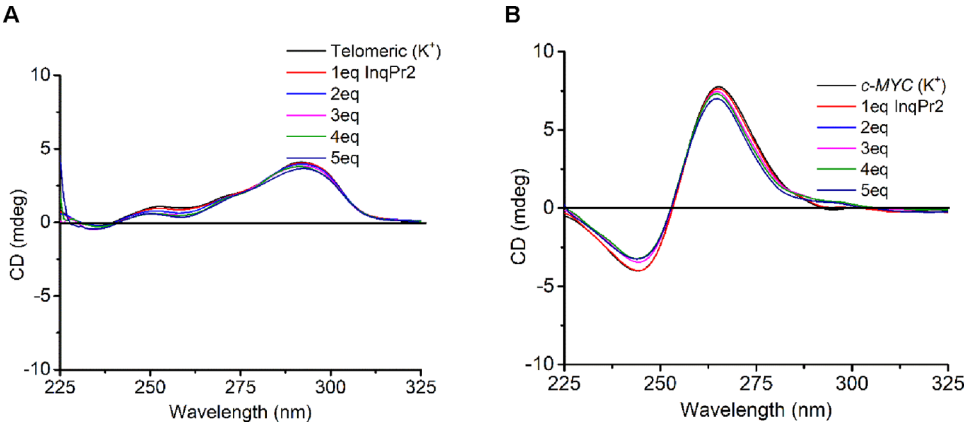

Figure 3. CD titration spectra of quadruplex DNAs (10 μM in 10 mM lithium cacodylate buffer, pH 7.2) in the presence of salt with **InqPr2** (0−5 equivalents). (A) Telomeric DNA (10 mM KCl and 90 mM LiCl); (B) *c-MYC* DNA (1 mM KCl and 99 mM LiCl).

CD Melting Studies. Melting experiment from CD was used to investigate ligand-induced thermal stability of G4 structures.[33] G4-forming and duplex DNA sequences used in the biophysical experiments are listed in Table S5, Supporting Information. We performed CD melting with 10 μM G4 DNAs in the presence and the absence of ligands by monitoring the CD signal intensity at the appropriate wavelengths, suitable salt, and buffer concentrations. Melting experiments with *c-MYC* G4 DNA were performed by monitoring the signal at 263 nm, which yielded a thermal melting temperature ($T_{1/2}$) of ∼58 °C.[34] After addition of 5 molar equivalents of ligand **InqPr2** to *c-MYC* G4 DNA, the $T_{1/2}$ value was increased by ∼10 °C (Figure 2A and Table 1). In contrast, ligands **InqEt1** and **InqEt2** could not enhance the $T_{1/2}$ to a notable extend (maximum $\Delta T_{1/2}$ ∼3.6 °C) at similar conditions. Similarly, the thermal stabilization of another parallel promoter, *c-KIT1* G4 DNA, was measured by monitoring the ellipticity changes at the same wavelength. In the absence of any ligand, *c-KIT1* G4 DNA in 10 mM KCl, showed $T_{1/2}$ of ∼46 °C. A high degree of stabilization was observed with 5 molar equivalents of ligand **InqPr2** by increasing in the $T_{1/2}$ value by up to ∼14 °C (Figure 2B and Table 1). The other two ligands exhibited a moderate increase in the melting temperatures ($\Delta T_{1/2}$ ∼ 9 °C for **InqEt1** and ∼11 °C for **InqEt2**) of *c-KIT1* G4 DNA (Figure 2B and Table 1). These results suggest that all three ligands stabilize the *c-MYC* and *c-KIT1* G4 DNAs.

To assess the stabilization property of these ligands with a particular G4 topology, we probed the effect of the ligand on the hybrid topology of telomeric G4 and the antiparallel topology of *h-RAS1* G4 DNAs. We performed melting studies with human telomeric and *h-RAS1* promoter G4 DNAs in the presence of K^+, which stabilize multiple G4 conformations in the former and antiparallel topology in the latter.[35,36] The melting experiments were performed with *h-RAS1* DNA by monitoring the wavelength at 290 nm to yield $T_{1/2}$ value of ∼53 °C (Figure S1, Supporting Information and Table 1).[35] Similarly, the $T_{1/2}$ value for telomeric DNA was found to be ∼54 °C (Figure S1, Supporting Information and Table 1).[34] Addition of any of the three ligands showed only a marginal change in the melting temperature (maximum $\Delta T_{1/2}$ ∼1 °C for telomeric DNA and maximum $\Delta T_{1/2}$ ∼3.4 °C for *h-RAS1* DNA) for both the G4 DNAs (Figure S1, Supporting Information and Table 1). After this, we measured CD melting with the duplex DNA by monitoring the CD ellipticity at 242 nm to explore the ligand selectivity toward quadruplex DNAs.[34,37] With 5 molar equivalents of ligands, we did not observe any stabilizing effect of these ligands on the duplex DNA (Figure S1, Supporting Information and Table 1).

Overall, CD melting experiments revealed that these ligands stabilize the *c-MYC* and *c-KIT1* parallel promoter over the antiparallel *h-RAS1*, hybrid telomeric G4 and duplex DNAs. Among the ligands studied, **InqPr2** was found to be the most promising one, and it was used for further evaluation.

CD Titration Studies. The CD spectrum of telomeric DNA in the presence of added metal ions consisted a small peak at 235 nm and a major peak at 290 nm along with a shoulder peak at 255 nm, which are the characteristic peaks of a (3 + 1) hybrid G4 structure[36] (Figure 3A). The addition of ligand **InqPr2** (0−5 equivalents) did not cause a

https://doi.org/10.1021/acs.biochem.2c00373
Biochemistry 2022, 61, 2546−2559

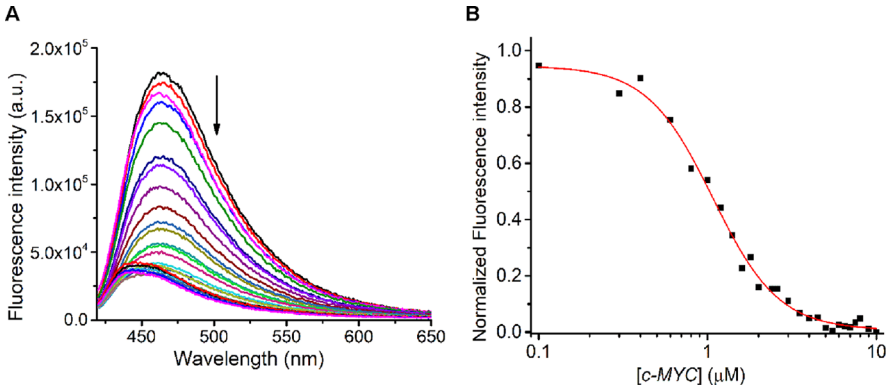

Figure 4. Emission spectra of **InqPr2** with (A) *c-MYC* G4 DNA (0–6 μM); (B) Plot of normalized fluorescence intensity of the ligand against the logarithm of an increasing concentration of *c-MYC* G4 DNA fitted into the Hill 1 equation. The titration was carried out in 100 mM KCl and 10 mM lithium cacodylate buffer at pH 7.2. (λ_{ex}—412 nm, λ_{em}—465 nm).

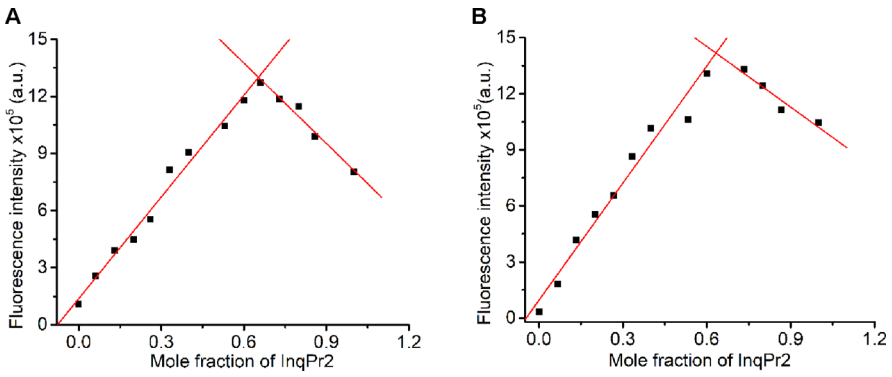

Figure 5. Job plot analysis of **InqPr2** with (A) *c-MYC* and (B) *c-KIT1* at an excitation wavelength of 412 nm and an emission wavelength of 465 nm. The overall molar concentration (ligand + DNA) was kept constant at 15 μM.

significant change in the peak ellipticity, which suggests that the prefolded topology of telomeric DNA remained the same (Figure 3A). *h-RAS1* DNA in the presence of added metal ions displayed a negative peak at 260 nm and a major positive peak at 290 nm, which are the characteristic peaks of an antiparallel G4 structure (Figure S2A Supporting Information).[35] Similarly, the CD ellipticities are almost unaffected in the presence of the **InqPr2** ligand, resulting in no changes in the topology of *h-RAS1* DNA. *c-MYC* and *c-KIT1* DNAs exhibited a major positive peak at 263 nm and a negative peak at 240 nm in the presence of added metal ions, which corresponds to parallel topology (Figure S2B Supporting Information and Figure 3B).[38] *c-MYC* and *c-KIT1* DNAs showed no major change in their ellipticities upon interacting with the ligand. Also, the addition of the ligand did not show any change in the position of the characteristic peak, indicating the parallel topology of the DNA is retained.

Fluorimetric Titration Experiments. Fluorimetric titration experiments were carried out to find the binding affinities of **InqPr2** with G4 and duplex DNAs. The ligand exhibited an emission peak at 465 nm upon excitation at 412 nm. The ligand fluorescence intensity gradually decreases upon the incremental addition of G4 and duplex DNAs. A blue shift of ~10 nm was observed on increasing the concentration of *c-MYC*, *c-KIT1*, and *h-RAS1* G4 DNAs (Figures 4A and S3, Supporting Information). The hypochromic and blue shift of ligand fluorescence suggests an effective interaction of **InqPr2** with the promoter G4 DNAs. The plot of normalized fluorescence intensity against the logarithm of the G4 concentration was fitted using the Hill 1 equation and the binding constants for *c-MYC*, *c-KIT1*, and *h-RAS1* G4 DNA were found to be K_a = 0.90 ± 0.03 × 10^6 M^{-1}, 1.28 ± 0.04 × 10^6 M^{-1}, and 0.35 ± 0.07 × 10^6 M^{-1}, respectively (Figures 4B and S3 Supporting Information). The binding constant values obtained for the parallel promoter G4 DNAs are in the range of favorable ligand–G4 binding interactions reported in the literature.[4,39] In contrast, negligible changes in the fluorescence intensity were observed with telomeric and duplex DNAs, which prevented us from calculating the binding constants. These results indicate the weak interaction of the ligand with telomeric and duplex DNAs (Figure S3, Supporting Information). Overall, fluorimetric titration studies likely indicate the favorable binding of **InqPr2** to *c-MYC* and *c-KIT1* G4s over other topologies.

Further, fluorescence property of **InqPr2** was used to probe the binding stoichiometry of the ligand and the DNAs, using Job plot analysis. The plot of fluorescence intensity versus the mole fraction (Figure 5) indicated a binding stoichiometry of 2:1 for the ligand-DNA interaction.

Taq DNA Polymerase Stop Assay. The preferential stabilizing effect of the lead ligand **InqPr2** toward parallel G4 DNA was further verified with the *Taq* DNA polymerase stop assay.[40] In the absence of added **InqPr2**, stop products were not observed in any reaction mixture containing telomeric, *c-MYC*, and muted *c-MYC* DNAs (Figures 6A and S4, Supporting Information) due to unstable G4 structures.

https://doi.org/10.1021/acs.biochem.2c00373
Biochemistry 2022, 61, 2546–2559

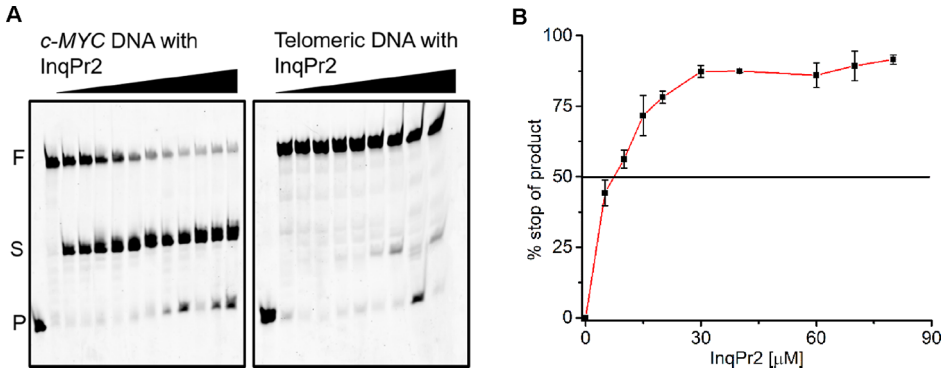

Figure 6. (A) 15% denaturing PAGE (7 M urea) of *Taq* DNA polymerase stop assay of the *c-MYC* DNA with an increasing concentration of **InqPr2** (0−80 μM) and Telomeric DNA with **InqPr2** (0−180 μM); (B) plot of the percentage of the stop product against the increasing concentration of **InqPr2**. Conditions: 0.2 μM primer, 0.1 μM template DNA, 0.2 mM dNTPs, and 1U *Taq* DNA polymerase enzyme in buffer (50 mM Tris−HCl, pH 7.2, 0.5 mM DTT, 0.1 mM EDTA, 5 mM $MgCl_2$, and 5 mM KCl). F, S, and P denote full length, stop product, and primer, respectively.

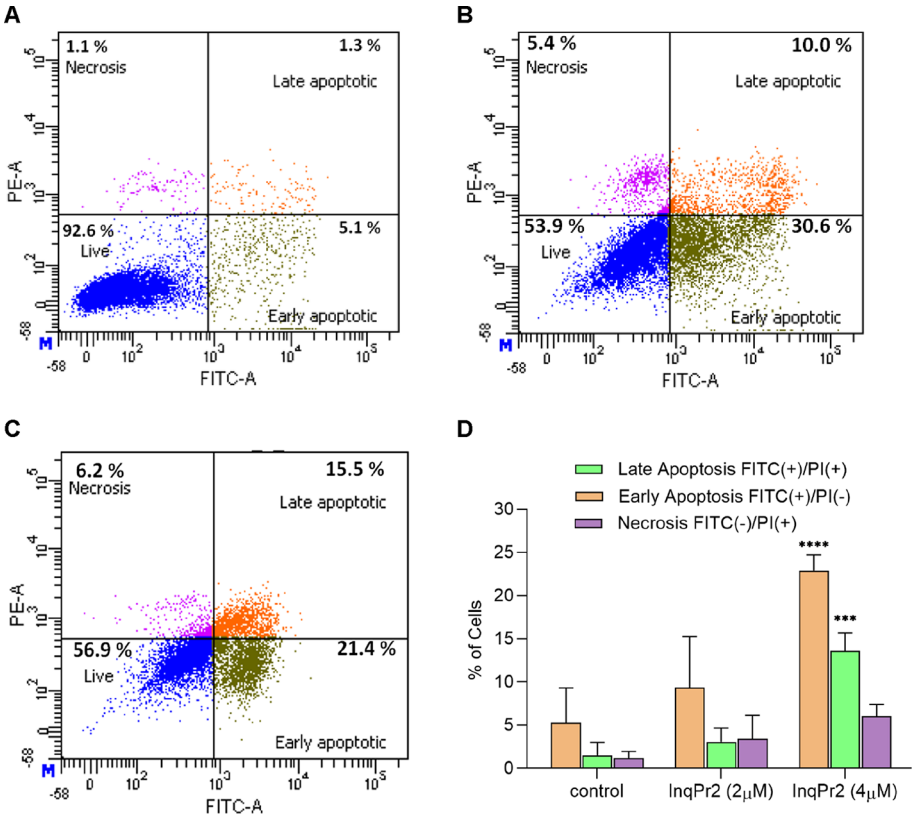

Figure 7. Apoptosis induction of HeLa cells (A) untreated, (B) on treatment with 2.0 μM, and (C) on treatment with 4.0 μM **InqPr2** for 24 h. (D) Cell percentages in early apoptosis, late apoptosis, and necrosis are shown in the bar graph as mean value ± SD. Apoptotic cells were stained with Annexin V/PI and analyzed by flow cytometry. The data are representative of three independent experiments. Asterisk *** and **** represent $p < 0.001$ and 0.0001, respectively. The results were considered significant as compared to untreated HeLa cells.

From the CD melting experiment, it is already proven that the **InqPr2** ligand can stabilize parallel G4 DNA; therefore, in the presence of the **InqPr2** ligand, stop products were detected with *c-MYC* DNA only. The plot of the percentage stop product against ligand concentration yielded ∼ 6.8 μM IC_{50} value (Figure 6B). Stop products were not observed even after adding up to 180 μM ligand concentration with telomeric or muted *c-MYC* DNA since **InqPr2** failed to stabilize other topologies of the G4 structure (Figure 6A and S4, Supporting Information). Therefore, apart from CD melting studies, polymerase stop assays suggested the stabilizing effects of the **InqPr2** ligand toward parallel G4 DNA.

Cytotoxicity and Apoptosis Studies. To investigate the antiproliferative activities of the most promising **InqPr2** ligand, we performed the luminometric cell viability assay using human cervical cancer (HeLa) and liver hepatocellular cancer (HepG2) cell lines.[41] After 24 h of treatment, **InqPr2** inhibited the cell proliferation in HeLa cell lines with an IC_{50} value of 2.2 ± 0.3 μM (Figure S5A, Supporting Information). Similarly, the ligand was able to impede the growth of the HepG2 cell having an IC_{50} value 2.6 ± 0.5 μM. We also

https://doi.org/10.1021/acs.biochem.2c00373
Biochemistry 2022, 61, 2546−2559

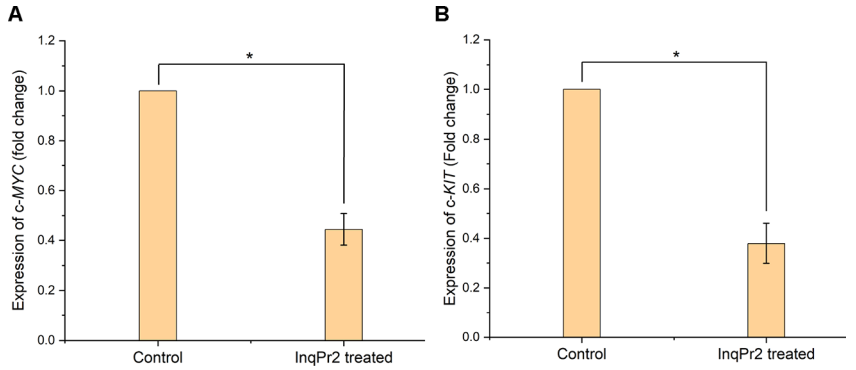

Figure 8. Effects of **InqPr2** (2 μM) on the expression of (A) *c-MYC* in HeLa and (B) c-*KIT* gene in HepG2 cell lines from qRT-PCR after 24 h of treatment. The fold change is calculated using the $2^{(-\Delta\Delta Ct)}$ method. Error bars represent the standard deviations derived from three independent experiments. * represents $p < 0.05$, which was considered a significant difference as compared to untreated cells (control).

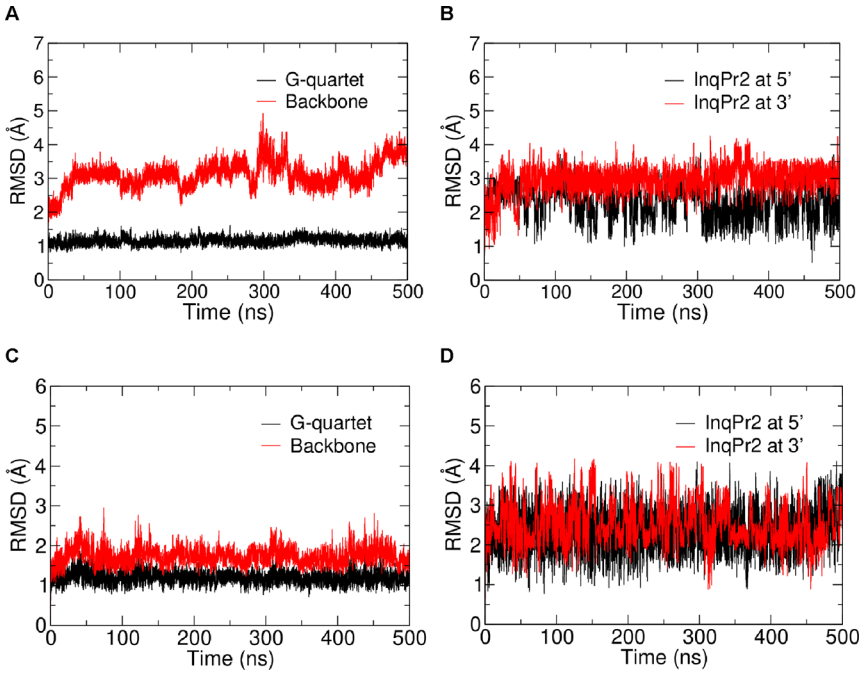

Figure 9. RMSD graphs of (A) G-quartets and backbone of *c-MYC*; (B) ligand in *c-MYC* G4; (C) G-quartets and backbone of *c-KIT1*; and (D) ligand in *c-KIT1* during the 500 ns simulation are plotted against time. The G-quartet core comprises the top, middle, and bottom G-quartets. The RMSD values are measured in Å.

checked the cytotoxicity of the ligand **InqPr2** in non-cancerous Lenti-X (human embryonic kidney). After 24 h of treatment with **InqPr2**, there was negligible death of Lenti-X cells, suggesting selective inhibition of the growth of cancer cell lines (Figure S5B, Supporting Information).

To evaluate the mechanism of **InqPr2**-induced cell death, a flow cytometry analysis was carried out using Annexin-V and PI dual staining assay (Figure 7). When HeLa cells were incubated with **InqPr2** (IC_{50} = 2.0 μM and 2 x IC_{50} = 4.0 μM) over a period of 24 h, the number of live cells decreased with an increase in apoptotic cells. The fraction of late apoptotic cells further increased when the ligand concentration was increased to 4.0 μM (Figure 7C). However, cell death *via* necrosis was insignificant, suggesting that apoptosis is the primary mechanism responsible for cell death induced by **InqPr2** (Figure 7D).

qRT-PCR Based Gene Expression Studies. qRT-PCR was used to evaluate the effects on gene expression upon ligand treatment.[42] As the ligand **InqPr2** stabilizes the promoter G4 DNA, we have investigated its influence on the *c-MYC* transcription in HeLa cells and c-*KIT* transcription in HepG2 cells by using qRT-PCR. The experiment was done utilizing a previously established procedure with slight modifications.[13,43] The cells were treated with 2 μM **InqPr2** for 24 h, and the expression of mRNA was quantified by the comparative threshold method by using β-actin as the housekeeping gene. The expressions of the target gene were normalized against constitutively expressed β-actin. Relative *c-MYC* and *c-KIT* expression levels in the treated HeLa and HepG2 cells were reduced by ~2-fold compared to untreated cells (Figure 8). These results indicate that **InqPr2** downregulates *c-MYC* and c-*KIT* gene transcription.

Molecular Modeling and Dynamics Studies. To examine the mode of binding and stability of the **InqPr2**-G4 complexes, molecular dynamics (MD) studies were carried out using *c-MYC* (PDB ID: 1XAV)[44] and *c-KIT1* (PDB ID: 2O3M)[45] G4 structures. The ligand was optimized (Figure S6, Supporting Information) in Gaussian 16[46] and

https://doi.org/10.1021/acs.biochem.2c00373
Biochemistry 2022, 61, 2546−2559

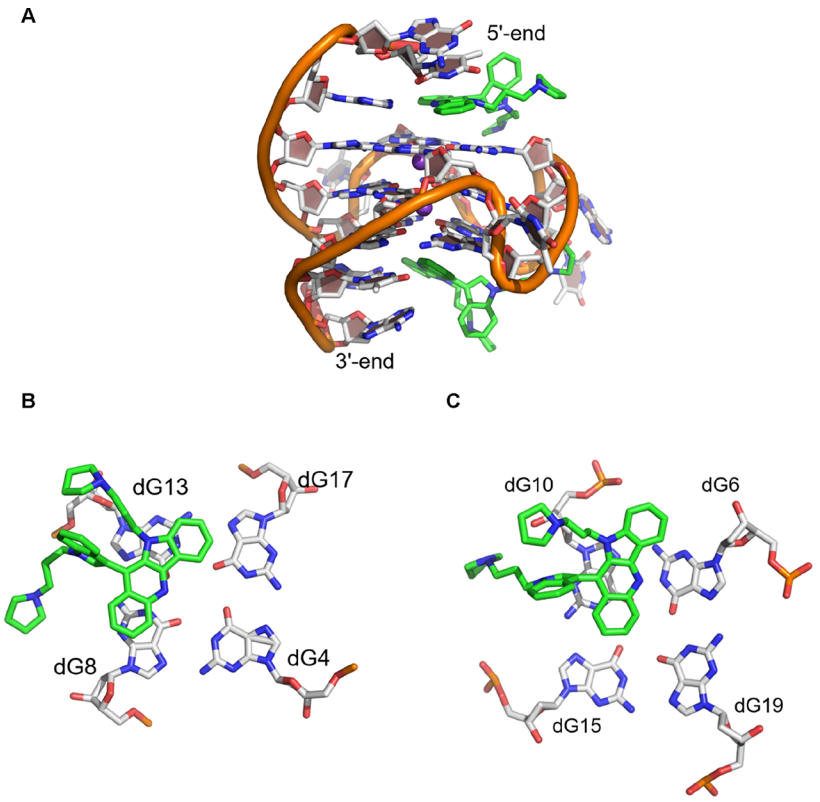

Figure 10. Representative structure of the major cluster from the 500 ns MD simulation. (A) **InqPr2** bound to 5′-end and 3′-end face of *c-MYC* DNA (side view); (B) axial view of the stacked ligand at the 5′-quartet of *c-MYC* G4 DNA; and (C) axial view of the stacked ligand at the 3′-quartet of *c-MYC* G4 DNA. The nitrogen atoms are represented in blue color, the phosphorous atoms are represented in orange, the oxygen atoms are represented in red, the carbon atoms of DNA are represented in white, and the carbon atoms of the ligand are represented in green. The backbone atoms of the DNA are represented in a cartoon form, and the ligand atoms in a stick form.

was then subjected to docking in AutoDock 4.2.6.[47] The 500 independent docked conformers were evaluated to find the various modes of binding of **InqPr2**. From the docked conformers, stacking over the G-quartets was found to be a probable binding mode. Therefore, the ligand poses, exhibiting the stacking mode at the 5′- and the 3′-ends with both *c-MYC* and *c-KIT1* G4s (Figure S7, Supporting Information), were chosen for molecular dynamics studies. This also agrees with the 2:1 binding stoichiometry revealed in the experimental studies. Structures showing stacking modes were subjected to ESP charge calculation, followed by RESP[48] charge fitting. Further, with the complexes generated, an unrestrained production run for 500 ns was carried out in the GPU-accelerated version of PMEMD[49−51] in AMBER 18.[52]

The conformational stability of the complexes was investigated by calculating the RMSD of the ligand, the backbone of the DNA, and the G quartets using the first frame of the simulation as a reference. Negligible variation was observed in the RMSD values of the G-quartet throughout the simulation in *c-MYC* and *c-KIT1* complexes (Figure 9). The movement of the loop and flanking nucleotides account for the slight changes in the DNA backbone RMSD in the *c-MYC* G4 complex. The RMSF values of the quartet-forming dG varied the least in both *c-MYC* and *c-KIT1* G4s, while the flanking nucleotides and the nucleotides in the loop region showed higher fluctuations (Figure S8, Supporting Information). These indicate the flexibility of the flanking and loop nucleotides upon ligand binding. Visualization of trajectories showed that the G4 flanking nucleotides rearranged to accommodate the ligand, specifically in *c-MYC* G4.

The trajectories of the 500 ns simulations were clustered into five ensembles. The major representative structures of *c-MYC* and *c-KIT1* G4 complexes revealed that stacking at the 5′- and the 3′-end are the primary binding modes. One major cluster existed for ∼60% of the simulation time for *c-MYC* (Figure 10), and ∼55% simulation time for *c-KIT1* G4 (Figure 11). While the quindolinium ring was stacked over the quartets, the indole ring was oriented perpendicular to the G-quartets. The flanking nucleotide dT5 stacked over the ligand binding at the 5′-quartet of the *c-MYC* G4 DNA (Figure 10). The nucleotide dA18 stacked over the ligand binding at the 3′-quartet of the *c-KIT1* G4 DNA. Visual inspection of the trajectories indicated that the ligand binding at the 5′-end showed slight reorientation over the G-quartets in the case of both *c-MYC* and *c-KIT1* G4 DNAs, while the ligands at the 3′-end showed negligible reorientation.

To probe noncovalent interactions between the ligand and nucleotides, the distances between the protonated nitrogen of the ligand and the negatively charged backbone of the G4 were calculated. Apart from stacking, multiple electrostatic interactions (Figures S9, S10, and Table S7, Supporting Information) also stabilize **InqPr2**-G4 structures. The primary electrostatic interaction persisting in the *c-MYC* G4 is N4 of the ligand bound at the 3′-quartet with the OP2 of the dT11 (Figure S9, Supporting Information). The N4 of the ligand bound at the 5′-quartet interacted with the OP1 of

https://doi.org/10.1021/acs.biochem.2c00373
Biochemistry 2022, 61, 2546−2559

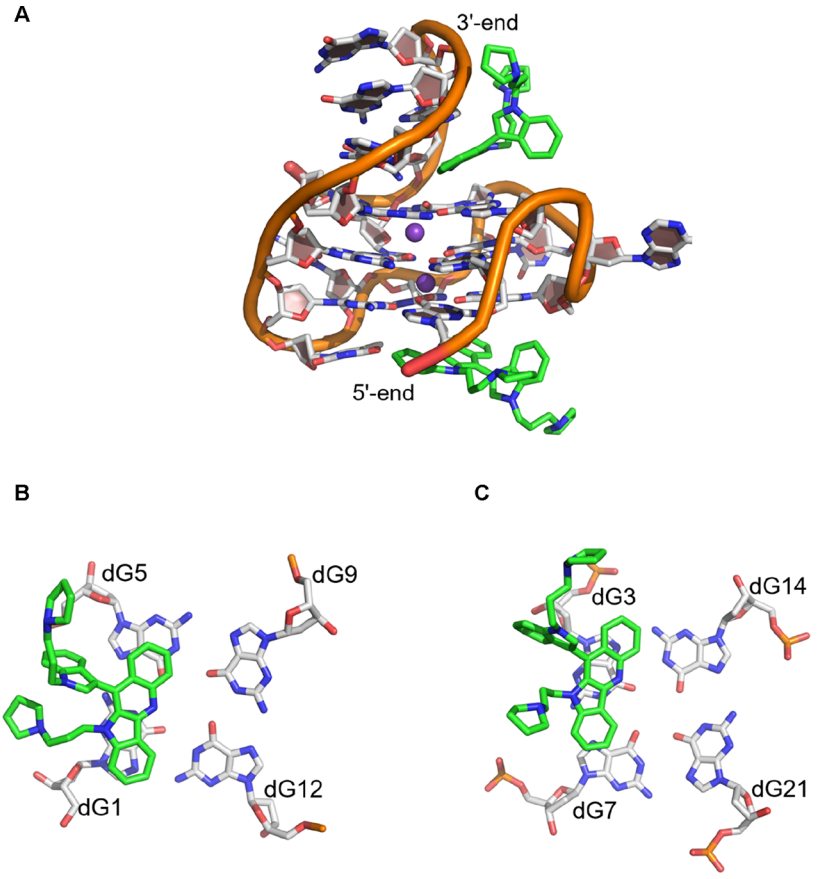

Figure 11. Representative structure of the major cluster from the 500 ns MD simulation. (A) **InqPr2** bound to 5′-end and 3′-end face of *c-KIT1* DNA (side view); (B) axial view of the stacked ligand at the 5′-quartet of *c-KIT1* G4 DNA; and (C) axial view of the stacked ligand at the 3′-quartet of *c-KIT1* G4 DNA. The nitrogen atoms are represented in blue color, the phosphorous atoms are represented in orange, the oxygen atoms are represented in red, the carbon atoms of DNA are represented in white, and the carbon atoms of the ligand are represented in green. The backbone atoms of the DNA are represented in a cartoon form, and the ligand atoms in a stick form.

dG13 in *c-MYC* G4 DNA (Figure S9, Supporting Information). In the case of *c-KIT1* G4, the most persistent electrostatic interactions are between N4 and N5 of the ligand bound at the 3′-quartet with OP1 of dG16 and dG17, respectively (Figure S10, Supporting Information).

The binding free energies of the **InqPr2**-bound G4s were estimated using the MM-PBSA[53] module of AMBER 18. Energy parameters (Tables S8 and S9, Supporting Information) showed that the entropy values are comparable in the case of *c-MYC* and *c-KIT1* complexes, while the enthalpy values are different (*c-KIT1* > *c-MYC*). This indicates that the enthalpy gain in the complex dictates the stabilization. In both cases, the binding to 3′-quartet is energetically more favorable.

To discern the selective binding of ligands to parallel G4s, we have also performed modeling studies with hybrid and antiparallel topologies. The ligand **InqPr2** was docked onto the telomeric hybrid-2 (PDB ID: 2JPZ)[54] and the antiparallel G4 (PDB ID: 143D)[55] DNAs. None of 500 independent docked conformers generated for each system could dock well to the G4 structures. In both cases, only partial access to the groove was observed for the ligand. Conformers with partial access to the groove were chosen as the starting structures for 500 ns MD simulations. No proper stacking or groove binding were observed in both the complexes during MD simulations (Figures S11 and S12, Supporting Information). The ligand did not fall off entirely or move away from the antiparallel G4 complex. In the hybrid G4, the ligand completely lost access to the groove in the first 100 ns and changed drastically from the docked structure. The indole ring is perpendicular to the quindolinium ring of the ligand, which prevents stacking or groove binding. This structural feature of **InqPr2** is likely responsible for the improved binding of the ligand toward parallel promoter G4 structures.

In conclusion, MD studies support 2:1 (**InqPr2**-G4) binding, and the stacking and electrostatic interactions account for the stability induced by **InqPr2** to the parallel G4s of *c-MYC* and *c-KIT1* DNAs. The ligand's structural features, particularly the indole ring's relative position to the quindolinium ring, result in enhanced binding toward the parallel G4 topology compared to the antiparallel and hybrid topologies.

CONCLUSIONS

In summary, we have synthesized three indole-fused quindoline derivatives as G4 stabilizers. Biophysical studies showed that ligands exhibit favorable stabilization of the parallel topology of the promoter G4 DNAs (*c-MYC* and *c-KIT1*) over the antiparallel promoter, hybrid topology of telomeric G4s and duplex DNAs. Of the three molecules, the one containing two propyl side chains, **InqPr2** was the most promising. **InqPr2** induces apoptotic cell death with the effective downregulation of *c-MYC* and *c-KIT* gene expression

https://doi.org/10.1021/acs.biochem.2c00373
Biochemistry 2022, 61, 2546−2559

in cells. Modeling studies revealed that along with stacking to quartets, the electrostatic interactions of the protonated side chains play a role in stabilizing G4 structures. The relative position of the indole ring with respect to the quindolinium ring is one of the critical structural features, which impart selectivity to the ligand toward parallel G4 DNAs. Our study demonstrates that with further fine tuning, these small molecule scaffolds could be promising candidates for anticancer drug development, harnessing G4 targets.

■ ASSOCIATED CONTENT

Supporting Information

The Supporting Information is available free of charge at https://pubs.acs.org/doi/10.1021/acs.biochem.2c00373.

General experiment details, synthetic procedures, details of mechanism, crystallographic data, CD melting and titration curves, fluorimetric titration curves, *Taq* polymerase stop assay results, cell viability assay curves, additional figures, plots and tables from molecular modeling and dynamics studies, sequences of DNAs used, and copies of ^{1}H NMR. ^{13}C NMR and HRMS spectra (PDF)

■ AUTHOR INFORMATION

Corresponding Author

P. I. Pradeepkumar − *Department of Chemistry, Indian Institute of Technology Bombay, Mumbai 400076, India;* orcid.org/0000-0001-9104-3708; Email: pradeep@chem.iitb.ac.in

Authors

Satendra Kumar − *Department of Chemistry, Indian Institute of Technology Bombay, Mumbai 400076, India*

Sushree Prangya Priyadarshinee Pany − *Department of Chemistry, Indian Institute of Technology Bombay, Mumbai 400076, India*

Sruthi Sudhakar − *Department of Chemistry, Indian Institute of Technology Bombay, Mumbai 400076, India*

Sushma B. Singh − *Department of Chemistry, Indian Institute of Technology Bombay, Mumbai 400076, India;* orcid.org/0000-0002-2615-7247

Chaitra S. Todankar − *Department of Chemistry, Indian Institute of Technology Bombay, Mumbai 400076, India*

Complete contact information is available at: https://pubs.acs.org/10.1021/acs.biochem.2c00373

Author Contributions

†S.K. and S.P.P.P. authors contributed equally.

Notes

The authors declare no competing financial interest.

■ ACKNOWLEDGMENTS

This work is supported by grants from the Science and Engineering Research Board (SERB), Government of India, to P.I.P. We are thankful to IIT Bombay for providing the FACS facility and grateful to IITB-Spacetime-HPC resources. We acknowledge the DST-FIST (grant no. SR/FST/CS-II/2017/37) for NMR and HRMS facilities. We also thank Prof. Ruchi Anand for providing access to her laboratory facilities. We thank Prof. Santosh G Gharpure for discussions on the reaction mechanism, Dr. S. Harikrishna for the guidance in the MD studies, Dr. Dipanjan Mondal for his assistance in the single crystal X-ray crystallographic analysis, and Dr. Saurja Dasgupta for the critical reading of the manuscript. S.P.P. thanks the Council of Scientific and Industrial Research (CSIR), S.K. thanks the University Grant Commission (UGC), and S.S. thanks the Prime Minister Research Fellowship (PMRF) for Ph.D. fellowships. C.S.T. thanks SERB and IRCC-IIT Bombay for the fellowships, and S.B.S. thanks IIT Bombay for the Institute Post-Doctoral Fellowship.

■ REFERENCES

(1) Burge, S.; Parkinson, G. N.; Hazel, P.; Todd, A. K.; Neidle, S. Quadruplex DNA: Sequence, Topology and Structure. *Nucleic Acids Res.* **2006**, *34*, 5402−5415.

(2) Ma, Y.; Iida, K.; Nagasawa, K. Topologies of G-Quadruplex: Biological Functions and Regulation by Ligands. *Biochem. Biophys. Res. Commun.* **2020**, *531*, 3−17.

(3) Dhamodharan, V.; Pradeepkumar, P. I. Specific Recognition of Promoter G-Quadruplex DNAs by Small Molecule Ligands and Light-up Probes. *ACS Chem. Biol.* **2019**, *14*, 2102−2114.

(4) Dhamodharan, V.; Pradeepkumar, P. I. Specific Recognition of Promoter G-Quadruplex DNAs by Small Molecule Ligands and Light-up Probes. *ACS Chem. Biol.* **2019**, *14*, 2102−2114.

(5) Mathad, R. I.; Hatzakis, E.; Dai, J.; Yang, D. c-MYC promoter G-quadruplex formed at the 5′-end of NHE III 1 element: insights into biological relevance and parallel-stranded G-quadruplex stability. *Nucleic Acids Res.* **2011**, *39*, 9023−9033.

(6) Chaudhuri, R.; Bhattacharya, S.; Dash, J.; Bhattacharya, S. Recent Update on Targeting C-MYC G-Quadruplexes by Small Molecules for Anticancer Therapeutics. *J. Med. Chem.* **2021**, *64*, 42−70.

(7) Hu, M.-H.; Wang, Y.-Q.; Yu, Z.-Y.; Hu, L.-N.; Ou, T.-M.; Chen, S.-B.; Huang, Z.-S.; Tan, J.-H. Discovery of a New Four-Leaf Clover-Like Ligand as a Potent c-MYC Transcription Inhibitor Specifically Targeting the Promoter G-Quadruplex. *J. Med. Chem.* **2018**, *61*, 2447−2459.

(8) Kumar, S.; Reddy Sannapureddi, R. K.; Todankar, C. S.; Ramanathan, R.; Biswas, A.; Sathyamoorthy, B.; Pradeepkumar, P. I. Bisindolylmaleimide Ligands Stabilize C-MYC G-Quadruplex DNA Structure and Downregulate Gene Expression. *Biochemistry* **2022**, *61*, 1064−1076.

(9) Dolomanov, O. V.; Bourhis, L. J.; Gildea, R. J.; Howard, J. A. K.; Puschmann, H. OLEX2: a complete structure solution, refinement and analysis program. *J. Appl. Crystallogr.* **2009**, *42*, 339−341.

(10) Sheldrick, G. M. A. A short history ofSHELX. *Acta Crystallogr., Sect. A: Found. Crystallogr.* **2008**, *64*, 112−122.

(11) Sheldrick, G. M. Crystal structure refinement withSHELXL. *Acta Crystallogr., Sect. C: Struct. Chem.* **2015**, *71*, 3−8.

(12) Carvalho, J.; Paiva, A.; Cabral Campello, M. P.; Paulo, A.; Mergny, J.-L.; Salgado, G. F.; Queiroz, J. A.; Cruz, C. Aptamer-Based Targeted Delivery of a G-Quadruplex Ligand in Cervical Cancer Cells. *Sci. Rep.* **2019**, *9*, 7945.

(13) Bookout, A. L.; Cummins, C. L.; Mangelsdorf, D. J.; Pesola, J. M.; Kramer, M. F. High-Throughput Real-Time Quantitative Reverse Transcription PCR. *Curr. Protoc. Mol. Biol.* **2006**, *73*, 1−28.

(14) Haider, S.; Neidle, S. Molecular modeling and simulation of G-quadruplexes and quadruplex-ligand complexes. *Methods Mol. Biol.* **2010**, *608*, 17−37.

(15) Wang, J.; Wang, W.; Kollman, P. A.; Case, D. A. Automatic Atom Type and Bond Type Perception in Molecular Mechanical Calculations. *J. Mol. Graph. Model.* **2006**, *25*, 247−260.

(16) Wang, J.; Wolf, R. M.; Caldwell, J. W.; Kollman, P. A.; Case, D. A. Development and Testing of a General Amber Force Field. *J. Comput. Chem.* **2004**, *25*, 1157−1174.

(17) Galindo-Murillo, R.; Robertson, J. C.; Zgarbová, M.; Šponer, J.; Otyepka, M.; Jurečka, P.; Cheatham, T. E. Assessing the Current

State of Amber Force Field Modifications for DNA. *J. Chem. Theory Comput.* **2016**, *12*, 4114−4127.
(18) Turq, P.; Lantelme, F.; Friedman, H. L. Brownian Dynamics: Its Application to Ionic Solutions. *J. Chem. Phys.* **1977**, *66*, 3039−3044.
(19) Berendsen, H. J. C.; Postma, J. P. M.; van Gunsteren, W. F.; DiNola, A.; Haak, J. R. Molecular Dynamics with Coupling to an External Bath. *J. Chem. Phys.* **1984**, *81*, 3684−3690.
(20) Roe, D. R.; Cheatham, T. E. PTRAJ and CPPTRAJ: Software for Processing and Analysis of Molecular Dynamics Trajectory Data. *J. Chem. Theory Comput.* **2013**, *9*, 3084−3095.
(21) Pettersen, E. F.; Goddard, T. D.; Huang, C. C.; Couch, G. S.; Greenblatt, D. M.; Meng, E. C.; Ferrin, T. E. UCSF Chimera?A visualization system for exploratory research and analysis. *J. Comput. Chem.* **2004**, *25*, 1605−1612.
(22) Gellért, E.; Raymond-Hamet; Schlittler, E. Die Konstitution Des Alkaloids Cryptolepin. *Helv. Chim. Acta* **1951**, *34*, 642−651.
(23) Tugusheva, N. Z.; Ryabova, S. Y.; Solov'eva, N. P.; Granik, V. G. Investigations of Indolo[3,2-b]Quinolines. *Chem. Heterocycl. Compd.* **1998**, *34*, 216−221.
(24) Suresh Kumar, E. V. K.; Etukala, J. R.; Ablordeppey, S. Y. Indolo[3,2-b]quinolines: Synthesis, Biological Evaluation and Structure Activity-Relationships. *Mini Rev. Med. Chem.* **2008**, *8*, 538−554.
(25) Dai, J.; Carver, M.; Hurley, L. H.; Yang, D. Solution Structure of a 2:1 Quindoline-c-MYC G-Quadruplex: Insights into G-Quadruplex-Interactive Small Molecule Drug Design. *J. Am. Chem. Soc.* **2011**, *133*, 17673−17680.
(26) Ou, T.-M.; Lu, Y.-J.; Zhang, C.; Huang, Z.-S.; Wang, X.-D.; Tan, J.-H.; Chen, Y.; Ma, D.-L.; Wong, K.-Y.; Tang, J. C.-O.; Chan, A. S.-C.; Gu, L.-Q. Stabilization of G-Quadruplex DNA and down-Regulation of Oncogene c-Myc by Quindoline Derivatives. *J. Med. Chem.* **2007**, *50*, 1465−1474.
(27) Mendes, I. M.; Bahls, A.; Aljnadi, E.; Paulo, A. Indoloquinolines as scaffolds for the design of potent G-quadruplex ligands. *Bioorg. Med. Chem. Lett.* **2022**, *72*, 128862.
(28) Lavrado, J.; Borralho, P. M.; Ohnmacht, S. A.; Castro, R. E.; Rodrigues, C. M. P.; Moreira, R.; Santos, D. J. V. A.; Neidle, S.; Paulo, A. Synthesis, G-Quadruplex Stabilisation, Docking Studies, and Effect on Cancer Cells of Indolo[3,2-b]Quinolines with One, Two, or Three Basic Side Chains. *ChemMedChem* **2013**, *8*, a−n.
(29) Funke, A.; Dickerhoff, J.; Weisz, K. Towards the Development of Structure-Selective G-Quadruplex-Binding Indolo[3,2-b]-quinolines. *Chem.—Eur. J.* **2016**, *22*, 3170−3181.
(30) Vianney, Y. M.; Weisz, K.Indoloquinoline Ligands Favor Intercalation at Quadruplex-Duplex Interfaces. *Chem.—Eur. J.*. **2022**, *28*(). DOI: 10.1002/chem.202103718.
(31) Diveshkumar, K. V.; Sakrikar, S.; Rosu, F.; Harikrishna, S.; Gabelica, V.; Pradeepkumar, P. I. Specific Stabilization of C-MYC and c-KIT G-Quadruplex DNA Structures by Indolylmethyleneindanone Scaffolds. *Biochemistry* **2016**, *55*, 3571−3585.
(32) Sharma, S.; Kundu, B. Unprecedented SnCl2·2H2O-mediated intramolecular cyclization of nitroarenes via C-N bond formation: a new entry to the synthesis of cryptotackieine and related skeletons. *Tetrahedron Lett.* **2008**, *49*, 7062−7065.
(33) Guédin, A.; Lacroix, L.; Mergny, J.-L.Thermal Melting Studies of Ligand DNA Interactions. In *Drug-DNA interaction protocols*; Springer, 2010, pp 25−35. DOI: 10.1007/978-1-60327-418-0_2
(34) Dhamodharan, V.; Harikrishna, S.; Jagadeeswaran, C.; Halder, K.; Pradeepkumar, P. I. Selective G-Quadruplex DNA Stabilizing Agents Based on Bisquinolinium and Bispyridinium Derivatives of 1,8-Naphthyridine. *J. Org. Chem.* **2012**, *77*, 229−242.
(35) Membrino, A.; Cogoi, S.; Pedersen, E. B.; Xodo, L. E. G4-DNA Formation in the HRAS Promoter and Rational Design of Decoy Oligonucleotides for Cancer Therapy. *PLoS One* **2011**, *6*, No. e24421.
(36) Ambrus, A.; Chen, D.; Dai, J.; Bialis, T.; Jones, R. A.; Yang, D. Human Telomeric Sequence Forms a Hybrid-Type Intramolecular G-Quadruplex Structure with Mixed Parallel/Antiparallel Strands in Potassium Solution. *Nucleic Acids Res.* **2006**, *34*, 2723−2735.
(37) Usatyi, A. F.; Shlyakhtenko, L. S. Temperature Dependence of CD Spectra of DNA from Various Sources. *Biopolymers* **1973**, *12*, 45−51.
(38) Dash, J.; Shirude, P. S.; Hsu, S.-T. D.; Balasubramanian, S. Diarylethynyl Amides That Recognize the Parallel Conformation of Genomic Promoter DNA G-Quadruplexes. *J. Am. Chem. Soc.* **2008**, *130*, 15950−15956.
(39) Luedtke, N. Targeting G-Quadruplex DNA with Small Molecules. *Chim. Int. J. Chem.* **2009**, *63*, 134−139.
(40) kong, J.-N.; Zhang, C.; Zhu, Y.-C.; Zhong, K.; Wang, J.; Chu, B.-B.; Yang, G.-Y. Identification and Characterization of G-Quadruplex Formation within the EP0 Promoter of Pseudorabies Virus. *Sci. Rep.* **2018**, *8*, 14029.
(41) Riss, T.; Moravec, R.; Niles, A. Selecting Cell-Based Assays for Drug Discovery Screening. *Cell Notes* **2005**, *13*, 16−21.
(42) Bustin, S. A.; Mueller, R. Real-Time Reverse Transcription PCR (QRT-PCR) and Its Potential Use in Clinical Diagnosis. *Clin. Sci.* **2005**, *109*, 365−379.
(43) Kramer, M. F.; Coen, D. M. Enzymatic Amplification of DNA by PCR: Standard Procedures and Optimization. *Curr. Protoc. Mol. Biol.* **2001**, *56*, 15.1.1−15.1.14 Chapter 15.
(44) Ambrus, A.; Chen, D.; Dai, J.; Jones, R. A.; Yang, D. Solution Structure of the Biologically Relevant G-Quadruplex Element in the Human c-MYC Promoter. Implications for G-Quadruplex Stabilization. *Biochemistry* **2005**, *44*, 2048−2058.
(45) Phan, A. T.; Kuryavyi, V.; Burge, S.; Neidle, S.; Patel, D. J. Structure of an Unprecedented G-Quadruplex Scaffold in the Human c-Kit Promoter. *J. Am. Chem. Soc.* **2007**, *129*, 4386−4392.
(46) Frisch, M. J.; Trucks, G. W.; Schlegel, H. B.; Scuseria, G. E.; Robb, M. a.; Cheeseman, J. R.; Scalmani, G.; Barone, V.; Petersson, G. a.; Nakatsuji, H.; Li, X.; Caricato, M.; Marenich, a. V.; Bloino, J.; Janesko, B. G.; Gomperts, R.; Mennucci, B.; Hratchian, H. P.; Ortiz, J. V.; Izmaylov, a. F.; Sonnenberg, J. L.; Williams; Ding, F.; Lipparini, F.; Egidi, F.; Goings, J.; Peng, B.; Petrone, A.; Henderson, T.; Ranasinghe, D.; Zakrzewski, V. G.; Gao, J.; Rega, N.; Zheng, G.; Liang, W.; Hada, M.; Ehara, M.; Toyota, K.; Fukuda, R.; Hasegawa, J.; Ishida, M.; Nakajima, T.; Honda, Y.; Kitao, O.; Nakai, H.; Vreven, T.; Throssell, K.; Montgomery, J. a., Jr.; Peralta, J. E.; Ogliaro, F.; Bearpark, M. J.; Heyd, J. J.; Brothers, E. N.; Kudin, K. N.; Staroverov, V. N.; Keith, T. a.; Kobayashi, R.; Normand, J.; Raghavachari, K.; Rendell, a. P.; Burant, J. C.; Iyengar, S. S.; Tomasi, J.; Cossi, M.; Millam, J. M.; Klene, M.; Adamo, C.; Cammi, R.; Ochterski, J. W.; Martin, R. L.; Morokuma, K.; Farkas, O.; Foresman, J. B.; Fox, D. J. G16_C01. 2016, p *Gaussian 16*, Revision C.01, Gaussian, Inc., Wallin.
(47) Morris, G. M.; Huey, R.; Lindstrom, W.; Sanner, M. F.; Belew, R. K.; Goodsell, D. S.; Olson, A. J. AutoDock4 and AutoDockTools4: Automated docking with selective receptor flexibility. *J. Comput. Chem.* **2009**, *30*, 2785−2791.
(48) Fox, T.; Kollman, P. A. Application of the RESP Methodology in the Parametrization of Organic Solvents. *J. Phys. Chem. B* **1998**, *102*, 8070−8079.
(49) Salomon-Ferrer, R.; Götz, A. W.; Poole, D.; Le Grand, S.; Walker, R. C. Routine Microsecond Molecular Dynamics Simulations with AMBER on GPUs. 2. Explicit Solvent Particle Mesh Ewald. *J. Chem. Theory Comput.* **2013**, *9*, 3878−3888.
(50) Götz, A. W.; Williamson, M. J.; Xu, D.; Poole, D.; Le Grand, S.; Walker, R. C. Routine Microsecond Molecular Dynamics Simulations with AMBER on GPUs. 1. Generalized Born. *J. Chem. Theory Comput.* **2012**, *8*, 1542−1555.
(51) Le Grand, S.; Götz, A. W.; Walker, R. C. SPFP: Speed without compromise-A mixed precision model for GPU accelerated molecular dynamics simulations. *Comput. Phys. Commun.* **2013**, *184*, 374−380.
(52) Case, D. A.; Ben-Shalom, I. Y.; Brozell, S. R.; Cerutti, D. S.; Cheatham, T. E., III; Cruzeiro, V. W. D.; Darden, T. A.; Duke, R.

E.; Ghoreishi, D.; Gilson, M. K.*AMBER 2018*; Univ. California: San Fr, 2018; Vol. *2018*.
(53) Kollman, P. A.; Massova, I.; Reyes, C.; Kuhn, B.; Huo, S.; Chong, L.; Lee, M.; Lee, T.; Duan, Y.; Wang, W.; Donini, O.; Cieplak, P.; Srinivasan, J.; Case, D. A.; Cheatham, T. E. Calculating Structures and Free Energies of Complex Molecules: Combining Molecular Mechanics and Continuum Models. *Acc. Chem. Res.* **2000**, *33*, 889−897.
(54) Dai, J.; Carver, M.; Punchihewa, C.; Jones, R. A.; Yang, D. Structure of the Hybrid-2 Type Intramolecular Human Telomeric G-Quadruplex in K+ Solution: Insights into Structure Polymorphism of the Human Telomeric Sequence. *Nucleic Acids Res.* **2007**, *35*, 4927−4940.
(55) Wang, Y.; Patel, D. J. Solution Structure of the Human Telomeric Repeat d[AG3(T2AG3)3] G-Tetraplex. *Structure* **1993**, *1*, 263−282.

https://doi.org/10.1021/acs.biochem.2c00373
Biochemistry 2022, 61, 2546−2559

Targeting Parallel Topology of G-Quadruplex Structures by Indole-fused Quindoline Scaffolds

Satendra Kumar†, Sushree Prangya Priyadarshinee Pany†, Sruthi Sudhakar, Sushma B. Singh, Chaitra S. Todankar and P. I. Pradeepkumar*

Department of Chemistry, Indian Institute of Technology Bombay, Powai, Mumbai-400076, India

Email: pradeep@chem.iitb.ac.in

†These authors contributed equally

TABLE OF CONTENTS

General Experimental Details

All chemicals and solvents used were obtained from commercial sources (Merck, India; Spectrochem, India; Sigma Aldrich, Germany and Alfa Aesar; UK). Dry solvents CH_3CN and EtOH were dried using calcium hydride and magnesium, respectively. Commercially obtained DMF was dried overnight under the nitrogen atmosphere by incubation in activated molecular sieves (4 Å). Thin-layer chromatography (TLC) was performed using silica gel plates (Merck, Germany) pre-coated with fluorescent indicator and further visualized under UV light (260 nm). Silica gel (100-200 mesh) and basic alumina (60-325 mesh BSS) were used for column chromatography to purify the compounds wherever required.^{1}H NMR and ^{13}C NMR were recorded on 400 MHz and 500 MHz instruments, respectively. The chemical shifts in parts per million (ppm) were recounted downfield to the TMS signal (0 ppm) and referenced from the TMS signal or residual proton signal of deuterated solvents: $CDCl_3$ (7.26 ppm), CD_3OD (3.31 ppm), and DMSO-d_6 (2.5 ppm) for ^{1}H NMR spectra; and $CDCl_3$ (77.2 ppm), CD_3OD (49.1 ppm), and DMSO- d_6 (39.5 ppm) for ^{13}C NMR spectra. Multiplicities of ^{1}H NMR spin couplings are reported as s (singlet), d (doublet), t (triplet), dd (doublet of doublets), and (q) quintet or m (multiplet and overlapping spin systems). Values for apparent coupling constants (J) are reported in Hz. High-resolution mass spectra (HRMS) were recorded using a Q-TOF analyzer in positive ion electrospray ionization (ESI) mode. HeLa (human cervical cancer) cell lines and liver hepatocellular cancer cell lines (HepG2) were obtained from NCCS, Pune. The enzymes (*Taq* DNA polymerase, PNK), dNTPs, Gene JET RNA purification kit and verso c-DNA synthesis kit were purchased from Thermo Scientific. Brilliant III Ultra-Fast SYBR green qPCR master mix was purchased from Agilent Technologies. All the media, serum, antibiotics and reagents used for cell-based experiments were purchased from HiMedia, MP Biomedicals and Glibco. The reagent used for cytotoxicity assay, Cell titer Glow was purchased from Promega.

Synthetic Procedures

3, 3'-((2-nitrophenyl)methylene)bis(1H-indole) (3)

A mixture of indole **1** (380 mg, 3.3 mmol), 2-nitrobenzaldehyde **2** (250 mg, 1.6 mmol) and I_2 (80 mg, 0.3 mmol) was stirred in ACN (10 mL) for 20 min. Then the solution of the reaction mixture was concentrated, and aqueous $Na_2S_2O_3$ (2 x 10 mL) was added. The compound was then extracted with ethyl acetate (2 x 150 mL). The solvent was evaporated to get the pure orange solid compound **3** (400 mg, 51 %). R_f = 0.5 (30% ethyl acetate in pet ether). ^{1}H NMR (400 MHz, $CDCl_3$) δ =7.85 (dd, J = 8.0, 1.0 Hz, 1H), 7.79 (br. s, 2H), 7.37−7.42 (m, 3H), 7.31-7.36 (m, 2H), 7.28 (d, J = 8.3 Hz, 2H), 7.18 (td, J = 7.24, 1.0 Hz, 2H), 7.04 (t, J = 14.9 Hz, 2H), 6.68 (s, 1H), 6.51 (s, 2H). ^{13}C NMR (100 MHz, $CDCl_3$): δ = 149.8, 138.1, 136.7, 132.5, 131.2, 127.3, 126.8, 124.4, 124.0 122.3, 119.7, 119.6,

117.6, 111.4, 34.8 HRMS (ESI): calcd for $C_{23}H_{17}N_3NaO_2$, $[M+Na]^+$ 390.1213; found, $[M+Na]^+$ 390.1213

11-(1H-indol-3-yl)-10H-indolo[3,2-b]quinoline (4)

A solution of compound **3** (130 mg, 0.4 mmol) and $SnCl_2.2H_2O$ (400 mg, 2.0 mmol) in methanol (2 mL) was refluxed for 1 h. Then the solution was allowed to cool and poured into ice cold water, and 5% $NaHCO_3$ (30 mL) solution was added to maintain the pH at 8.0. Ethyl acetate (2 x 50 mL) was added and filtered through a celite bed. The organic layer was dried over $MgSO_4$, and the solvent was evaporated. The residue was purified by column chromatography (20% ethyl acetate in pet ether) to yield the bright yellow solid compound **4 (**80 mg, 64%). R_f= 0.45 (30% ethyl acetate in pet ether). ^{1}H NMR (400 MHz, DMSO-d_6): δ = 11.81 (s, 1H), 10.89 (s, 1H), 8.40 (d, J = 7.7 Hz, 1H), 8.27 (d, J = 8.4 Hz, 1H), 7.96 (d, J = 8.5 Hz, 1H), 7.88 (d, J = 2.4 Hz, 1H), 7.62-7.68 (m, 2H), 7.52-7.60 (m, 2H), 7.44-7.48 (m, 1H), 7.22-7.30 (m, 2H), 7.14 (d, J = 7.6 Hz, 1H), 7.04 (t, J = 7.1 Hz, 1H). ^{13}C NMR (100 MHz, CD_3OD): δ = 145.6, 144.6, 144.4, 137.0, 132.1, 129.8, 129.6, 127.3, 127.1, 126.3, 126.2, 125.9, 124.9, 122.2, 121.8, 121.7, 120.6, 120.1, 119.8, 119.7, 112.5, 112.3, 107.8 HRMS (ESI): calcd for $C_{23}H_{16}N_3$, $[M+H]^+$ 334.1338; found, $[M+H]^+$334.1339 (Δm = 0.0001 and error = 0.2 ppm)

10-(3-bromopropyl)-11-(1-(3-bromopropyl)-1H-indol-3-yl)-10H-indolo[3,2-b]quinoline (5)

To a solution of **4** (100 mg, 0.3 mmol) in dry ACN (4 mL), Cs_2CO_3 (400 mg, 1.2 mmol) was added and refluxed at 80 °C for 1 h. 1,2 dibromoprpopane (800 mg, 4 mmol) was added to the heated solution and further refluxed at the same temperature for 24 h. The solvent was evaporated and the solid residue was dissolved in ethyl acetate (2 x 50 mL) and washed with H_2O (2 x 20 mL). The organic layer was concentrated under reduced pressure and purified by column chromatography (15% ethyl acetate in pet ether) to yield the yellow solid compound **7 (**110 mg, 60 %). R_f = 0.9 (30% ethyl acetate in pet ether). ^{1}H NMR (500 MHz, $CDCl_3$) : δ = 8.63 (d, J = 7.5 Hz, 1H), 8.40 (dd, J = 8.3, 0.6 Hz, 1H), 7.72 (dd, J = 8.5, 0.8 Hz, 1H), 7.61-7.67 (m, 2H), 7.57 (d, J = 8.3 Hz, 1H), 7.34- 7.40 (m, 5H), 7.17(d, J = 7.9 Hz, 1H), 7.10 (td, J = 7.1, 0.6 Hz, 1H), 4.53 (t, J = 6.5 Hz,2H), 3.89-4.03 (m, 2H), 3.45-3.49 (m, 2H), 2.81 (dt, J = 10.1, 5.9 Hz, 1H), 2.46 − 2.57 (m, 3H), 1.73 − 1.92 (m, 2H).^{13}C NMR (100 MHz, $CDCl_3$): δ = 146.5, 145.1, 144.0, 135.9, 132.0, 129.8, 129.3, 129.2, 128.3, 128.2, 126.4, 125.3, 125.1, 123.0, 122.1, 122.0, 120.7, 120.2, 120.2, 119.1, 109.9, 109.0, 108.8, 44.5, 42.8, 32.8, 31.7, 30.2, 30.0. HRMS (ESI): calcd for $C_{29}H_{25}Br_2N_3$, $[M+H]^+$ 574.0486; found, $[M]^+$ 574.0488

11-(1-(2-(pyrrolidin-1-yl)ethyl)-1H-indol-3-yl)-10H-indolo[3,2-b]quinolone (InqEt1) and **10-(2-(pyrrolidin-1-yl)ethyl)-11-(1-(2-(pyrrolidin-1-yl)ethyl)-1H-indol-3-yl)-10H-indolo[3,2-b] quinoline** (**InqEt2**)

To a solution of **4** (100 mg, 0.3 mmol) in dry ACN (10 mL), Cs_2CO_3 (488.7 mg, 1.5 mmol) was added and refluxed at 80 °C for 1 h. 1-(2-chloroethyl) pyrrolidine hydrogen chloride (204 mg, 1.2 mmol) was added to the heated solution and refluxed at the same temperature for 48 h. The solvent was

evaporated, and the solid residue was dissolved in ethyl acetate (2 x 50 mL) and washed with H_2O (2 x 20 mL). The organic layer was concentrated under reduced pressure and purified by column chromatography (8% MeOH in DCM) to yield the brown solid **InqEt1** and a yellow solid **InqEt2.**

InqEt1 (39 mg, 30%). R_f = 0.5 (10% MeOH in ethyl acetate). ^{1}H NMR (400 MHz, CD_3OD): δ = 8.56 (d, *J* = 7.7 Hz, 1H), 8.24 (d, *J* = 8.4 Hz, 1H), 7.59-7.71(m, 4H), 7.5 (s, 1H), 7.50 (d, *J* = 8.2 Hz, 1H), 7.33-7.38(m, 2H), 7.24 (td, *J* = 6.9, 1 Hz, 1H), 6.98-7.06 (m, 2H), 4.01-4.19 (m, 2H), 2.20-2.44 (m, 2H), 1.78-1.99 (m, 4H),1.53 (m, 4H). ^{13}C NMR (100 MHz, MeOD): δ = 146.9, 146.5, 144.5, 137.9, 133.4, 131.5, 130.0, 129.7, 128.6, 127.9, 126.9, 126.9, 126.2, 123.6, 123.0, 122.8, 122.4, 121.4, 121.3, 120.2, 113.1, 110.5, 109.2, 54.4, 54.1, 43.4, 24.0. HRMS (ESI): calcd for $C_{29}H_{27}N_4$, $[M+H]^+$ 431.2230; found, $[M]^+$ 431.2230.

InqEt2 (34 mg, 21%). R_f= 0.4 (10% MeOH in ethyl acetate). ^{1}H NMR (400 MHz, $CDCl_3$): δ = 8.61 (d, *J* =7.5 Hz, 1H), 8.35 (d, *J* =7.9 Hz, 1H), 7.72 (dd, *J* = 8.5, 0.8 Hz, 1H), 7.60-7.64 (m, 2H), 7.53 (d, *J* =8.3 Hz, 1 H), 7.43 (d, *J* =8.2 Hz, 1 H), 7.38 (s, 1H), 7.28 − 7.36 (m, 3H), 7.18 (d, *J* =7.8 Hz, 1H), 7.07 (td, *J* = 7.1, 0.6 Hz, 1H), 4.44 (t, *J* =14.5 Hz, 2H), 3.99 − 4.17 (m, 2H), 3.37 - 3.49 (m, 1H), 3.04 (t, *J* =7.3 Hz, 2H), 2.63 − 2.69 (m, 4H), 2.44 (td, *J* =11.3, 5.2 Hz, 1H), 2.25 (td, *J* =11.4, 5.4 Hz, 1H), 1.93 − 1.99 (m, 2H), 1.78 − 1.85 (m, 5H), 1.51-1.54 (m, 4H). ^{13}C NMR (100 MHz, $CDCl_3$): δ = 145.3, 144.1, 136.3, 132.3, 129.9, 129.5, 129.3, 128.7, 128.5, 126.3, 125.6, 125.0, 122.7, 122.2, 120.6, 120.5, 120.1, 119.4, 109.8, 109.3, 108.5, 56.1, 54.6, 53.8, 53.5, 46.1, 43.1, 23.8, 23.4. HRMS (ESI): calcd for $C_{35}H_{37}N_5$, $[M+H]^+$ 528.3122; found, $[M+H]^+$ 528.3122

3-(3-(10-(3-(dimethylammonio)propyl)-10H-indolo[3,2-b]quinolin-11-yl)-1H-indol-1-yl)-N,N-dimethylpropan-1-aminium (InqPr1)

To a solution of **4** (100 mg, 0.3 mmol) in dry ACN (10 mL), Cs_2CO_3 (488.7 mg, 1.5 mmol) was added and refluxed at 80 °C for 1 h. 3-chloro-N,N-dimethylpropan-1-amine hydrogen chloride (292 mg, 1.5 mmol) was added to the heated solution and refluxed at the same temperature for 48 h. The solvent was evaporated, and the solid residue was dissolved in ethyl acetate (2 x 50 mL) and washed with H_2O (2 x 20 mL). The organic layer was concentrated under reduced pressure and purified by column chromatography. The purified compound was protonated by adding 0.2 mL HCl in DCM (5ml) to obtain a precipitate. The precipitate was then washed with DCM to get **InqPr1** as a yellow solid.

(73 mg, 42 %). R_f = 0.2 (10% MeOH in ethyl acetate). ^{1}H NMR (400 MHz, D_2O): δ = 8.1 (t, *J* = 9.5 Hz, 1H), 7.93 (t, *J* =9.5 Hz, 1H), 7.8 (d, *J* =6.4 Hz, 1H), 7.72-7.6 (m, 3H), 7.5-7.25 (m, 4H), 7.1-7.03 (m, 1H), 6.87-6.81 (m, 1H), 6.72 (t, *J* =8.7 Hz, 1H), 4.6 - 4.4 (m, 2H), 4.0 -3.83 (m, 2H), 3.4-3.2 (m, 2H), 2.27 (s, 6H), 2.4-2.37 (m, 3H), 2.32 (s, 3H), 2.11 (s, 3H), 1.65-1.13 (m, 3H).^{13}C NMR (100 MHz, D_2O): δ = 145.7, 136.8, 135.8, 134.2, 133.2, 131.9, 131.7, 131.6, 130.0, 128.1, 127.2, 126.7, 126.6, 123.6, 122.8, 121.9, 121.4, 119.3, 119.1, 113.0, 111.1, 110.9, 105.3, 55.1, 54.1, 43.4, 42.9,

42.9, 42.7, 41.8, 41.2, 25.4, 23.8. HRMS (ESI): calcd for $C_{37}H_{41}N_5$, $[M/2]^+$ 252.6597; found, $[M/2]^+$ 252.6599

10-(3-(pyrrolidin-1-yl)propyl)-11-(1-(3-(pyrrolidin-1-yl)propyl)-1H-indol-3-yl)-10H-indolo[3,2-b] quinoline (**InqPr2**)

A solution of compound **5** (60 mg, 0.1 mmol) and pyrrolidine (40 mg, 0.6 mmol) was refluxed at 80 °C for 12 h. After completion of the reaction, the solvent was evaporated. The residue was purified by column chromatography (2% methanol in ethyl acetate) to yield the yellow solid ligand **InqPr2** (50 mg, 86 %). R_f = 0.6 (10% MeOH in ethyl acetate). ^{1}H NMR (400 MHz, $CDCl_3$): δ = 8.61 (d, J = 7.3 Hz, 1H), 8.36 (dd, J =8.4, 0.6 Hz, 1H), 7.71 (dd, J =8.5, 0.8 Hz, 1H), 7.55-7.64 (m, 3H), 7.39 (d, J =8.2 Hz, 1H), 7.28-7.35 (m, 4H), 7.14 (d, J =7.6 Hz, 1H), 7.04 (td, J =7.4, 0.6 Hz, 1H), 4.42 (t, J =6.8 Hz, 2H), 3.84-3.99 (m, 2H), 2.54-2.58 (m, 6H), 2.14-2.23 (m, 6H), 1.90-1.97 (m, 2H), 1.79-1.82 (m, 4H), 1.65-1.69 (m, 6H).^{13}C NMR (100 MHz, $CDCl_3$): δ = 146.4, 145.2, 143.9, 136.0, 133.0, 129.6, 129.3, 129.1, 128.4, 128.3, 126.1, 125.4, 124.9, 122.4, 122.0, 121.9, 120.2, 120.2, 119.8, 119.3, 110.0, 109.2, 108.4, 54.1, 53.7, 53.1, 53.0, 44.5, 42.0, 29.6, 27.9, 23.5, 23.3. HRMS (ESI): calcd for $C_{37}H_{41}N_5$, $[M+H]^+$ 556.3435; found, $[M]^+$ 556.3435

The detailed mechanism on the formation of compound 4

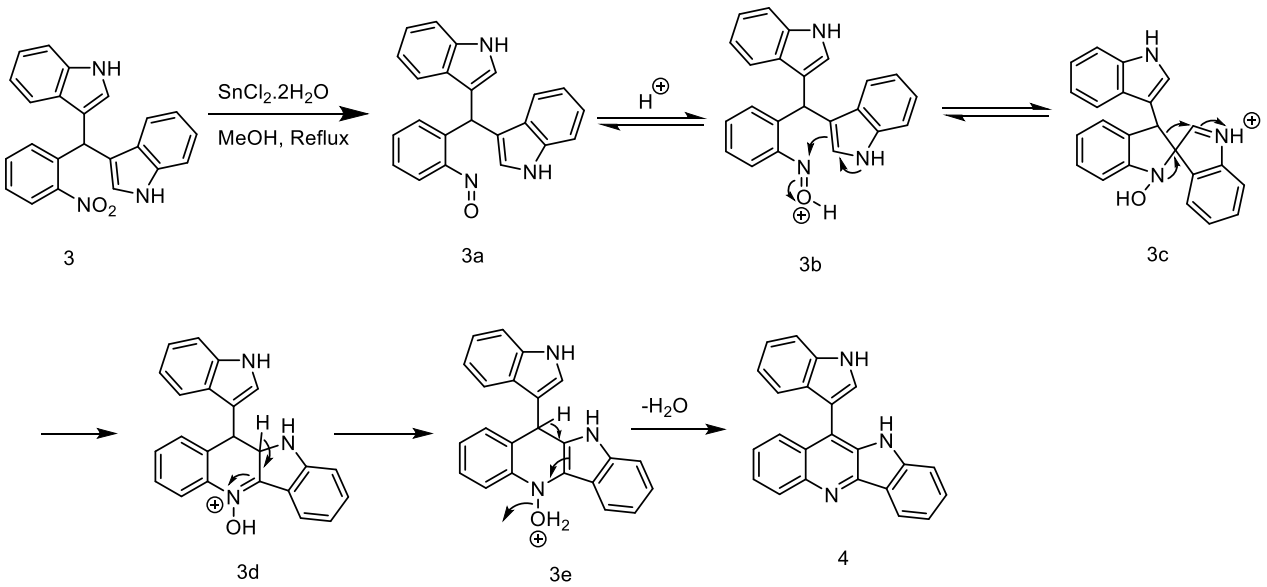

Scheme S1. Proposed mechanism on the formation of compound **4**

The synthetic scheme for the formation of InqPr1

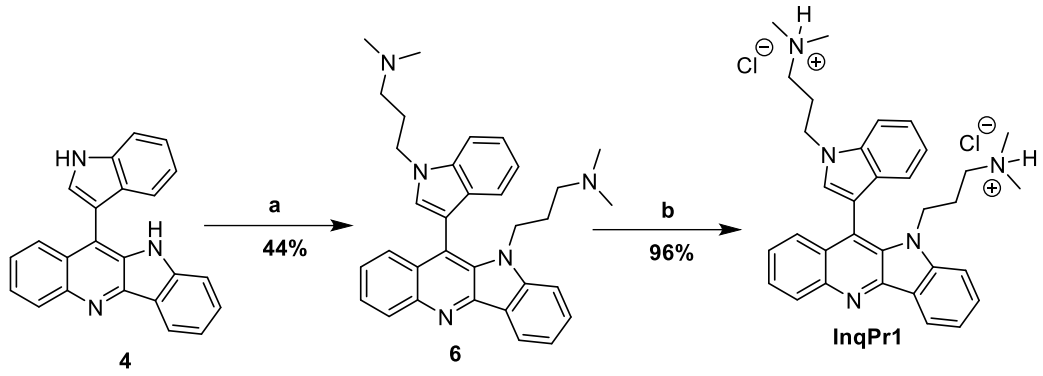

Scheme S2. (a) 3-chloro-N,N-dimethylpropan-1-amine hydrogen chloride, Cs_2CO_3, ACN, 80 °C, 48 h; (B) HCl, DCM, RT, 2 h

Normalized CD melting curves of *h-RAS1*, telomeric and duplex DNAs

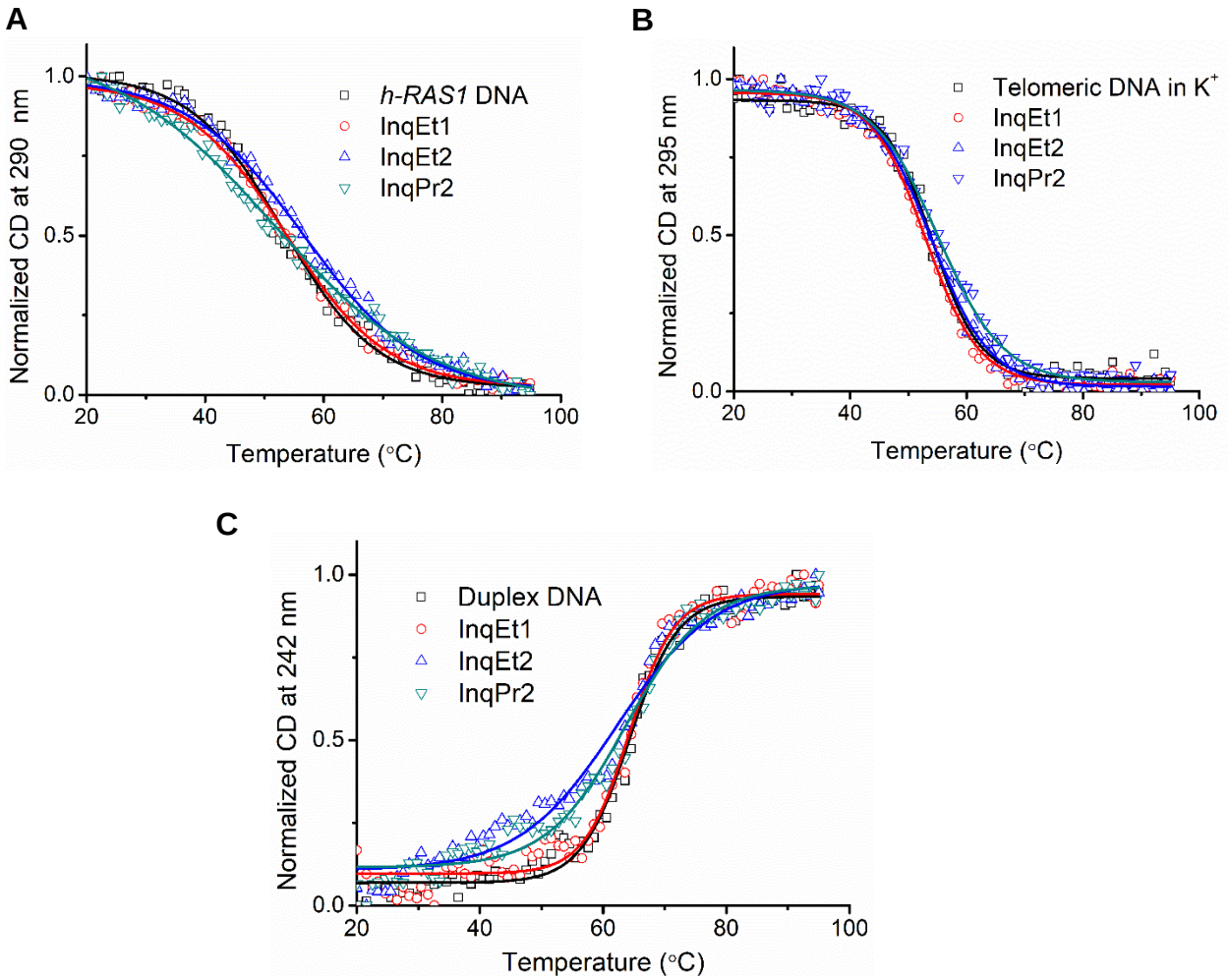

Figure S1. Normalized CD melting curves of various quadruplex DNAs (10 μM) and duplex DNA (15 μM in 10 mM lithium cacodylate buffer, pH 7.2) in the absence and the presence of 5 equivalents of ligands. (A) *h-RAS1* DNA (50 mM KCl and 50 mM LiCl); (B) telomeric DNA (10 mM KCl and 90 mM LiCl); and (C) Duplex DNA (10 mM KCl and 90 mM LiCl).

CD spectra of ligands with *h-RAS1* and *c-KIT1* DNAs in the presence of added metal cations

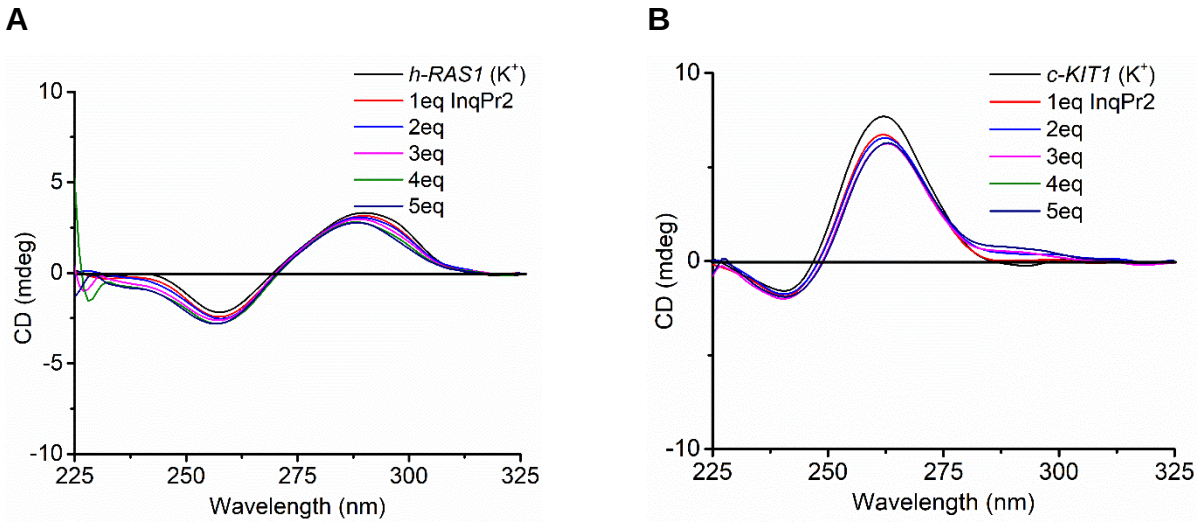

Figure S2. CD titration spectra of quadruplex DNAs (10 μM in 10 mM lithium cacodylate buffer, pH 7.2) in the presence of salt with **InqPr2** (0-5 equivalents). (A) *h-RAS1* G4 DNA (50 mM KCl and 50 mM LiCl); and (B) *c-KIT1* DNA (10 mM KCl and 90 mM LiCl).

Fluorimetric titration curves of ligand InqPr2 with *c-KIT1*, *h-RAS1*, telomeric and duplex DNAs

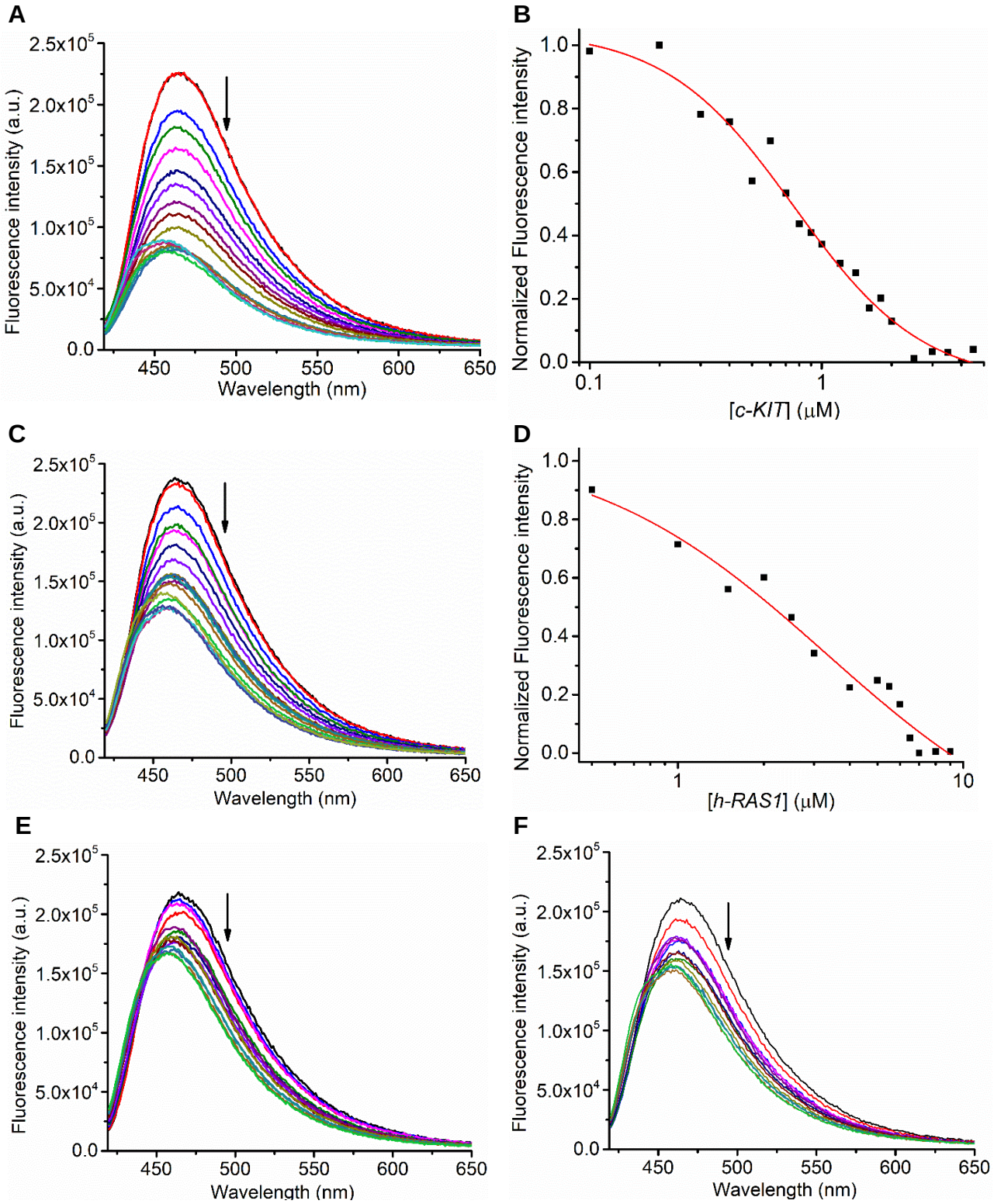

Figure S3. Fluorimetric titration of **InqPr2** (100 μM in 100 mM KCl and 10 mM lithium cacodylate buffer, pH 7.2) with increasing concentration of G4 and duplex DNAs. Emission spectra of **InqPr2** with (A) *c-KIT1* G4 DNA (0-6 μM); (C) *h-RAS1* G4 DNA (0-10 μM); (E) telomeric G4 DNA (0-10 μM); (F) duplex DNA (0-10 μM); (B) plot of normalized fluorescence intensity against the logarithm of an increasing concentration of *c-KIT* DNA; and (D) *h-RAS1* DNA.

***Taq* DNA polymerase stop assay of mutated *c-MYC* with InqPr2**

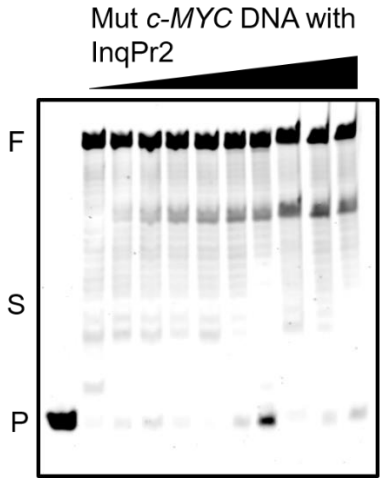

Figure S4. 15% denaturing PAGE (7 M urea) of *Taq* DNA polymerase stop assay of the mutated *c-MYC* DNA with an increasing concentration of **InqPr2** (0–180 μM). Conditions: 0.2 μM primer, 0.1 μM template DNA, 0.2 mM dNTPs and 1U *Taq* DNA polymerase enzyme in buffer (50 mM Tris-HCl, pH 7.2, 0.5 mM DTT, 0.1 mM EDTA, 5 mM MgCl2, 5 mM KCl). F, S and P denote full length, stop product and primer product respectively.

Cell viability assay of HeLa, HepG2 and Lenti-X with InqPr2

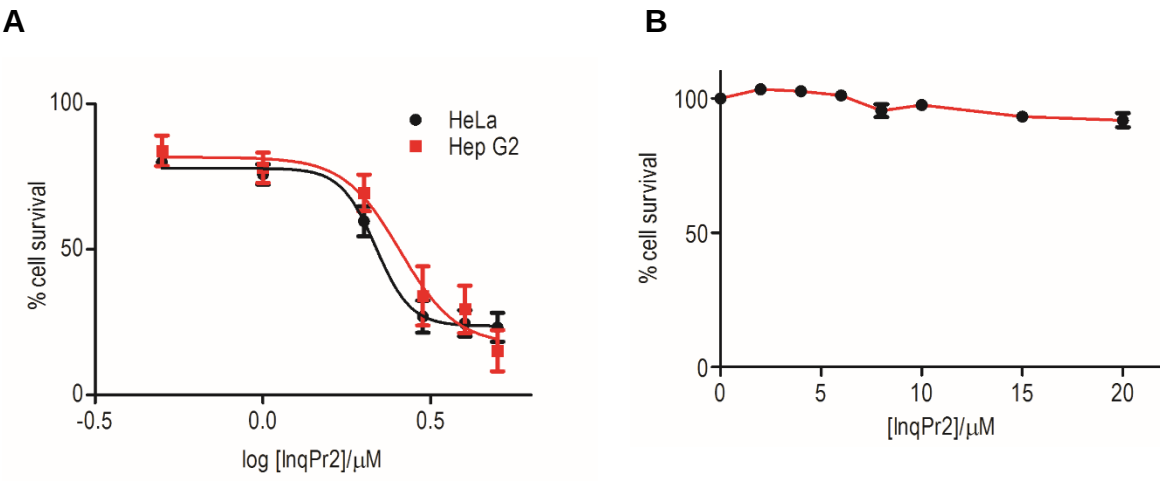

Figure S5. (A) Plot for the cell viability by MTT assay. HeLa and HepG2 cell lines with increasing concentration of **InqPr2** (0-10 μM). (B) Representative graph for cell viability in Lenti-X cell with arrange of concentration of **InqPr2** (0-20 μM). The curves in A were fitted using the dose-response equation; Error bars represent the standard deviations from three independent experiments.

Optimized structure, cartesian coordinates and RESP charges of InqPr2 used for docking

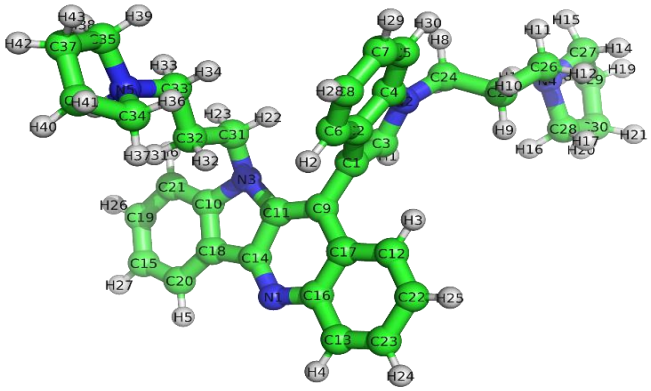

@<TRIPOS>MOLECULE
INQ
85 92 1 0 0
SMALL
Resp
@<TRIPOS>ATOM

1	C1	-0.5150	0.0210	0.5710	cc	1	INQ	-0.072185
2	C2	-0.3960	-1.3150	1.1150	ca	1	INQ	0.162984
3	C3	-1.6180	0.0080	-0.2060	cd	1	INQ	-0.117893
4	H1	-2.0360	0.8120	-0.7800	h4	1	INQ	0.185911
5	C4	-1.4640	-2.0630	0.6030	ca	1	INQ	0.108132
6	C5	-1.6430	-3.4090	0.9330	ca	1	INQ	-0.280835
7	C6	0.5130	-1.9200	1.9910	ca	1	INQ	-0.230888
8	H2	1.3130	-1.3450	2.4250	ha	1	INQ	0.162022
9	C7	-0.7320	-3.9840	1.7920	ca	1	INQ	-0.117754
10	C8	0.3390	-3.2450	2.3230	ca	1	INQ	-0.165114
11	C9	0.3560	1.2050	0.8050	ca	1	INQ	0.037142
12	C10	2.4490	2.1820	-1.9700	ca	1	INQ	0.316059
13	C11	1.2300	1.6880	-0.1240	ca	1	INQ	-0.004146
14	C12	-0.5930	1.5570	3.1010	ca	1	INQ	-0.164341
15	H3	-1.1710	0.6560	3.0120	ha	1	INQ	0.120856
16	C13	0.8890	3.9020	3.3680	ca	1	INQ	-0.290800
17	H4	1.4660	4.8050	3.4400	ha	1	INQ	0.184304
18	C14	1.8960	2.9350	0.1150	cp	1	INQ	0.441162
19	C15	4.0520	4.3190	-2.6900	ca	1	INQ	-0.228699
20	C16	0.9910	3.1500	2.1690	ca	1	INQ	0.507573
21	C17	0.2490	1.9550	2.0260	ca	1	INQ	-0.150436
22	C18	2.6570	3.2390	-1.0900	cp	1	INQ	-0.135858
23	C19	3.8450	3.2530	-3.5660	ca	1	INQ	-0.059752
24	C20	3.4540	4.3200	-1.4430	ca	1	INQ	-0.064079
25	H5	3.5970	5.1330	-0.7550	ha	1	INQ	0.155983
26	C21	3.0440	2.1730	-3.2240	ca	1	INQ	-0.319263
27	H6	2.8800	1.3790	-3.9300	ha	1	INQ	0.169358

28	C22	-0.6690	2.2950	4.2420	ca	1	INQ	-0.145054
29	C23	0.0850	3.4850	4.3820	ca	1	INQ	-0.101119
30	N1	1.7900	3.6350	1.1890	nb	1	INQ	-0.639745
31	N2	-2.2070	-1.2400	-0.2180	na	1	INQ	-0.183286
32	C24	-3.5160	-1.5230	-0.7500	c3	1	INQ	-0.071540
33	H7	-3.6610	-0.8680	-1.6050	h1	1	INQ	0.091940
34	H8	-3.5290	-2.5390	-1.1300	h1	1	INQ	0.091940
35	C25	-4.6230	-1.3360	0.3000	c3	1	INQ	0.036405
36	H9	-4.5890	-0.3270	0.6970	hc	1	INQ	0.083580
37	H10	-4.4180	-1.9940	1.1380	hc	1	INQ	0.083580
38	C26	-6.0310	-1.6840	-0.1800	c3	1	INQ	-0.426241
39	H11	-6.0440	-2.6350	-0.6990	hx	1	INQ	0.214537
40	H12	-6.7130	-1.7510	0.6570	hx	1	INQ	0.214537
41	C27	-7.9370	-1.1170	-1.7260	c3	1	INQ	-0.129454
42	C28	-6.8920	0.6960	-0.5230	c3	1	INQ	-0.129454
43	H13	-5.9920	-0.5510	-1.8880	hn	1	INQ	0.281125
44	C29	-8.5050	0.1740	-2.2880	c3	1	INQ	0.003644
45	H14	-8.5440	-1.5130	-0.9220	hx	1	INQ	0.124239
46	H15	-7.7470	-1.8970	-2.4490	hx	1	INQ	0.124239
47	C30	-8.1790	1.2070	-1.1990	c3	1	INQ	0.003644
48	H16	-6.0280	1.3160	-0.7100	hx	1	INQ	0.124239
49	H17	-7.0040	0.5710	0.5430	hx	1	INQ	0.124239
50	H18	-8.0190	0.4230	-3.2260	hc	1	INQ	0.060169
51	H19	-9.5660	0.0910	-2.4820	hc	1	INQ	0.060169
52	H20	-8.0450	2.2010	-1.6030	hc	1	INQ	0.060169
53	H21	-8.9790	1.2560	-0.4710	hc	1	INQ	0.060169
54	N3	1.5830	1.2190	-1.4070	na	1	INQ	-0.407152
55	C31	1.8540	-0.1840	-1.6580	c3	1	INQ	-0.035126
56	H22	1.0250	-0.7710	-1.2950	h1	1	INQ	0.097077
57	H23	1.8980	-0.3300	-2.7310	h1	1	INQ	0.097077
58	H24	0.0140	4.0580	5.2890	ha	1	INQ	0.152712
59	H25	-1.3050	1.9730	5.0480	ha	1	INQ	0.149283
60	H26	4.3060	3.2740	-4.5370	ha	1	INQ	0.147140
61	H27	4.6720	5.1430	-2.9920	ha	1	INQ	0.169015
62	H28	1.0100	-3.7190	3.0170	ha	1	INQ	0.151840
63	H29	-0.8500	-5.0150	2.0720	ha	1	INQ	0.155232
64	H30	-2.4580	-3.9900	0.5410	ha	1	INQ	0.180137
65	N4	-6.6300	-0.6760	-1.1190	n4	1	INQ	0.044166
66	C32	3.1670	-0.6560	-1.0080	c3	1	INQ	0.050703
67	H31	3.9870	-0.0590	-1.4000	hc	1	INQ	0.029774
68	H32	3.1140	-0.4760	0.0590	hc	1	INQ	0.029774
69	C33	3.4270	-2.1320	-1.2830	c3	1	INQ	-0.236312
70	H33	3.3800	-2.3450	-2.3450	hx	1	INQ	0.132628
71	H34	2.7170	-2.7710	-0.7740	hx	1	INQ	0.132628
72	C34	5.0400	-2.5420	0.6480	c3	1	INQ	-0.104491
73	C35	5.1690	-3.9530	-1.2580	c3	1	INQ	-0.104491
74	H35	5.4560	-1.9250	-1.2520	hn	1	INQ	0.313577
75	C36	6.3520	-3.3070	0.7940	c3	1	INQ	-0.020643

76	H36	4.2070	-3.0570	1.1070	hx	1	INQ	0.125152
77	H37	5.0730	-1.5230	1.0030	hx	1	INQ	0.125152
78	C37	6.3400	-4.3510	-0.3470	c3	1	INQ	-0.020643
79	H38	5.3990	-3.9470	-2.3140	hx	1	INQ	0.125152
80	H39	4.2960	-4.5700	-1.0950	hx	1	INQ	0.125152
81	H40	7.1920	-2.6300	0.6870	hc	1	INQ	0.062466
82	H41	6.4280	-3.7590	1.7730	hc	1	INQ	0.062466
83	H42	7.2760	-4.3460	-0.8890	hc	1	INQ	0.062466
84	H43	6.1900	-5.3550	0.0270	hc	1	INQ	0.062466
85	N5	4.7920	-2.5590	-0.8330	n4	1	INQ	-0.020497

@<TRIPOS>BOND

1	1	2	1
2	1	3	2
3	1	11	1
4	2	5	ar
5	2	7	ar
6	3	4	1
7	3	31	1
8	5	6	ar
9	5	31	1
10	6	9	ar
11	6	64	1
12	7	8	1
13	7	10	ar
14	9	10	ar
15	9	63	1
16	10	62	1
17	11	13	ar
18	11	21	ar
19	12	22	ar
20	12	26	ar
21	12	54	1
22	13	18	ar
23	13	54	1
24	14	15	1
25	14	21	ar
26	14	28	ar
27	16	17	1
28	16	20	ar
29	16	29	ar
30	18	22	1
31	18	30	ar
32	19	23	ar
33	19	24	ar
34	19	61	1
35	20	21	ar
36	20	30	ar
37	22	24	ar

38	23	26	ar
39	23	60	1
40	24	25	1
41	26	27	1
42	28	29	ar
43	28	59	1
44	29	58	1
45	31	32	1
46	32	33	1
47	32	34	1
48	32	35	1
49	35	36	1
50	35	37	1
51	35	38	1
52	38	39	1
53	38	40	1
54	38	65	1
55	41	44	1
56	41	45	1
57	41	46	1
58	41	65	1
59	42	47	1
60	42	48	1
61	42	49	1
62	42	65	1
63	43	65	1
64	44	47	1
65	44	50	1
66	44	51	1
67	47	52	1
68	47	53	1
69	54	55	1
70	55	56	1
71	55	57	1
72	55	66	1
73	66	67	1
74	66	68	1
75	66	69	1
76	69	70	1
77	69	71	1
78	69	85	1
79	72	75	1
80	72	76	1
81	72	77	1
82	72	85	1
83	73	78	1
84	73	79	1
85	73	80	1

```
86          73          85          1
87          74          85          1
88          75          78          1
89          75          81          1
90          75          82          1
91          78          83          1
92          78          84          1
      @<TRIPOS>SUBSTRUCTURE
 1          INQ          1          TEMP          0          ****          ****          0          ROOT
```

Figure S6. The optimized structure of **InqPr2,** which was used for docking studies. The ligand was optimized at HF/6-31+G** theory level in Gaussian 16. The ESP charges were then calculated in Gaussian 16. The Cartesian coordinates and RESP charges were then calculated in SYBL Mol2 format using antechamber in AMBER 18. Carbon atoms are represented using green, nitrogen atoms using blue and hydrogen atoms using light grey.

Docked structures of InqPr2 used for simulation

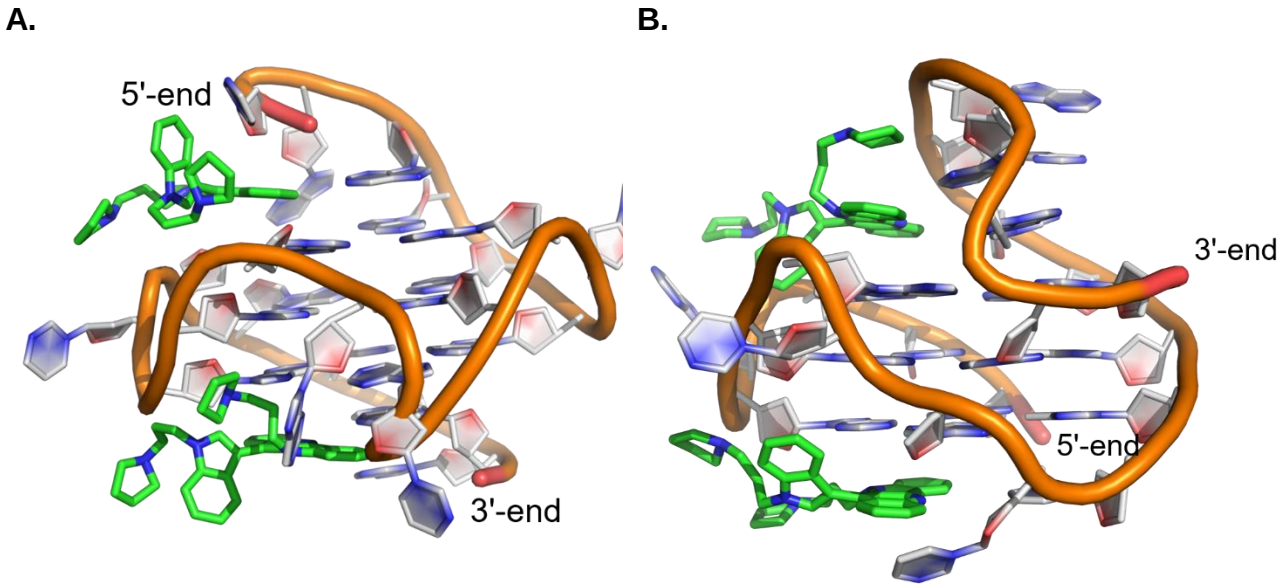

Figure S7. Selected conformers for MD studies out of the 500 independent docked conformers generated with (A) *c-MYC*; and (B) *c-KIT1* G4 DNA in AutoDock 4.2.6.

Per-nucleotide RMSF values of InqPr2 with *c-MYC* and *c-KIT1*

A

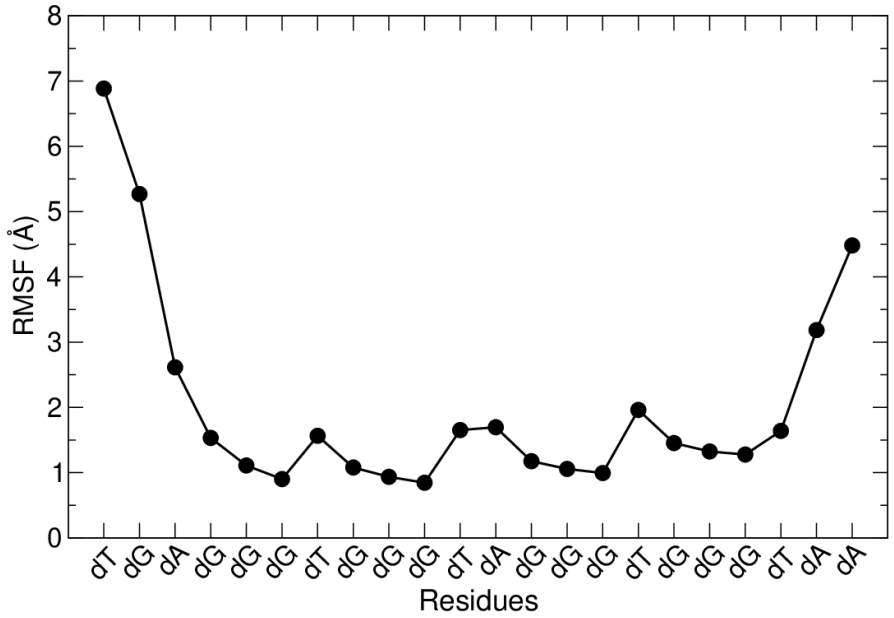

B

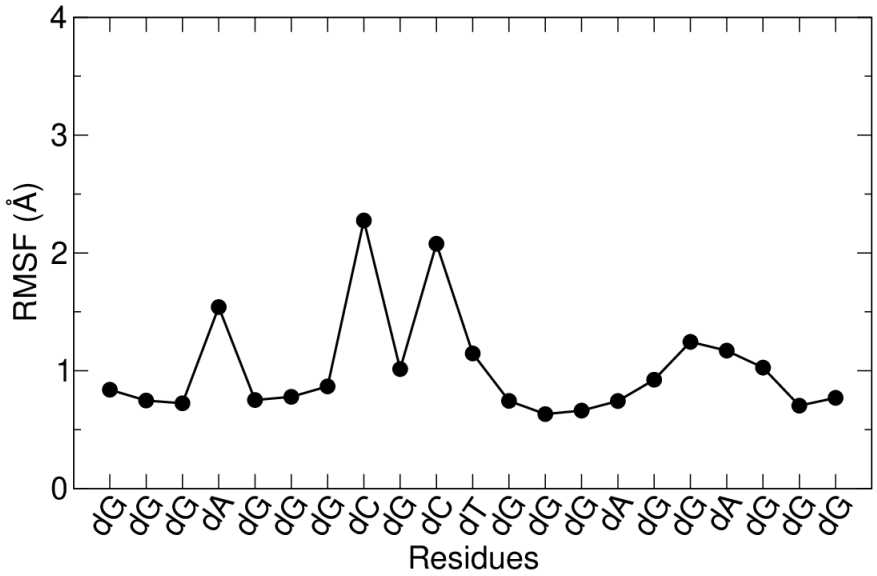

Figure S8. Per-nucleotide RMSF values of (A) *c-MYC* DNA; and (B) *c-KIT1* G4 DNA. The graphs plotted are fluctuations of the nucleotides numbered from 5′ to 3′.

Major electrostatic interactions of InqPr2 with *c-MYC* G4 DNA

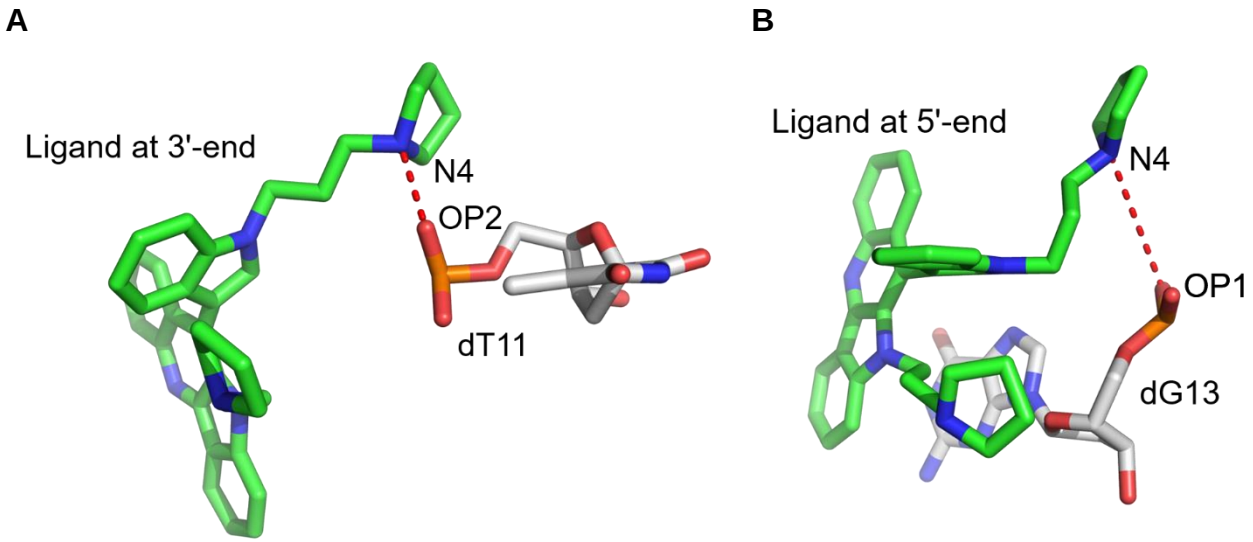

Figure S9. The electrostatic interactions of **InqPr2** with *c-MYC* G4 residues. The interaction is represented with red dashed lines. The electrostatic interactions between (A) the N4 and OP2 of dT11; and (B) N4 and OP1 of dG13 are represented.

Major electrostatic interactions of InqPr2 with *c-KIT1* G4 DNA

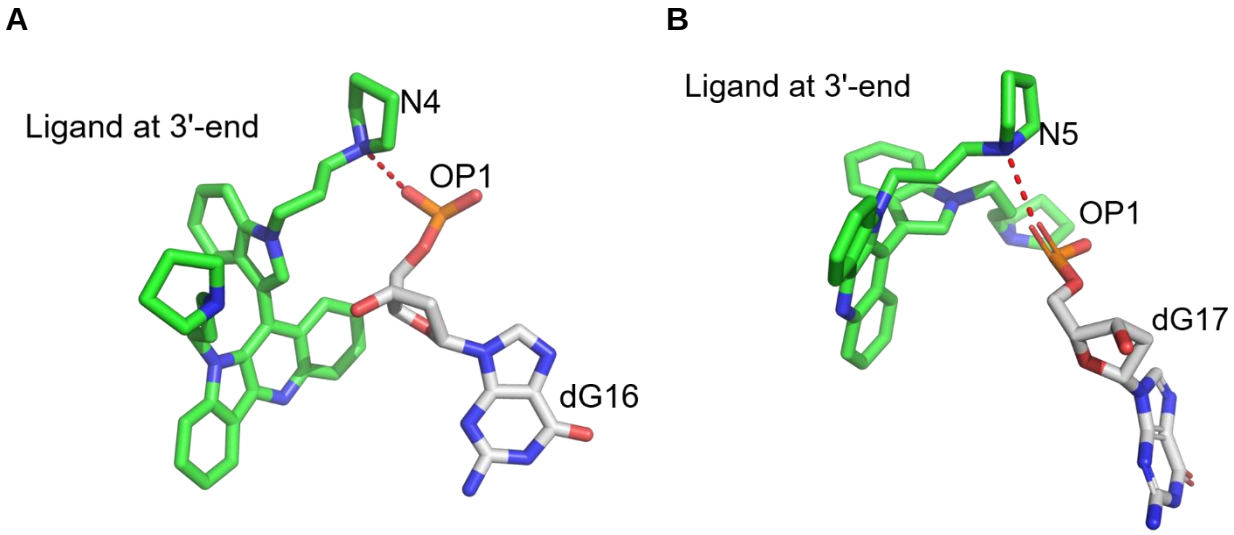

Figure S10. The electrostatic interactions of **InqPr2** with *c-KIT1* G4 residues. The interaction is represented with red dashed lines. The electrostatic interactions between (A) the N4 and OP1 of dG16; (B) N5 and OP1 of dG17 are represented.

Orientation of InqPr2 with telomeric hybrid 2 G4 DNA

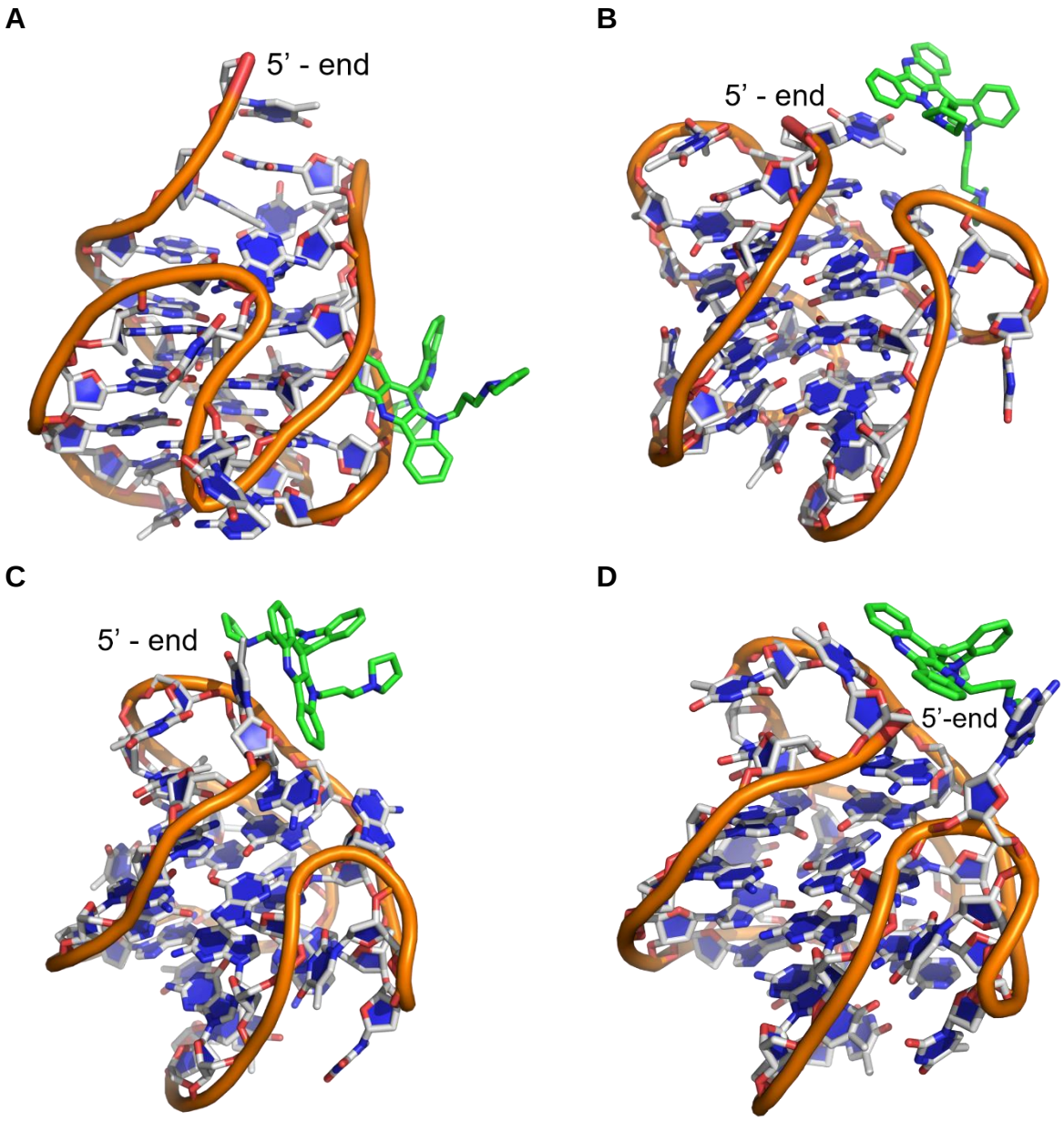

Figure S11. Reorientation of **InqPr2** during the simulation with telomeric hybrid DNA (PDB ID: 2JPZ). Frame at (A) 0.1 ns; (B) 100 ns; (C) 300 ns; and (D) 500 ns

Orientation of InqPr2 with telomeric antiparallel G4 DNA

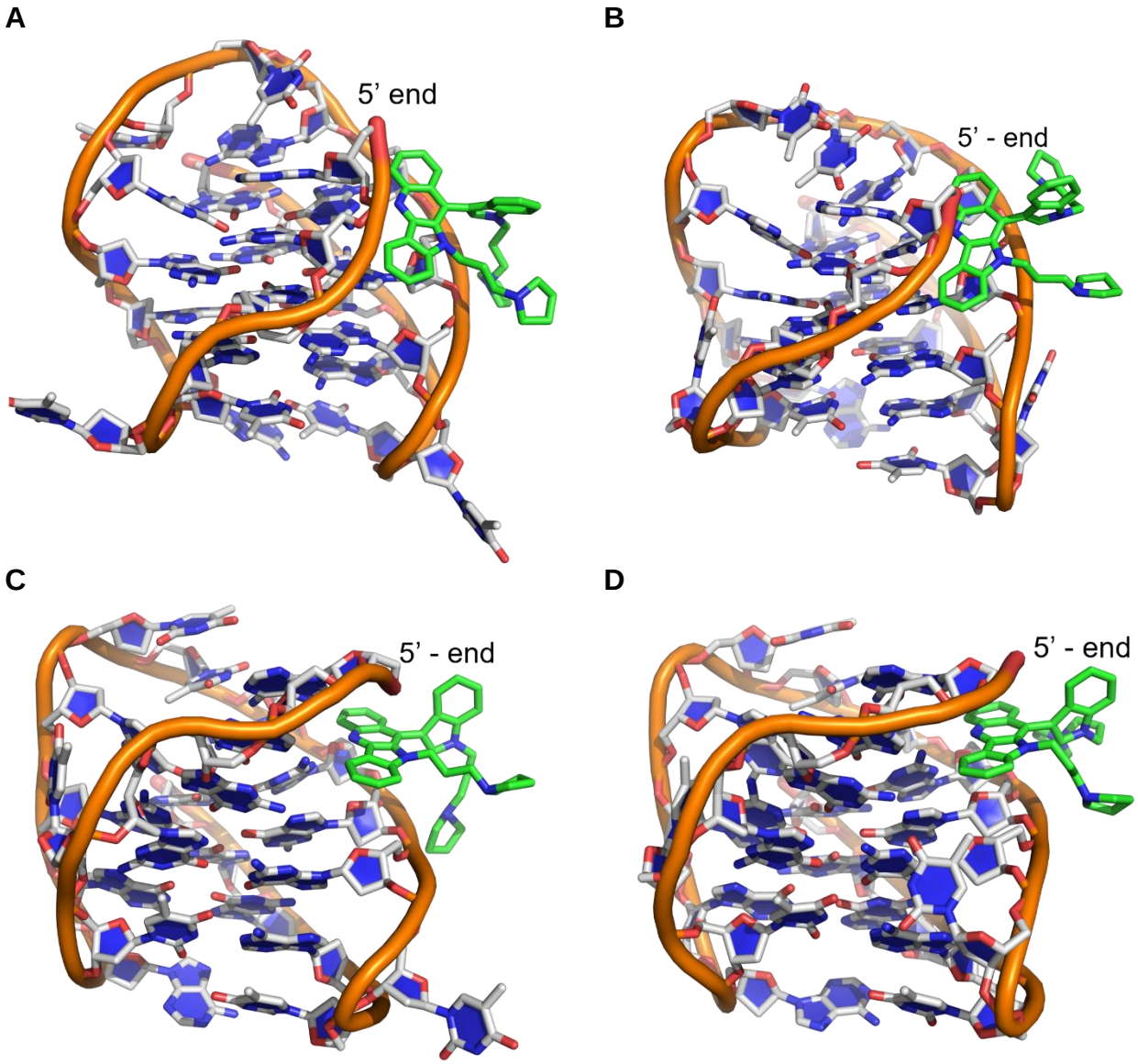

Figure S12. Reorientation of **InqPr2** during the simulation with telomeric antiparallel DNA (PDB ID: 143D). Frame at (A) 100 ns; (B) 300 ns; (C) 400 ns; and (D) 500 ns

Details of single crystal structure information of compound 4

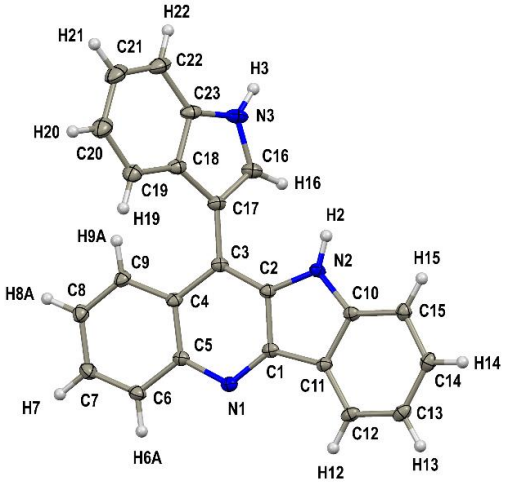

ORTEP diagram of compound **4** with 50% ellipsoid probability (CCDC 2009565)

Selected crystallographic data of compound 4

Table S1. Crystal data and structure refinement data for compound **4**

Empirical formula	$C_{95}H_{67}N_{12}$
Formula weight	1376.60
Temperature/K	293(2)
Crystal system	triclinic
Space group	P-1
a/Å	11.6632(4)
b/Å	12.5674(6)
c/Å	25.4481(9)
α/°	100.530(3)
β/°	90.315(3)
γ/°	99.551(3)
Volume/Å^3	3614.0(3)
Z	2
ρ_{calc}g/cm^3	1.265
μ/mm^{-1}	0.076

F(000)	1442.0
Crystal size/mm^3	0.98 × 0.68 × 0.56
Radiation	MoKα (λ = 0.71073)
2Θ range for data collection/°	3.258 to 50
Index ranges	$-13 \leq h \leq 13$, $-14 \leq k \leq 14$, $-30 \leq l \leq 30$
Reflections collected	72755
Independent reflections	12709 [R_{int} = 0.1453, R_{sigma} = 0.1062]
Data/restraints/parameters	12709/933/965
Goodness-of-fit on F^2	1.025
Final R indexes [I>=2σ (I)]	R_1 = 0.0904, wR_2 = 0.2322
Final R indexes [all data]	R_1 = 0.1479, wR_2 = 0.3026
Largest diff. peak/hole / e $Å^{-3}$	0.45/-0.46

Bond lengths [Å] and angles [°] for Compound 4

Table S2. Bond lengths and bond parameters for compound **4**

Bond Lengths (Å)

Atom	Atom	Length/Å	Atom	Atom	Length/Å
N8	C56	1.383(5)	C12	C13	1.381(6)
N8	C48	1.376(5)	C12	C11	1.392(6)
N4	C24	1.323(5)	C35	C36	1.381(6)
N4	C28	1.360(5)	C6	C7	1.368(6)
N1	C5	1.371(5)	C60	C61	1.399(6)
N1	C1	1.333(5)	C27	C26	1.427(6)
N5	C33	1.385(5)	C27	C28	1.443(6)
N5	C25	1.379(5)	C25	C26	1.372(6)
N2	C2	1.380(5)	C17	C18	1.443(6)
N2	C10	1.375(5)	C17	C16	1.368(6)
N10	C70	1.318(5)	C26	C40	1.487(5)
N10	C74	1.373(5)	C37	C38	1.373(6)
N7	C47	1.331(5)	C37	C36	1.404(6)
N7	C51	1.370(5)	C18	C23	1.432(6)

N11	C79	1.384(5)	C18	C19	1.397(6)
N11	C71	1.382(5)	C64	C63	1.448(6)
N9	C62	1.361(5)	C64	C69	1.405(6)
N9	C69	1.373(6)	C64	C65	1.399(6)
N3	C23	1.364(6)	C72	C73	1.428(6)
N3	C16	1.367(5)	C72	C71	1.374(6)
N6	C39	1.372(5)	C72	C86	1.490(6)
N6	C42	1.375(6)	C81	C80	1.391(6)
N12	C85	1.370(6)	C81	C82	1.370(6)
N12	C88	1.389(6)	C52	C51	1.412(6)
C4	C5	1.421(6)	C52	C53	1.358(6)
C4	C9	1.411(6)	C62	C63	1.366(6)
C4	C3	1.433(6)	C8	C7	1.396(6)
C24	C34	1.449(6)	C73	C74	1.429(6)
C24	C25	1.439(5)	C73	C78	1.421(6)
C70	C80	1.451(6)	C69	C68	1.374(6)
C70	C71	1.431(6)	C74	C75	1.428(6)
C2	C1	1.429(6)	C23	C22	1.401(6)
C2	C3	1.370(6)	C78	C77	1.369(6)
C33	C34	1.406(6)	C46	C45	1.386(6)
C33	C38	1.403(6)	C77	C76	1.398(6)
C5	C6	1.408(6)	C84	C83	1.370(6)
C9	C8	1.369(6)	C76	C75	1.358(6)
C34	C35	1.390(5)	C65	C66	1.380(6)
C10	C15	1.391(6)	C54	C53	1.412(7)
C10	C11	1.415(6)	C28	C29	1.419(6)
C1	C11	1.438(6)	C87	C86	1.441(6)
C50	C49	1.421(6)	C87	C88	1.407(6)
C50	C55	1.423(6)	C87	C92	1.388(6)
C50	C51	1.441(6)	C40	C39	1.381(6)
C3	C17	1.480(6)	C85	C86	1.374(6)
C15	C14	1.386(6)	C29	C30	1.342(6)
C59	C58	1.394(6)	C82	C83	1.419(7)
C59	C60	1.390(6)	C30	C31	1.412(6)

C49	C48	1.385(6)	C42	C43	1.400(6)
C49	C63	1.471(6)	C68	C67	1.383(7)
C58	C57	1.393(6)	C88	C89	1.386(6)
C55	C54	1.366(6)	C22	C21	1.352(8)
C14	C13	1.403(6)	C19	C20	1.376(7)
C79	C80	1.406(6)	C44	C45	1.388(7)
C79	C84	1.389(6)	C44	C43	1.356(7)
C47	C48	1.431(6)	C89	C90	1.373(7)
C47	C57	1.445(6)	C66	C67	1.393(7)
C56	C61	1.392(6)	C92	C91	1.383(7)
C56	C57	1.400(6)	C90	C91	1.403(7)
C32	C27	1.418(6)	C21	C20	1.421(7)
C32	C31	1.361(6)	C93	C93[1]	1.530(11)
C41	C46	1.387(6)	C93	C94	1.521(8)
C41	C40	1.448(6)	C94	C95	1.500(8)
C41	C42	1.410(6)			

Bond Angles (°)

Atom	Atom	Atom	Angle/°	Atom	Atom	Atom	Angle/°
C48	N8	C56	108.8(3)	C19	C18	C23	118.8(4)
C24	N4	C28	115.7(4)	C69	C64	C63	106.9(4)
C1	N1	C5	115.4(3)	C65	C64	C63	134.1(4)
C25	N5	C33	109.0(3)	C65	C64	C69	119.0(4)
C10	N2	C2	109.3(3)	C73	C72	C86	123.7(4)
C70	N10	C74	114.9(4)	C71	C72	C73	115.4(4)
C47	N7	C51	116.5(4)	C71	C72	C86	120.9(4)
C71	N11	C79	108.7(3)	C82	C81	C80	119.7(4)
C62	N9	C69	109.4(4)	C37	C38	C33	117.6(4)
C23	N3	C16	109.3(4)	C53	C52	C51	121.5(4)
C39	N6	C42	109.6(4)	N9	C62	C63	110.3(4)
C85	N12	C88	109.1(4)	C79	C80	C70	106.1(4)
C5	C4	C3	119.5(4)	C81	C80	C70	133.9(4)
C9	C4	C5	117.7(4)	C81	C80	C79	119.9(4)
C9	C4	C3	122.7(4)	N7	C51	C50	122.8(4)

N4	C24	C34	128.6(4)	N7	C51	C52	118.0(4)
N4	C24	C25	124.7(4)	C52	C51	C50	119.3(4)
C25	C24	C34	106.7(4)	C56	C61	C60	117.0(4)
N10	C70	C80	128.4(4)	C64	C63	C49	128.3(4)
N10	C70	C71	125.1(4)	C62	C63	C49	125.7(4)
C71	C70	C80	106.5(3)	C62	C63	C64	105.9(4)
N2	C2	C1	108.1(4)	C9	C8	C7	120.4(4)
C3	C2	N2	130.9(4)	C72	C73	C74	119.5(4)
C3	C2	C1	120.9(4)	C78	C73	C72	123.1(4)
N5	C33	C34	110.0(4)	C78	C73	C74	117.3(4)
N5	C33	C38	129.2(4)	N9	C69	C64	107.4(4)
C38	C33	C34	120.8(4)	N9	C69	C68	129.9(4)
N1	C5	C4	123.7(4)	C68	C69	C64	122.7(4)
N1	C5	C6	116.7(4)	N10	C74	C73	123.9(4)
C6	C5	C4	119.5(4)	N10	C74	C75	116.8(4)
C8	C9	C4	121.4(4)	C75	C74	C73	119.3(4)
C33	C34	C24	106.1(3)	N3	C23	C18	107.7(4)
C35	C34	C24	133.2(4)	N3	C23	C22	130.6(4)
C35	C34	C33	120.7(4)	C22	C23	C18	121.6(5)
N2	C10	C15	128.9(4)	C77	C78	C73	121.6(4)
N2	C10	C11	109.5(4)	C45	C46	C41	118.7(4)
C15	C10	C11	121.5(4)	N11	C71	C70	108.6(4)
N1	C1	C2	124.6(4)	C72	C71	N11	130.3(4)
N1	C1	C11	128.4(4)	C72	C71	C70	121.1(4)
C2	C1	C11	107.0(3)	C78	C77	C76	120.5(4)
C49	C50	C55	123.1(4)	C83	C84	C79	118.2(4)
C49	C50	C51	119.9(4)	C6	C7	C8	119.9(4)
C55	C50	C51	117.0(4)	C75	C76	C77	120.3(4)
C4	C3	C17	122.7(4)	C66	C65	C64	118.2(5)
C2	C3	C4	115.9(4)	C55	C54	C53	119.8(4)
C2	C3	C17	121.3(4)	N4	C28	C27	123.8(4)
C14	C15	C10	117.6(4)	N4	C28	C29	117.9(4)
C60	C59	C58	120.4(4)	C29	C28	C27	118.3(4)
C50	C49	C63	123.2(4)	C88	C87	C86	107.1(4)

C48	C49	C50	115.8(4)	C92	C87	C86	135.0(4)
C48	C49	C63	121.0(4)	C92	C87	C88	117.8(4)
C57	C58	C59	118.3(4)	C41	C40	C26	129.6(4)
C54	C55	C50	122.2(4)	C39	C40	C41	106.5(4)
C15	C14	C13	121.4(4)	C39	C40	C26	123.7(4)
N11	C79	C80	110.0(4)	N3	C16	C17	110.4(4)
N11	C79	C84	129.0(4)	N12	C85	C86	109.8(4)
C84	C79	C80	121.0(4)	C30	C29	C28	121.6(4)
N7	C47	C48	124.0(4)	C58	C57	C47	133.0(4)
N7	C47	C57	129.4(4)	C58	C57	C56	120.8(4)
C48	C47	C57	106.6(3)	C56	C57	C47	106.1(4)
N8	C56	C61	128.5(4)	C87	C86	C72	129.2(4)
N8	C56	C57	110.1(4)	C85	C86	C72	124.1(4)
C61	C56	C57	121.4(4)	C85	C86	C87	106.6(4)
C31	C32	C27	121.3(4)	N6	C39	C40	109.4(4)
C46	C41	C40	134.5(4)	C81	C82	C83	119.7(4)
C46	C41	C42	118.9(4)	C84	C83	C82	121.6(4)
C42	C41	C40	106.6(4)	C35	C36	C37	120.7(4)
C13	C12	C11	118.9(4)	C29	C30	C31	120.6(4)
C12	C13	C14	120.8(4)	C32	C31	C30	120.2(4)
C36	C35	C34	118.3(4)	N6	C42	C41	107.9(4)
C7	C6	C5	120.9(4)	N6	C42	C43	130.1(4)
C59	C60	C61	122.1(4)	C43	C42	C41	122.0(5)
C32	C27	C26	123.3(4)	C76	C75	C74	120.8(4)
C32	C27	C28	117.9(4)	C69	C68	C67	117.7(5)
C26	C27	C28	118.8(4)	N12	C88	C87	107.3(4)
N5	C25	C24	108.2(3)	C89	C88	N12	129.0(4)
C26	C25	N5	131.4(4)	C89	C88	C87	123.6(5)
C26	C25	C24	120.4(4)	C52	C53	C54	120.3(4)
C18	C17	C3	128.5(4)	C21	C22	C23	117.5(5)
C16	C17	C3	124.9(4)	C20	C19	C18	119.2(5)
C16	C17	C18	106.6(4)	C43	C44	C45	121.8(5)
C10	C11	C1	106.1(3)	C90	C89	C88	116.5(5)
C12	C11	C10	119.8(4)	C65	C66	C67	121.8(5)

C12	C11	C1	134.1(4)	C46	C45	C44	121.2(5)
N8	C48	C49	130.5(4)	C44	C43	C42	117.4(5)
N8	C48	C47	108.4(4)	C91	C92	C87	120.0(5)
C49	C48	C47	121.1(4)	C89	C90	C91	122.1(5)
C27	C26	C40	123.1(4)	C92	C91	C90	120.0(5)
C25	C26	C27	116.5(4)	C68	C67	C66	120.7(5)
C25	C26	C40	120.4(4)	C22	C21	C20	122.4(5)
C38	C37	C36	121.8(4)	C19	C20	C21	120.4(5)
C23	C18	C17	106.0(4)	C94	C93	C93[1]	115.8(6)
C19	C18	C17	135.2(4)	C95	C94	C93	113.1(5)

Details of single crystal structure information of InqPr1

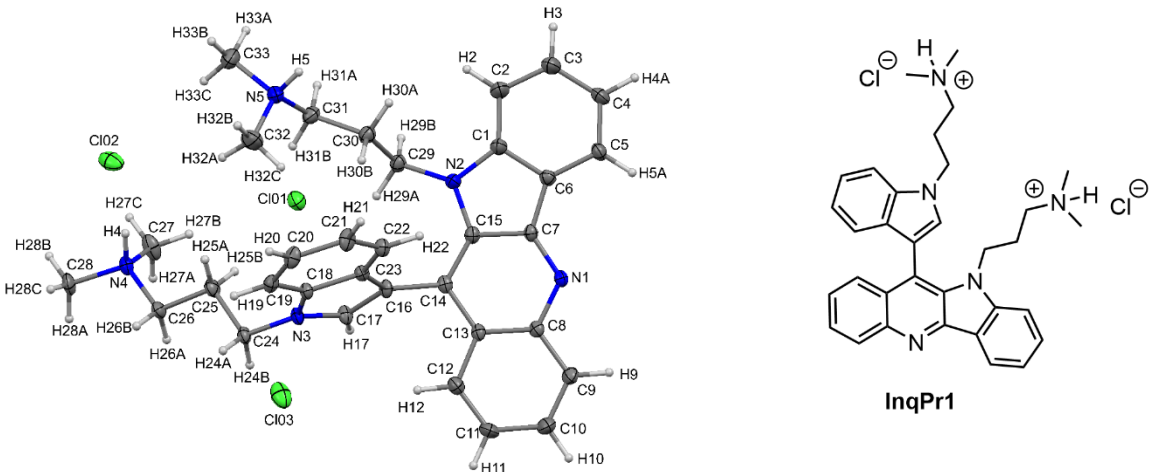

ORTEP diagram and structure of the alkylated product **InqPr1** (CCDC 2113444)

Selected crystallographic data of InqPr1

Table S3. Crystal data and structure refinement data for **InqPr1**

Empirical formula	$C_{33}H_{43}Cl_3N_5O_2$
Formula weight	648.07
Temperature/K	150.00
Crystal system	triclinic
Space group	P-1
a/Å	10.7323(4)
b/Å	11.1110(6)

c/Å	16.7890(9)
α/°	76.812(4)
β/°	76.009(4)
γ/°	64.298(4)
Volume/Å^3	1732.95(16)
Z	2
ρ_{calc}g/cm^3	1.242
μ/mm^{-1}	2.676
F(000)	686.0
Crystal size/mm^3	0.21 × 0.135 × 0.12
Radiation	CuKα (λ = 1.54184)
2Θ range for data collection/°	5.48 to 145.602
Reflections collected	20518
Independent reflections	6676 [R_{int} = 0.0940]
Data/restraints/parameters	6676/0/398
Goodness-of-fit on F^2	1.169
R_1	0.0911
wR_2	0.3055
Largest diff. peak/hole / e Å^{-3}	0.98/-1.05

Bond lengths [Å] and angles [°] for InqPr1

Table S4. Bond lengths and bond parameters for **InqPr1**

Bond Lengths (Å)

Atom	Atom	Length/Å	Atom	Atom	Length/Å
N1	C8	1.379(4)	C6	C7	1.414(5)
N1	C7	1.332(4)	C6	C1	1.414(5)
N3	C18	1.376(4)	C6	C36	1.406(5)
N3	C17	1.381(4)	N5	C31	1.484(5)
N3	C24	1.457(4)	N5	C33	1.494(5)
N2	C15	1.391(5)	N5	C32	1.475(6)
N2	C1	1.400(5)	C22	C21	1.380(5)
N2	C29	1.461(4)	C17	C16	1.377(4)
N4	C28	1.487(4)	C14	C16	1.469(4)
N4	C26	1.499(5)	C1	C2	1.389(6)
N4	C27	1.480(5)	C20	C21	1.404(5)
C18	C23	1.418(4)	C9	C10	1.369(6)
C18	C19	1.397(5)	C25	C24	1.526(5)
C15	C7	1.430(4)	C25	C26	1.524(4)
C15	C14	1.388(5)	C29	C30	1.516(5)
C23	C22	1.396(4)	C36	C4	1.372(6)
C23	C16	1.443(4)	C12	C11	1.358(6)
C13	C8	1.423(4)	C2	C3	1.394(6)
C13	C14	1.423(5)	C4	C3	1.409(6)
C13	C12	1.433(5)	C30	C31	1.541(5)
C8	C9	1.403(5)	C10	C11	1.403(6)
C19	C20	1.386(5)			

Bond Angles (°)

Atom	Atom	Atom	Angle/°	Atom	Atom	Atom	Angle/°
C7	N1	C8	120.6(3)	C32	N5	C33	109.9(4)
C18	N3	C17	108.9(2)	C21	C22	C23	118.6(3)
C18	N3	C24	125.1(3)	N1	C7	C15	121.5(3)
C17	N3	C24	125.6(3)	N1	C7	C6	129.6(3)

C15	N2	C1	108.0(3)	C6	C7	C15	109.0(3)
C15	N2	C29	127.6(3)	C16	C17	N3	110.1(3)
C1	N2	C29	121.5(3)	C15	C14	C13	116.3(3)
C28	N4	C26	110.2(3)	C15	C14	C16	124.0(3)
C27	N4	C28	110.5(3)	C13	C14	C16	119.3(3)
C27	N4	C26	112.8(3)	N2	C1	C6	110.0(3)
N3	C18	C23	107.7(3)	C2	C1	N2	128.6(3)
N3	C18	C19	130.0(3)	C2	C1	C6	121.4(3)
C19	C18	C23	122.3(3)	C19	C20	C21	121.4(3)
N2	C15	C7	107.4(3)	C23	C16	C14	123.7(3)
C14	C15	N2	131.7(3)	C17	C16	C23	106.3(3)
C14	C15	C7	120.8(3)	C17	C16	C14	129.4(3)
C18	C23	C16	107.0(3)	C10	C9	C8	119.1(3)
C22	C23	C18	119.3(3)	C26	C25	C24	109.1(3)
C22	C23	C16	133.6(3)	N3	C24	C25	110.4(3)
C8	C13	C12	115.9(3)	N2	C29	C30	114.0(3)
C14	C13	C8	121.4(3)	C22	C21	C20	121.5(3)
C14	C13	C12	122.5(3)	C4	C36	C6	118.4(3)
N1	C8	C13	119.1(3)	C11	C12	C13	121.1(3)
N1	C8	C9	118.5(3)	N4	C26	C25	111.4(3)
C9	C8	C13	122.3(3)	C1	C2	C3	117.0(4)
C20	C19	C18	117.0(3)	C36	C4	C3	120.5(4)
C1	C6	C7	105.6(3)	C29	C30	C31	109.0(3)
C36	C6	C7	133.9(3)	N5	C31	C30	111.5(3)
C36	C6	C1	120.5(3)	C2	C3	C4	122.3(4)
C31	N5	C33	112.0(3)	C9	C10	C11	120.3(4)
C32	N5	C31	111.8(3)	C12	C11	C10	121.3(4)

Oligonucleotides used for various biophysical and biochemical experiments

Table S5. DNA sequences used for the experiments in 5' to 3' direction

DNA	Sequence
Telomeric DNA	5'-AGGGTTAGGGTTAGGGTTAGGG-3'
c-MYC DNA	5'-TGAGGGTGGGTAGGGTGGGTAA-3'
c-KIT1 DNA	5'-GGGAGGGCGCTGGGAGGAGGG-3'
h-RAS DNA	5'- TCGGGTTGCGGGCGCAGGGCACGGGCG -3'
Duplex-17 (DS17)	5'-CCAGTTCGTAGTAACCC-3' 5'-GGGTTACTA CGAACTGG-3'
Primer for stop assay	5'-ACGACTCACTATAGCAATTGCG-3’
Template of *c-MYC* DNA	5'-TGAGGGTGGGTAGGGTGGGTAAGCCACCGCAATT GCTATAGTGAGTCGT-3'
Template of mutated *c-MYC* DNA	5'-TGAGGGTGGGTAGAGTGGGTAAGCCACCGCAATT GCTATAGTGAGTCGT-3'
Template of telomeric DNA	5'-AGGGTTAGGGTTAGGGTTAGGGGCCACCGCAATT GCTATAGTGAGTCGT-3'

Primers used for qRT-PCR experiments

Table S6. List of primers used for the qRT-PCR experiments in 5' to 3' direction

Description	Sequence
c-MYC forward primer	5′-TGAGGAGACACCGCCCAC-3′
c-MYC reverse primer	5′-CAACATCGATTTCTTCCTCATCTTC-3′
c-KIT forward primer	5′-CGTGGAAAAGAGAAAACAGTCA-3′
c-KIT reverse primer	5′-CACCGTGATGCCAGCTATTA-3′
β-actin forward primer	5′-TGCGTGACATTAAGGAGAA-3′
β-actin reverse primer	5′-CTGCATCCTGTCGGCAATG-3′

Average distances and percentage occupancies of major electrostatic interaction of InqPr2 with *c-MYC* and *c-KIT1* G4 DNAs

Table S7. Average distances and percentages of major electrostatic interactions

DNA	Residue-interacting atom	Protonated nitrogen of the ligand	Percentage occupancy	Average distance (Å)
c-MYC	dT11-OP2	N4 of the ligand at the 3′-end	91.3	3.5
	dG13-OP1	N4 of the ligand at the 5′-end	52.5	7.1
c-KIT1	dG16-OP1	N4 of the ligand at the 3′-end	44.2	5.5
	dG17-OP1	N5 of the ligand at the 3′-end	55.3	5.1
	dG17-OP2	N4 of the ligand at the 3′-end	35	5.9

The distances were calculated using CPPTRAJ module of AMBER 18. All the distances between the protonated nitrogen and the backbone atoms of G4 below 5.0 Å were considered. Percentage occupancies when the distance is less than 5.0 Å are mentioned. The average distance represents the distance during the whole 500 ns trajectory.

Binding free energy values of InqPr2 with *c-MYC* G4 DNA

Table S8. Binding free energy components of *c-MYC* G4 DNA and **InqPr2** complex

	5′-quartet bound	3′-quartet bound	Dual bound
ΔE_{ELEC}	−829.95 ± 26.33	−850.80 ± 20.70	−1680.75 ± 31.92
ΔE_{VDW}	−45.95 ± 5.05	−47.23 ± 3.63	−93.18 ± 5.64
$\Delta E_{MM}(\Delta E_{ELEC} + \Delta E_{VDW})$	−875.39 ± 28.06	−897.51 ± 22.48	−1773.93 ± 33.96
ΔPB_{np}	−3.50 ± 0.35	−4.02 ± 0.23	−7.51 ± 0.41
ΔPB_{cal}	842.29 ± 27.82	860.90 ± 21.10	1702.76 ± 33.28
$\Delta PB_{solv}(\Delta PB_{np} + \Delta PB_{cal})$	838.79 ± 27.74	856.89 ± 20.95	1695.24 ± 33.19
$\boldsymbol{\Delta H_{PB}(\Delta E_{MM} + \Delta PB_{solv})}$	**−36.59 ± 5.04**	**−40.62 ± 4.94**	**−78.69 ± 6.89**
$\boldsymbol{T\Delta S}$	**−18.80 ± 5.92**	**−19.53 ± 6.14**	**−31.36 ± 7.85**
$\boldsymbol{\Delta G(\Delta H_{PB} - T\Delta S)}$	**−17.80 ± 7.82**	**−21.09 ± 7.77**	**−47.33 ± 10.89**

Binding free energy components have been calculated from the last 20 ns of the 500 ns simulation by considering every 5th frame from a total of 2000 frames. The molecular-mechanical energy calculations were performed using MM/PBSA, and entropy calculations using nmode analysis. ΔE_{ELEC} is the electrostatic contribution. ΔE_{VDW} is the Vander Waals contribution. ΔE_{MM} is the total molecular mechanical energy. ΔPB_{np} is the non-polar contribution to the solvation energy. ΔPB_{cal} is the electrostatic contribution to the solvation energy. ΔPB_{solv} is the total solvation energy. $T\Delta S$ is the solute entropic contributions. ΔG *(*$\Delta H - T\Delta S$) is the estimated binding free energy. All the values are reported in kcal mol^{-1}. For nmode analysis parameters used were: drms = 0.5; dielec (distance dependent dielec) = 4; maxcyc = 10,000 and AMBER prescribed default values were used for PB calculations

Binding free energy values of InqPr2 with *c-KIT1* G4 DNA

Table S9. Binding free energy components of *c-KIT1* G4 DNA and **InqPr2** complex

	5′-quartet bound	**3′-quartet bound**	**Dual bound**
ΔE_{ELEC}	−677.39 ± 30.89	−945.09 ± 20.19	−1622.48 ± 36.82
ΔE_{VDW}	−34.69 ± 4.94	−57.65 ± 3.72	−92.35 ± 5.94
$\Delta E_{MM}(\Delta E_{ELEC} + \Delta E_{VDW})$	−711.57 ± 34.47	−1002.23 ± 20.98	−1714.83 ± 39.92
ΔPB_{np}	−2.94 ± 0.32	−4.40 ± 0.19	−7.34 ± 0.36
ΔPB_{cal}	685.79 ± 32.28	947.65 ± 20.10	1633.29 ± 37.71
$\Delta PB_{solv}(\Delta PB_{np} + \Delta PB_{cal})$	682.85 ± 32.02	943.24 ± 19.99	1625.94 ± 37.46
$\boldsymbol{\Delta H_{PB}(\Delta E_{MM} + \Delta PB_{solv})}$	**−28.72 ± 4.29**	**−58.99 ± 4.54**	**−88.88 ± 6.09**
$\boldsymbol{T\Delta S}$	**−17.81 ± 5.66**	**−22.04 ± 5.56**	**−34.39 ± 6.90**
$\boldsymbol{\Delta G(\Delta H_{PB} - T\Delta S)}$	**−10.91 ± 6.36**	**−36.94 ± 7.27**	**−54.50 ± 8.97**

Binding free energy components have been calculated from the last 20 ns of the 500 ns simulation by considering every 5th frame from a total of 2000 frames. The molecular-mechanical energy calculations were performed using MM/PBSA, and entropy calculations using nmode analysis. ΔE_{ELEC} is the electrostatic contribution. ΔE_{VDW} is the Vander Waals contribution. ΔE_{MM} is the total molecular mechanical energy. ΔPB_{np} is the non-polar contribution to the solvation energy. ΔPB_{cal} is the electrostatic contribution to the solvation energy. ΔPB_{solv} is the total solvation energy. $T\Delta S$ is the solute entropic contributions. ΔG ($\Delta H - T\Delta S$) is the estimated binding free energy. All the values are reported in kcal mol^{-1}. For nmode analysis parameters used were: drms = 0.5; dielec (distance dependent dielec) = 4; maxcyc = 10,000 and AMBER prescribed default values were used for PB calculations

^{1}H and ^{13}C NMR spectrum of compound 3, (G: Grease, I: Impurity)

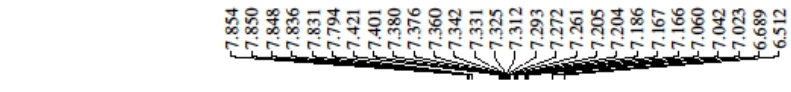

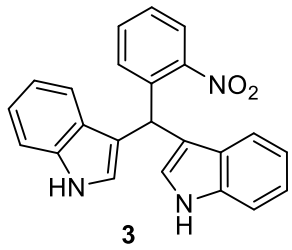

3

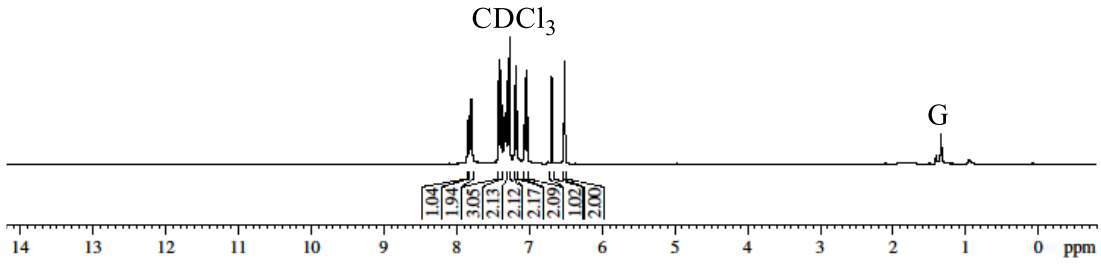

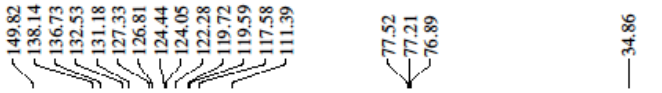

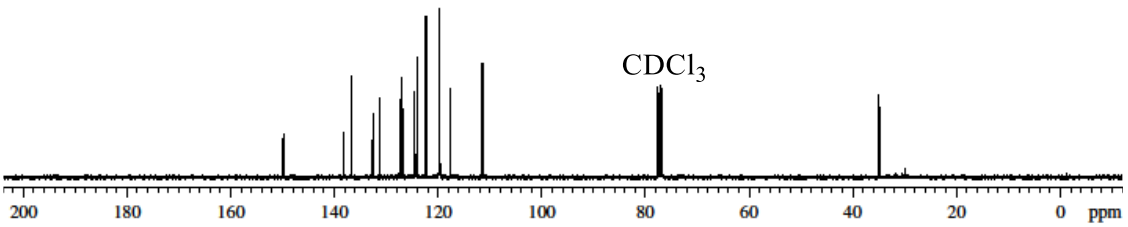

^{1}H and ^{13}C NMR spectrum of compound 4

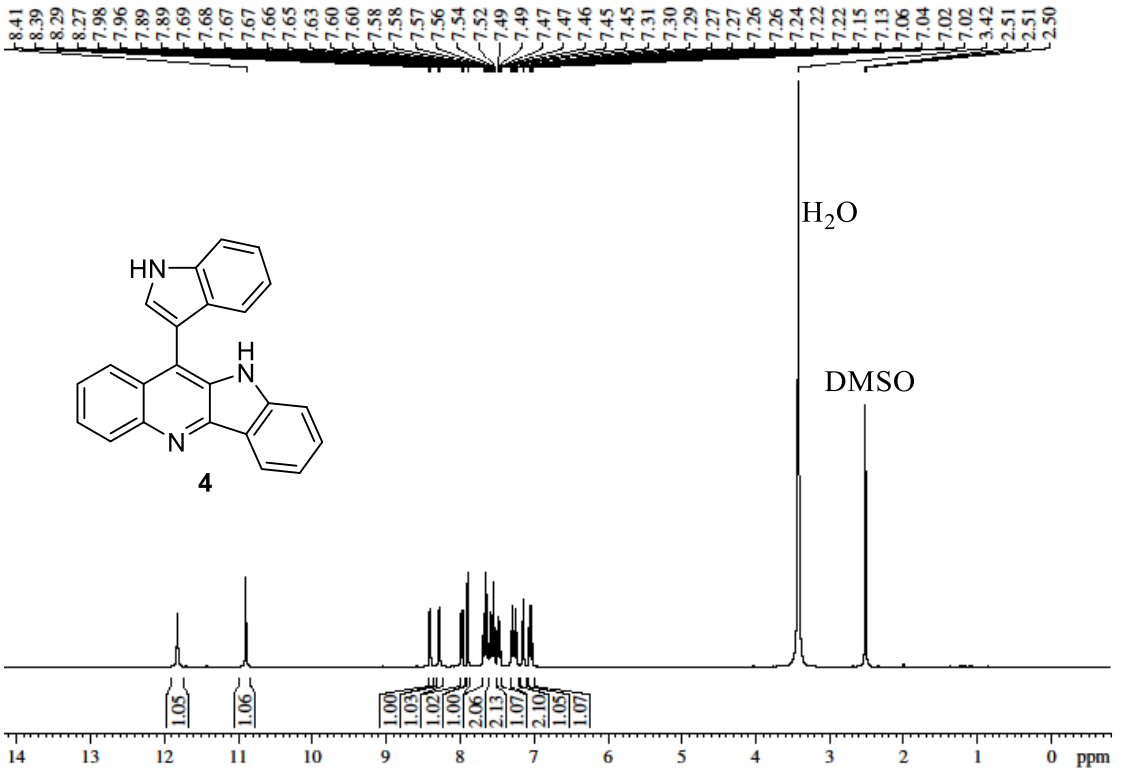

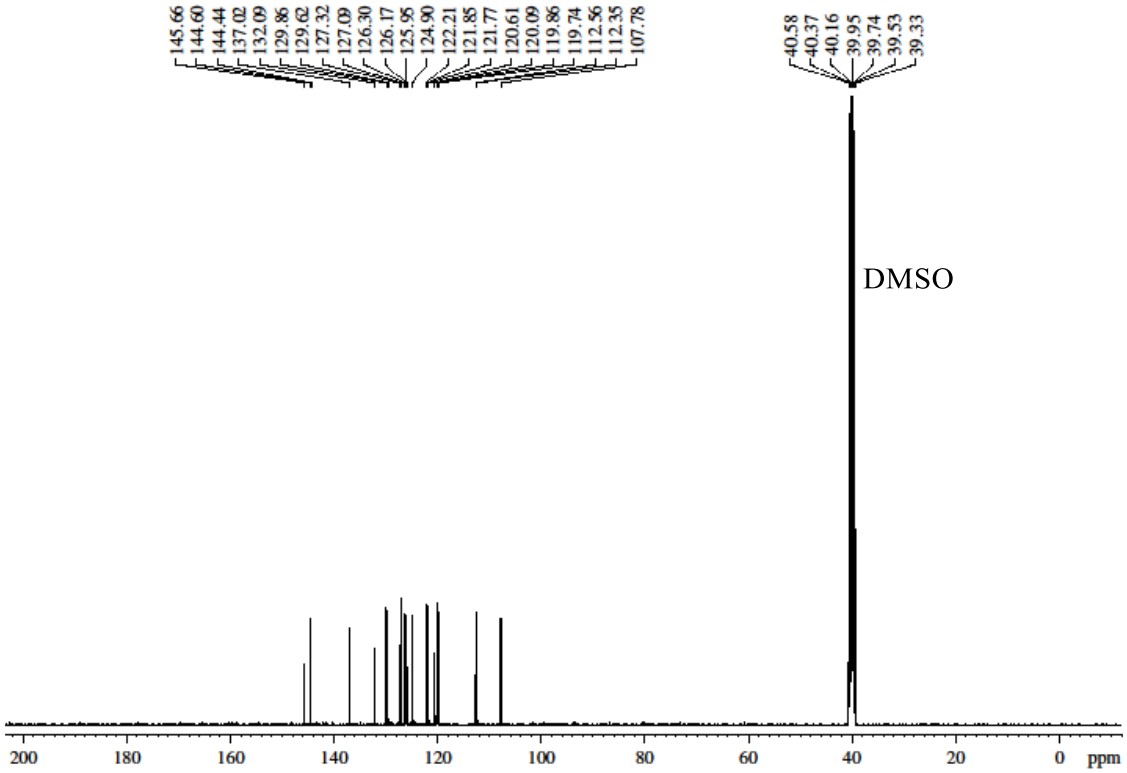

^{1}H and ^{13}C NMR spectrum of compound InqEt1

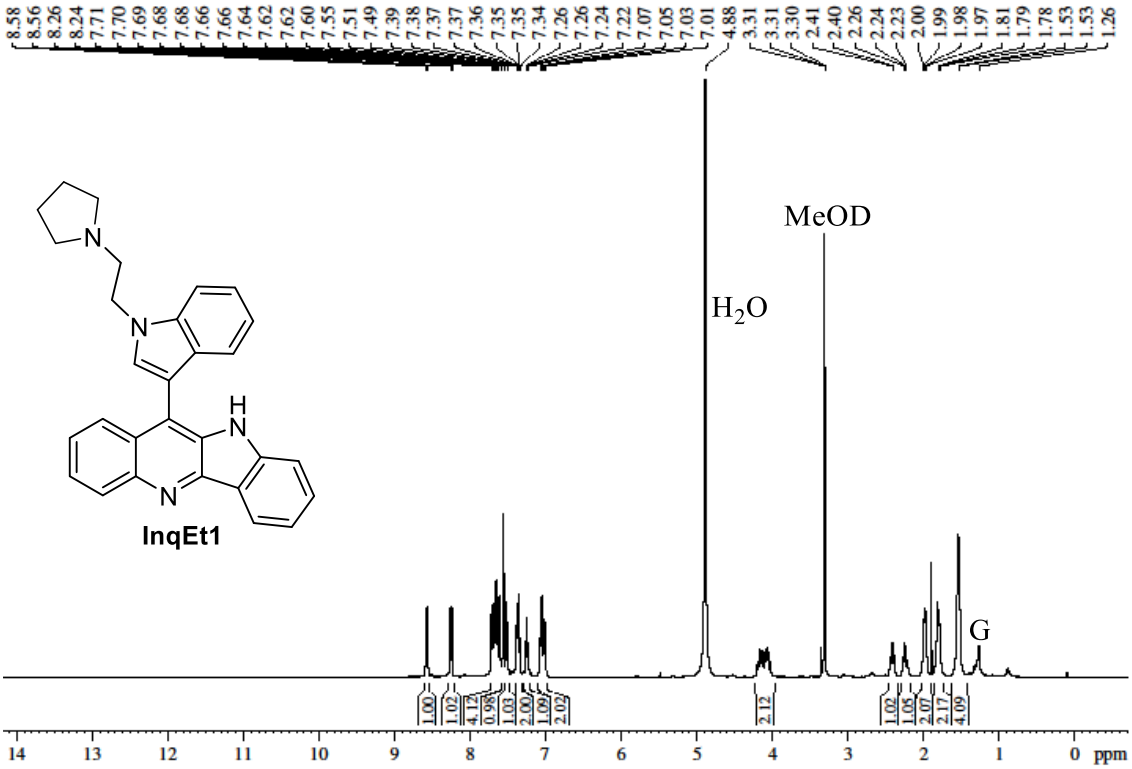

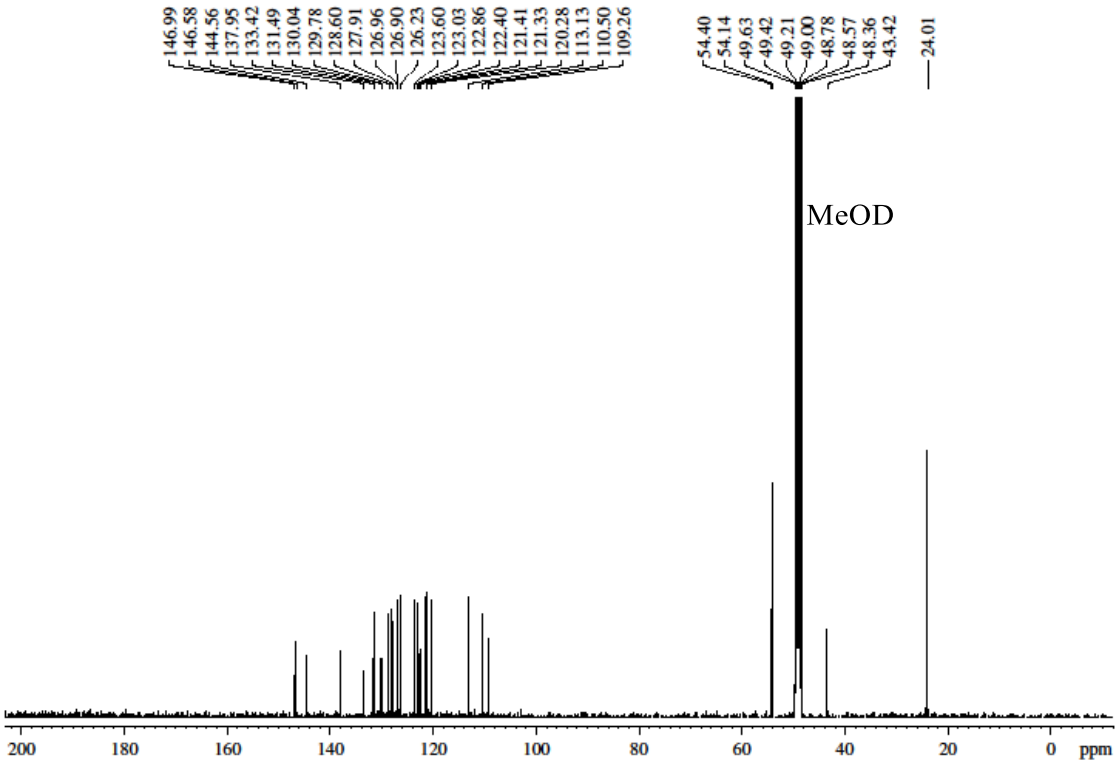

^{1}H and ^{13}C NMR spectrum of compound InqEt2

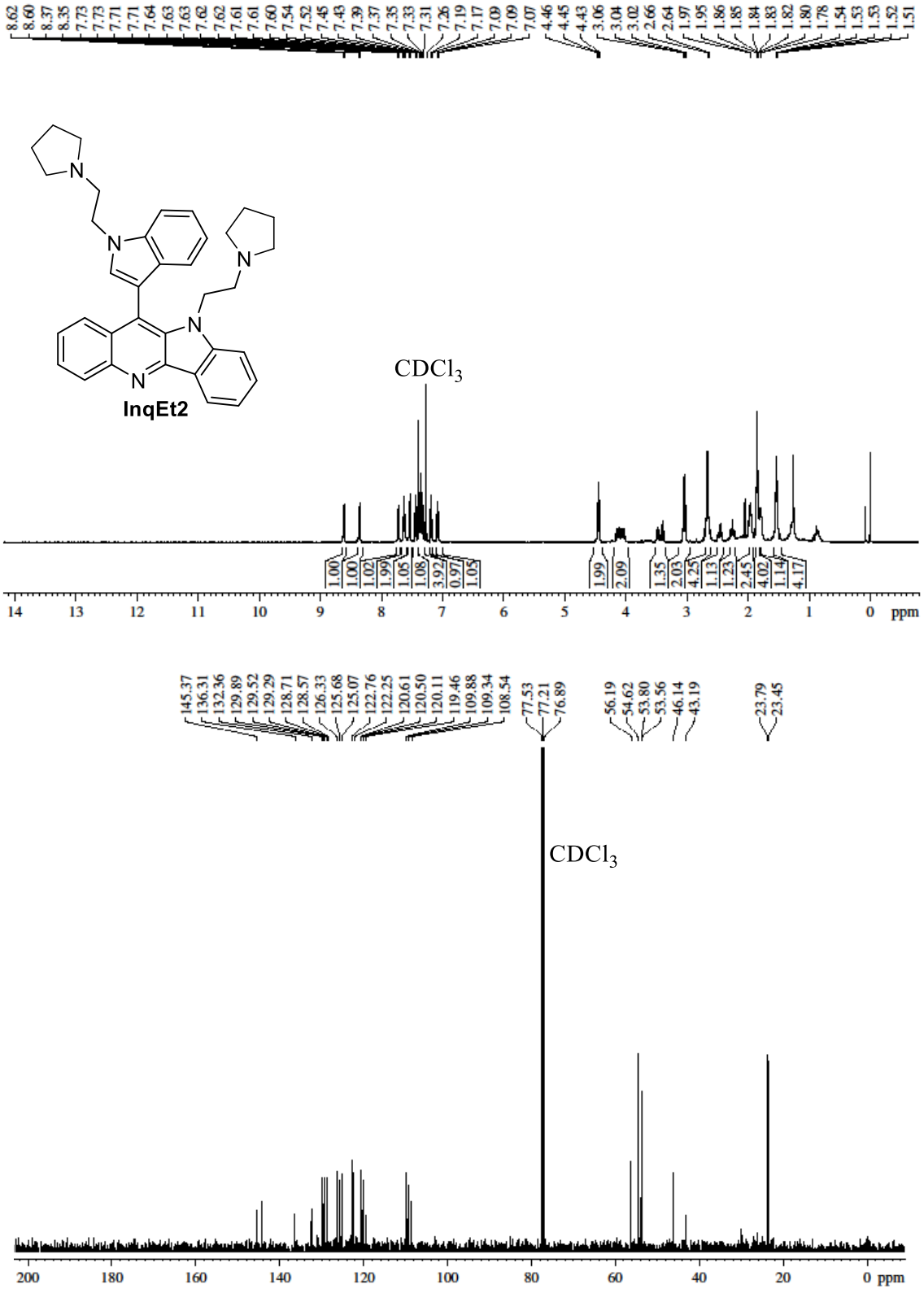

^{1}H and ^{13}C NMR spectrum of compound 5

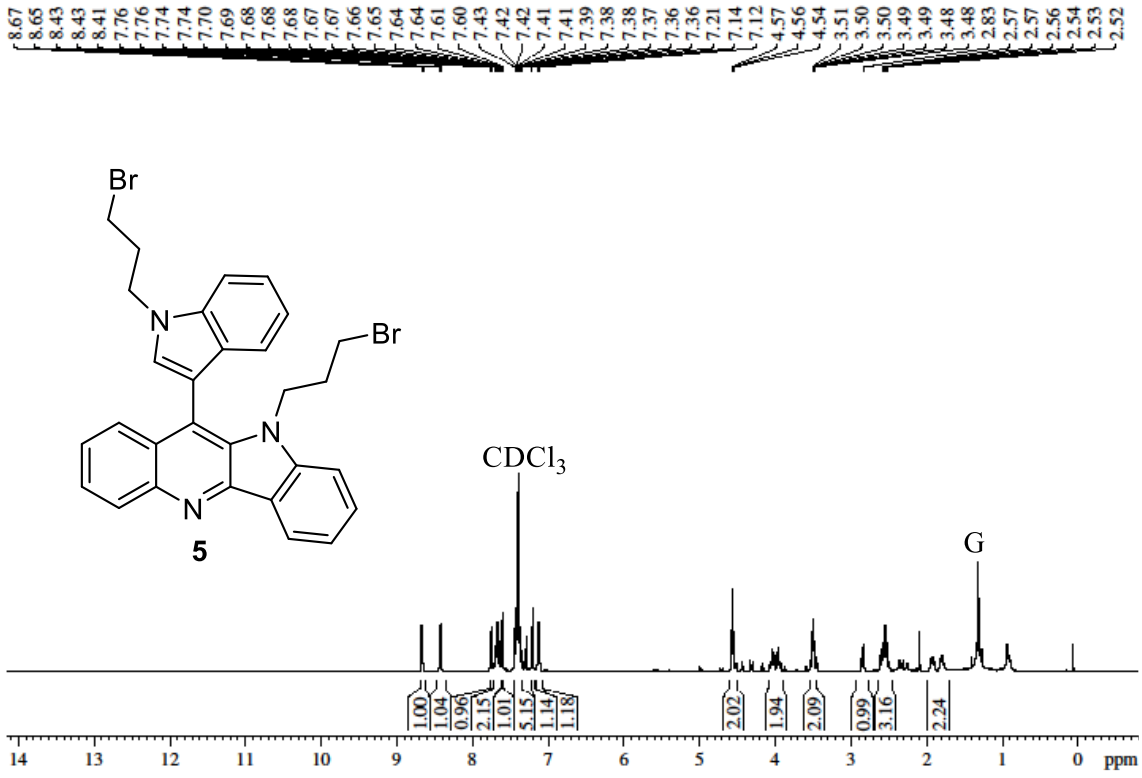

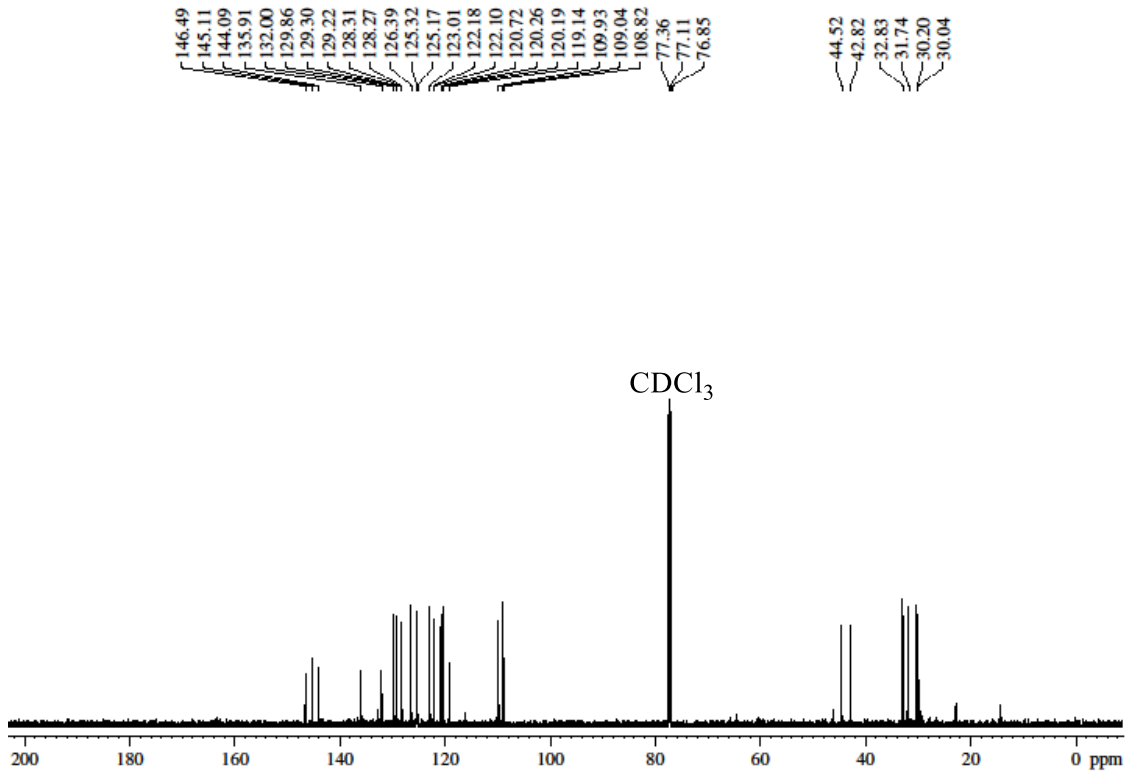

^{1}H and ^{13}C NMR spectrum of compound InqPr1

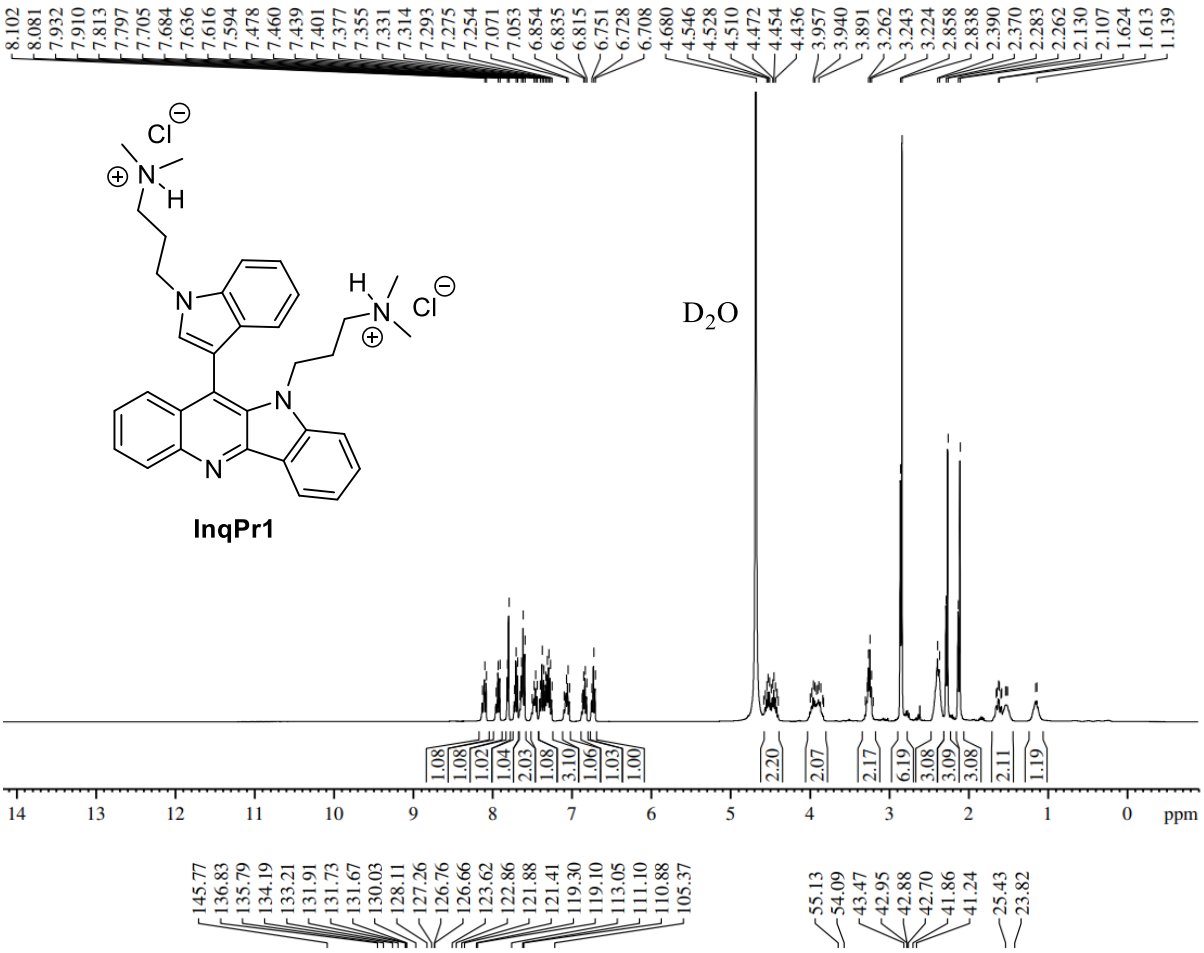

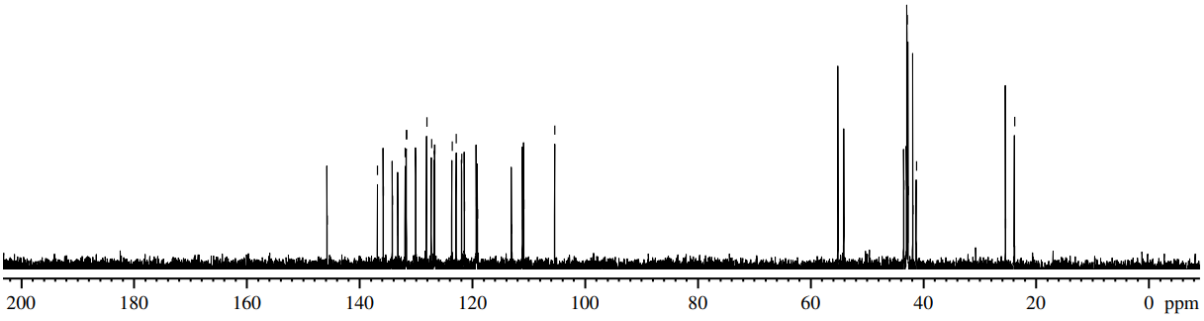

^{1}H and ^{13}C NMR spectrum of compound InqPr2

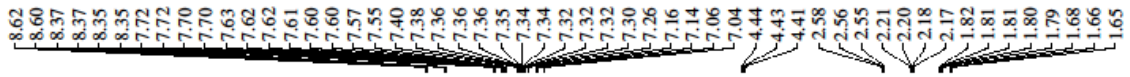

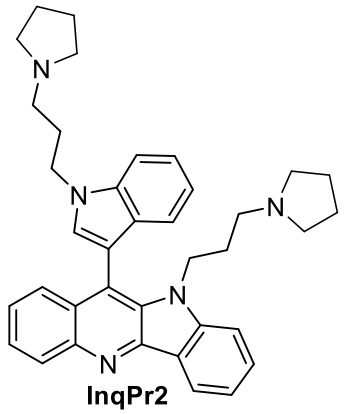

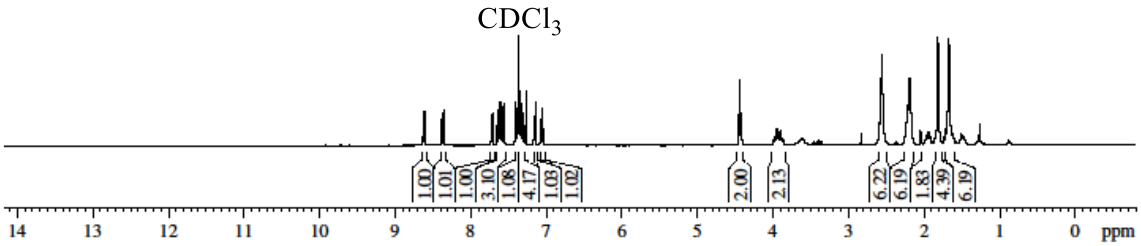

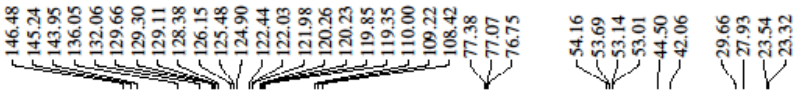

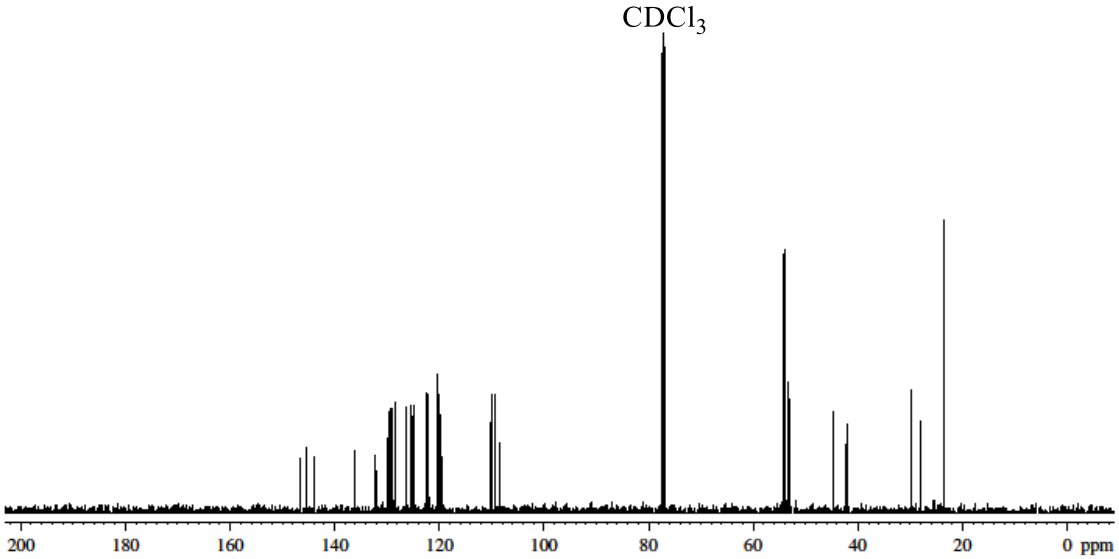

HRMS spectra of compound 3

DEPARTMENT OF CHEMISTRY, I.I.T.(B)

Analysis Info

Analysis Name	D:\Data\backup_PPI\PK-SP-bisindole.d	Acquisition Date	10/25/2018 2:47:07 AM
Method	Tune_pos_NAF-1500A.m	Operator	PPIOUT
Sample Name	PK-SP-bisindole	Instrument	maXis impact 282001.00081
Comment	C23H17N3O2		

Acquisition Parameter

Source Type	ESI	Ion Polarity	Positive	Set Nebulizer	0.5 Bar
Focus	Active	Set Capillary	3700 V	Set Dry Heater	180 °C
Scan Begin	50 m/z	Set End Plate Offset	-500 V	Set Dry Gas	4.0 l/min
Scan End	1500 m/z	Set Charging Voltage	2000 V	Set Divert Valve	Source
		Set Corona	0 nA	Set APCI Heater	0 °C

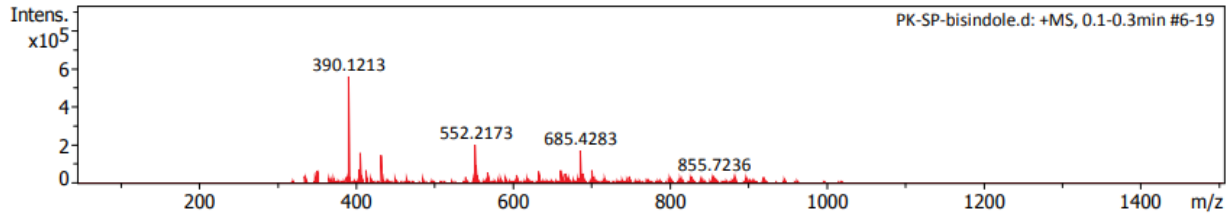

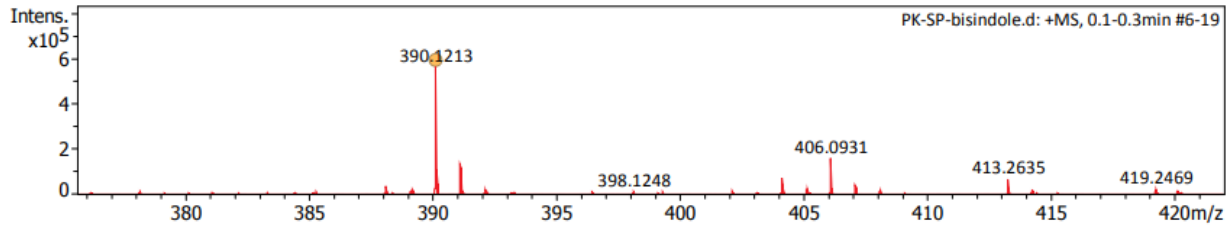

Meas. m/z	#	Ion Formula	m/z	err [ppm]	mSigma	# mSigma	Score	rdb	e⁻ Conf	N-Rule
390.1213	1	C23H17N3NaO2	390.1213	-0.1	13.5	1	100.00	17.0	even	ok

HRMS spectra of compound 4

DEPARTMENT OF CHEMISTRY, I.I.T.(B)

Analysis Info

Analysis Name	D:\Data\backup_PPI\PK-SP-CRPT-CORE@.d	Acquisition Date	10/25/2018 2:55:52 AM
Method	Tune_pos_NAF-1500A.m	Operator	PPIOUT
Sample Name	PK-SP-CRPT-CORE@	Instrument	maXis impact 282001.00081
Comment	C23H15N3		

Acquisition Parameter

Source Type	ESI	Ion Polarity	Positive	Set Nebulizer	0.5 Bar
Focus	Active	Set Capillary	3700 V	Set Dry Heater	180 °C
Scan Begin	50 m/z	Set End Plate Offset	-500 V	Set Dry Gas	4.0 l/min
Scan End	1500 m/z	Set Charging Voltage	2000 V	Set Divert Valve	Source
		Set Corona	0 nA	Set APCI Heater	0 °C

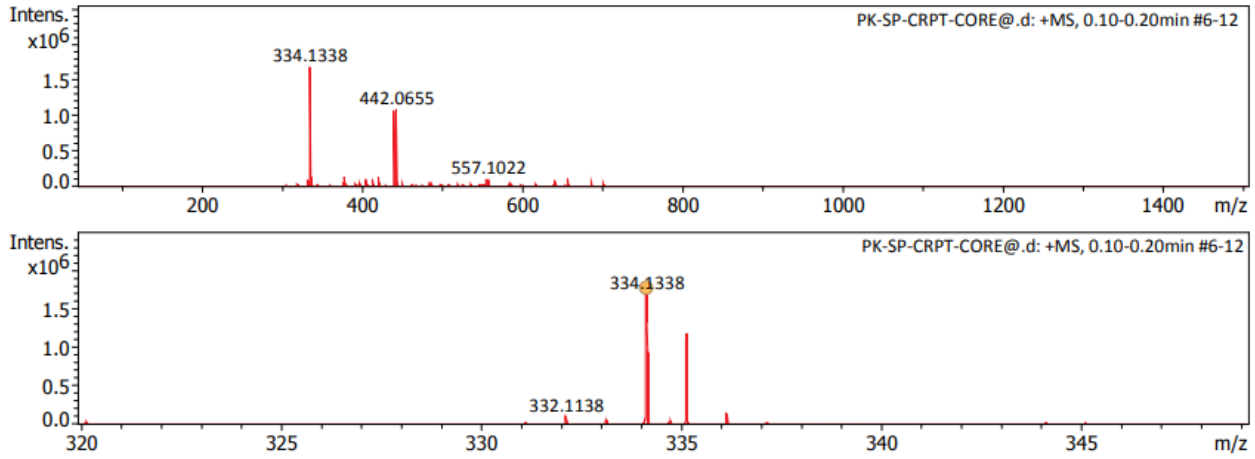

Meas. m/z	#	Ion Formula	m/z	err [ppm]	mSigma	# mSigma	Score	rdb	e¯ Conf	N-Rule
334.1338	1	C23H16N3	334.1339	0.2	258.5	1	100.00	18.0	even	ok

HRMS spectra of InEt1

DEPARTMENT OF CHEMISTRY, I.I.T.(B)

Analysis Info

Analysis Name	D:\Data\backup_PPI\PK-SP-CR-PY-1@.d	Acquisition Date	11/20/2017 10:22:12 AM
Method	Tune_pos_NAF-1000A.m	Operator	KPK OUT
Sample Name	PK-SP-CR-PY-1@	Instrument	maXis impact 282001.00081
Comment	C30H40O5Si		

Acquisition Parameter

Source Type	ESI	Ion Polarity	Positive	Set Nebulizer	0.5 Bar
Focus	Active	Set Capillary	3700 V	Set Dry Heater	180 °C
Scan Begin	50 m/z	Set End Plate Offset	-500 V	Set Dry Gas	4.0 l/min
Scan End	1000 m/z	Set Charging Voltage	2000 V	Set Divert Valve	Source
		Set Corona	0 nA	Set APCI Heater	0 °C

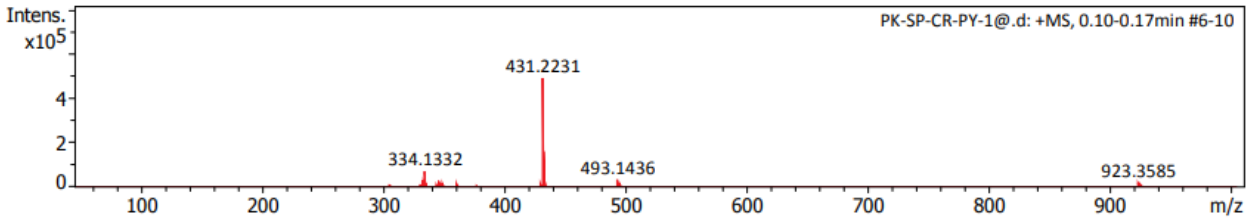

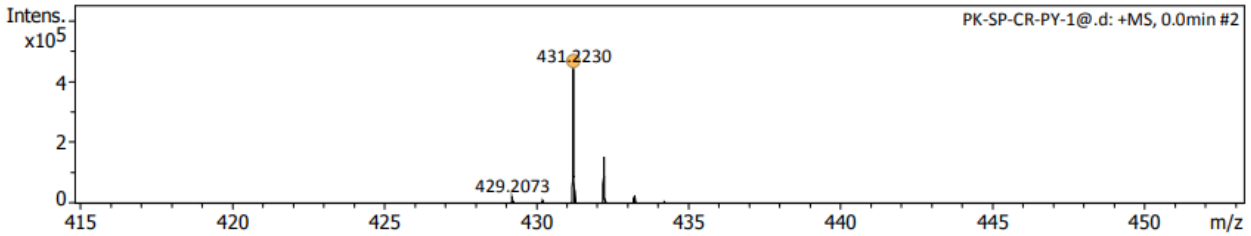

Meas. m/z	#	Ion Formula	m/z	err [ppm]	mSigma	# mSigma	Score	rdb	e¯ Conf	N-Rule
431.2230	1	C29H27N4	431.2230	-0.0	4.5	1	100.00	19.0	even	ok

HRMS spectra of InEt2

DEPARTMENT OF CHEMISTRY, I.I.T.(B)

Analysis Info

Analysis Name	D:\Data\AUG-2022\PK-SS-InqEtPy2 final.d	Acquisition Date	8/2/2022 10:50:04 AM
Method	NaICsI_pos_1000-a.m	Operator	GKL-LS-out
Sample Name	PK-SS-InqEtPy2 final	Instrument	maXis impact 282001.00081
Comment	C35H37N5		

Acquisition Parameter

Source Type	ESI	Ion Polarity	Positive	Set Nebulizer	0.3 Bar
Focus	Not active	Set Capillary	3700 V	Set Dry Heater	180 °C
Scan Begin	50 m/z	Set End Plate Offset	-500 V	Set Dry Gas	4.0 l/min
Scan End	1000 m/z	Set Charging Voltage	2000 V	Set Divert Valve	Source
		Set Corona	0 nA	Set APCI Heater	0 °C

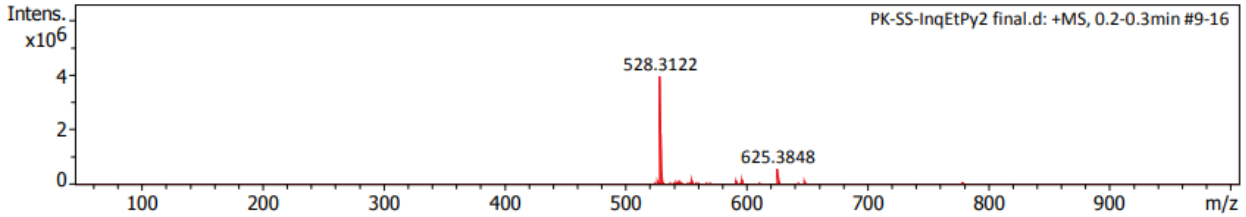

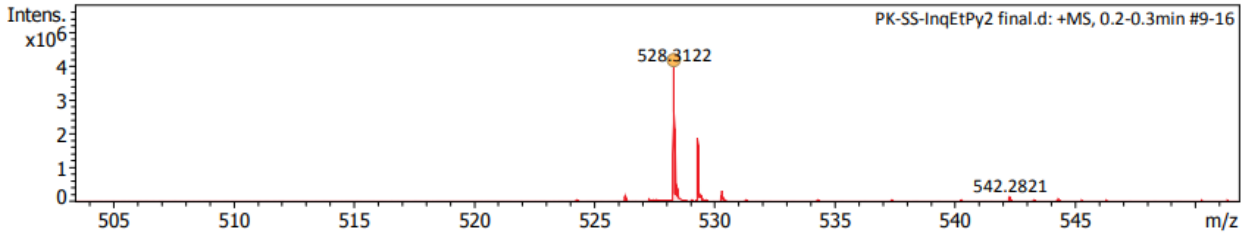

Meas. m/z	#	Ion Formula	m/z	err [ppm]	mSigma	# mSigma	Score	rdb	e⁻ Conf	N-Rule
528.3122	1	C35H38N5	528.3122	-0.1	31.4	1	100.00	20.0	even	ok

HRMS spectra of compound 5

DEPARTMENT OF CHEMISTRY, I.I.T.(B)

Analysis Info

Analysis Name	D:\Data\backup_PPI\PK-SP-CRPT-PRBR2.d	Acquisition Date	10/25/2018 2:13:19 AM
Method	Tune_pos_NAF-1500A.m	Operator	PPIOUT
Sample Name	PK-SP-CRPT-PRBR2	Instrument	maXis impact 282001.00081
Comment	C37H41N5		

Acquisition Parameter

Source Type	ESI	Ion Polarity	Positive	Set Nebulizer	0.5 Bar
Focus	Active	Set Capillary	3700 V	Set Dry Heater	180 °C
Scan Begin	50 m/z	Set End Plate Offset	-500 V	Set Dry Gas	4.0 l/min
Scan End	1500 m/z	Set Charging Voltage	2000 V	Set Divert Valve	Source
		Set Corona	0 nA	Set APCI Heater	0 °C

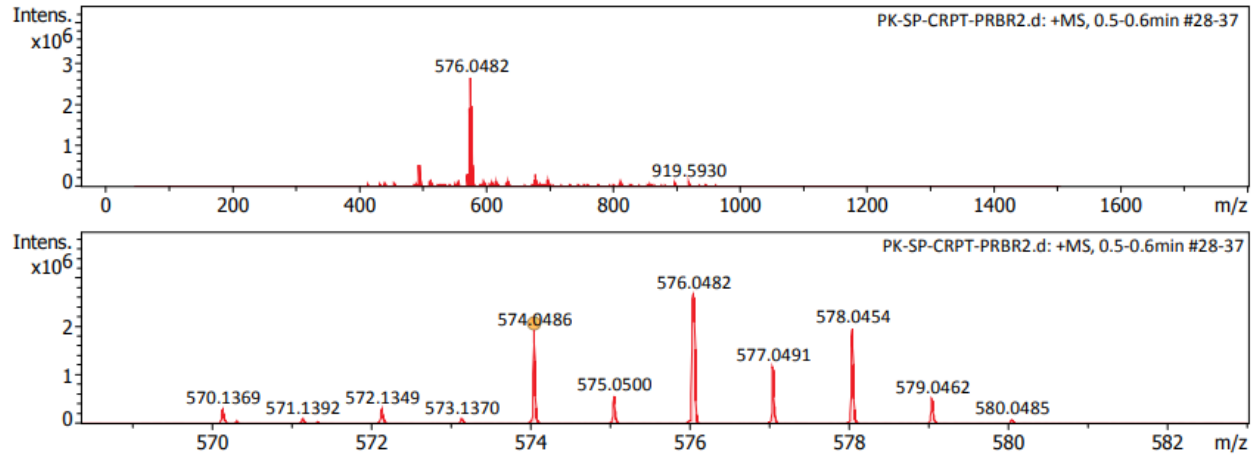

Meas. m/z	#	Ion Formula	m/z	err [ppm]	mSigma	# mSigma	Score	rdb	e⁻ Conf	N-Rule
574.0486	1	C29H26Br2N3	574.0488	0.3	123.9	1	100.00	22.0	even	ok

HRMS spectra of InqPr1

DEPARTMENT OF CHEMISTRY, I.I.T.(B)

Analysis Info

Analysis Name	D:\Data\JULY-2022\PK-SS-CryptnmE2@.d	Acquisition Date	7/8/2022 10:04:18 PM
Method	Low_mass- NaICsI.m	Operator	PPIIN
Sample Name	PK-SS-CryptnmE2@	Instrument	maXis impact 282001.00081
Comment	C33H39N5		

Acquisition Parameter

Source Type	ESI	Ion Polarity	Positive	Set Nebulizer	0.3 Bar
Focus	Not active	Set Capillary	4000 V	Set Dry Heater	180 °C
Scan Begin	50 m/z	Set End Plate Offset	-500 V	Set Dry Gas	4.0 l/min
Scan End	650 m/z	Set Charging Voltage	2000 V	Set Divert Valve	Source
		Set Corona	0 nA	Set APCI Heater	0 °C

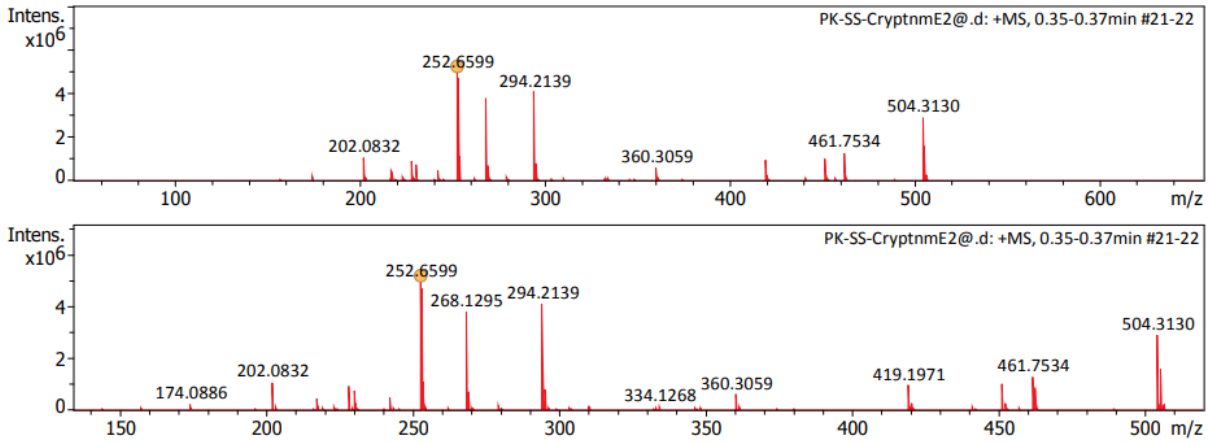

Meas. m/z	#	Ion Formula	m/z	err [ppm]	mSigma	# mSigma	Score	rdb	e⁻ Conf	N-Rule
252.6599	1	C33H39N5	252.6597	-0.5	297.8	1	100.00	18.0	even	ok

HRMS spectra of InqPr2

DEPARTMENT OF CHEMISTRY, I.I.T.(B)

Analysis Info

Analysis Name	D:\Data\backup_PPI\PK-SP-CRPT-PRPY2@.d	Acquisition Date	10/25/2018 2:05:38 AM
Method	Tune_pos_NAF-1500A.m	Operator	PPIOUT
Sample Name	PK-SP-CRPT-PRPY2@	Instrument	maXis impact 282001.00081
Comment	C37H41N5		

Acquisition Parameter

Source Type	ESI	Ion Polarity	Positive	Set Nebulizer	0.5 Bar
Focus	Active	Set Capillary	3700 V	Set Dry Heater	180 °C
Scan Begin	50 m/z	Set End Plate Offset	-500 V	Set Dry Gas	4.0 l/min
Scan End	1500 m/z	Set Charging Voltage	2000 V	Set Divert Valve	Source
		Set Corona	0 nA	Set APCI Heater	0 °C

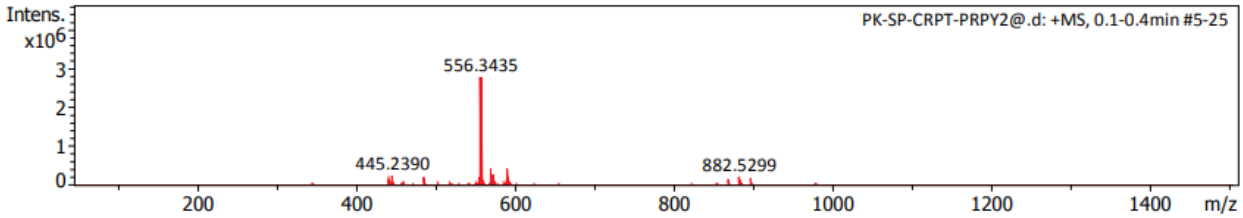

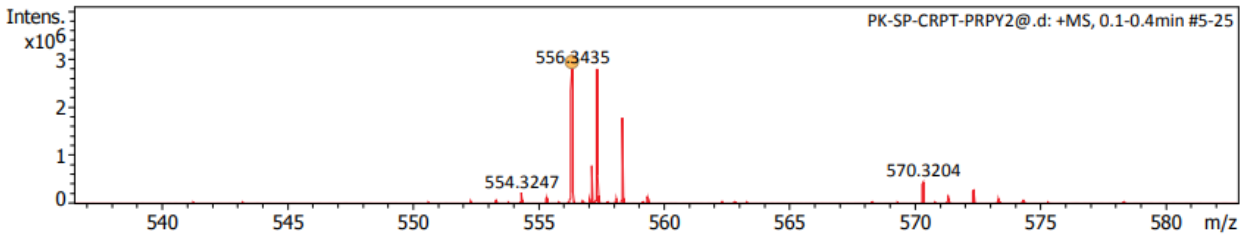

Meas. m/z	#	Ion Formula	m/z	err [ppm]	mSigma	# mSigma	Score	rdb	e⁻ Conf	N-Rule
556.3435	1	C37H42N5	556.3435	-0.1	398.4	1	100.00	20.0	even	ok